IMPROVED CHARACTERIZATION AND MODELING OF TIGHT OIL FORMATIONS FOR CO_2 ENHANCED OIL RECOVERY POTENTIAL AND STORAGE CAPACITY ESTIMATION

Final Report

Prepared for:

AAD Document Control

National Energy Technology Laboratory
U.S. Department of Energy
626 Cochrans Mill Road
PO Box 10940, MS 921-107
Pittsburgh, PA 15236-0940

Project Reporting Period: November 1, 2014 – October 31, 2017
Cooperative Agreement No. DE-FE0024454
DUNS No. 102280781

Prepared by:

James A. Sorensen
Steven A. Smith
Bethany A. Kurz
Steven B. Hawthorne
Lu Jin
Nicholas W. Bosshart
José A. Torres
Carolyn M. Nyberg
Loreal V. Heebink
John P. Hurley

Energy & Environmental Research Center
University of North Dakota
15 North 23rd Street, Stop 9018
Grand Forks, ND 58202-9018
Phone (701) 777-5287; Fax (701) 777-5181
jsorensen@undeerc.org

2018-EERC-03-04 March 2018

EERC DISCLAIMER

LEGAL NOTICE This research report was prepared by the Energy & Environmental Research Center (EERC), an agency of the University of North Dakota, as an account of work sponsored by the U.S. Department of Energy (DOE) National Energy Technology Laboratory. Because of the research nature of the work performed, neither the EERC nor any of its employees makes any warranty, express or implied, or assumes any legal liability or responsibility for the accuracy, completeness, or usefulness of any information, apparatus, product, or process disclosed or represents that its use would not infringe privately owned rights. Reference herein to any specific commercial product, process, or service by trade name, trademark, manufacturer, or otherwise does not necessarily constitute or imply its endorsement or recommendation by the EERC.

ACKNOWLEDGMENTS

The material presented in this report is based upon work supported by the U.S. Department of Energy National Energy Technology Laboratory under Award No. DE-FE0024454. Additional financial support for the project was provided by the North Dakota Industrial Commission through the North Dakota Oil and Gas Research Program and the Lignite Energy Council. The authors also thank Marathon Oil Company and the North Dakota Geological Survey for providing invaluable access to core samples.

DOE DISCLAIMER

This report was prepared as an account of work sponsored by an agency of the United States Government. Neither the United States Government, nor any agency thereof, nor any of their employees, makes any warranty, express or implied, or assumes any legal liability or responsibility for the accuracy, completeness, or usefulness of any information, apparatus, product, or process disclosed, or represents that its use would not infringe privately owned rights. Reference herein to any specific commercial product, process, or service by trade name, trademark, manufacturer, or otherwise does not necessarily constitute or imply its endorsement, recommendation, or favoring by the United States Government or any agency thereof. The views and opinions of authors expressed herein do not necessarily state or reflect those of the United States Government or any agency thereof.

NDIC DISCLAIMER

This report was prepared by the EERC pursuant to an agreement partially funded by the Industrial Commission of North Dakota, and neither the EERC nor any of its subcontractors nor the North Dakota Industrial Commission nor any person acting on behalf of either:

(A) Makes any warranty or representation, express or implied, with respect to the accuracy, completeness, or usefulness of the information contained in this report or that the use of

any information, apparatus, method, or process disclosed in this report may not infringe privately owned rights; or

(B) Assumes any liabilities with respect to the use of, or for damages resulting from the use of, any information, apparatus, method, or process disclosed in this report.

Reference herein to any specific commercial product, process, or service by trade name, trademark, manufacturer, or otherwise does not necessarily constitute or imply its endorsement, recommendation, or favoring by the North Dakota Industrial Commission. The views and opinions of authors expressed herein do not necessarily state or reflect those of the North Dakota Industrial Commission.

IMPROVED CHARACTERIZATION AND MODELING OF TIGHT OIL FORMATIONS FOR CO_2 ENHANCED OIL RECOVERY POTENTIAL AND STORAGE CAPACITY ESTIMATION

ABSTRACT

Tight oil formations such as those in the Bakken petroleum system are known to hold hundreds of billions of barrels of oil in place; however, the primary recovery factor for these plays is typically less than 10%. Tight oil formations, including the Bakken Formation, therefore, may be attractive candidates for enhanced oil recovery (EOR) using CO_2. Multiphase fluid behavior and flow in fluid-rich shales can vary substantially depending on the size of pore throats, and properties such as fluid viscosity and density are much different in nanoscale pores than in macroscale pores. Thus it is critical to understand the nature and distribution of nano-, micro-, and macroscale pores and fracture networks. To address these issues, the Energy & Environmental Research Center (EERC) has been conducting a research program entitled "Improved Characterization and Modeling of Tight Oil Formations for CO_2 Enhanced Oil Recovery Potential and Storage Capacity Estimation." The objectives of the project are 1) the use of advanced characterization methods to better understand and quantify the petrophysical and geomechanical factors that control CO_2 and oil mobility within tight oil formation samples, 2) the determination of CO_2 permeation and oil extraction rates in tight reservoir rocks and organic-rich shales of the Bakken, and 3) the integration of the laboratory-based CO_2 permeation and oil extraction data and the characterization data into geologic models and dynamic simulations to develop predictions of CO_2 storage resource and EOR in the Bakken tight oil formation.

A combination of standard and advanced petrophysical characterization techniques were applied to characterize samples of Bakken Formation tight reservoir rock and shales from multiple wells. Techniques included advanced computer tomography (CT) imaging, scanning electron microscopy (SEM) techniques, whole-core and micro x-ray CT imaging, field emission (FE) SEM, and focused ion beam (FIB) SEM. Selected samples were also analyzed for geomechanical properties. X-ray CT imaging yielded information on the occurrence of fractures, bedding planes, fossils, and bioturbation in core, as well as data on bulk density and photoelectric factor logs, which were used to interpret porosity, organic content, and mineralogy. FESEM was used for characterization of nano- and microscale features, including nanoscale pore visualization and micropore and pore throat mineralogy. FIBSEM yielded micro- to nanoscale visualization of fracture networks, porosity and pore-size distribution, connected versus isolated porosity, and distribution of organics. Results from the characterization activities provide insight on nanoscale fracture properties, pore throat mineralogy and connectivity, rock matrix characteristics, mineralogy, and organic content. Laboratory experiments demonstrated that CO_2 can permeate the tight matrix of Bakken shale and nonshale reservoir samples and mobilize oil from those samples. Geologic models were created at scales ranging from the core plug to the reservoir, and dynamic simulations were conducted. The data from the characterization and laboratory-based activities were integrated into modeling research activities to determine the fundamental mechanisms controlling fluid transport in the Bakken, which support EOR scheme design and estimation of CO_2 storage potential in tight oil formations. Simulation results suggest a CO_2 storage resource estimate range of 169 million to 1.5 billion tonnes for the Bakken in North Dakota, possibly resulting in 1.8 billion to 16 billion barrels of incremental oil.

TABLE OF CONTENTS

Continued . . .

TABLE OF CONTENTS (continued)

Continued . . .

TABLE OF CONTENTS (continued)

LIST OF FIGURES

Continued . . .

LIST OF FIGURES (continued)

Continued . . .

LIST OF FIGURES (continued)

Continued . . .

LIST OF FIGURES (continued)

LIST OF TABLES

IMPROVED CHARACTERIZATION AND MODELING OF TIGHT OIL FORMATIONS FOR CO_2 ENHANCED OIL RECOVERY POTENTIAL AND STORAGE CAPACITY ESTIMATION

EXECUTIVE SUMMARY

Tight oil formations are known to hold hundreds of billions of barrels of oil in place; however, the primary recovery factor for these plays is typically less than 10%. Therefore, tight oil formations may be attractive candidates for enhanced oil recovery (EOR) using CO_2. To design effective CO_2 injection and EOR schemes, it is necessary to better understand fluid permeation and transport within tight reservoirs. The Energy & Environmental Research Center (EERC) has conducted a research program entitled "Improved Characterization and Modeling of Tight Oil Formations for CO_2 Enhanced Oil Recovery Potential and Storage Capacity Estimation." Advanced characterization methods were applied to better understand and quantify the petrophysical factors that control CO_2 and oil mobility within tight oil formation samples. The ability of CO_2 to permeate the shale and nonshale rocks of the Bakken while mobilizing oil was described through a series of laboratory experiments. The unique data sets generated by the characterization and laboratory activities were integrated into geocellular models that were then used to develop new insight into CO_2 storage and EOR in tight oil formations.

A combination of industry standard scanning electron microscopy (SEM) and petrophysical characterization techniques, as well as advanced techniques that included whole-core and micro x-ray computer tomography (CT) imaging, field emission (FE)–SEM, and focused ion beam (FIB)–SEM, were applied. The characterization work yielded detailed, high-resolution information on the occurrence of fractures and inorganic and organic pore throat networks in both shale and nonshale reservoir rock samples. As expected, porosity in shales was found to be low but more connected than previously thought, with most of the connected porosity being associated with the organic matrix. In the nonshale reservoir rocks, a key finding was that, although microfractures are often filled with clays, the pore throats within the clay filling are predominantly connected, which indicates that those microfractures can still serve as fluid flow pathways.

Laboratory-based permeation and extraction studies were conducted on Bakken shale and nonshale samples. Those tests clearly demonstrated the ability of CO_2 to permeate both Bakken shale and nonshale rocks and extract oil from them. Although the permeation into and oil extraction rates from the shales were substantially slower than the nonshale reservoir rocks, with sufficient exposure time and rock surface area, significant recovery of the oil was obtained from both the Middle Bakken reservoir rocks and the Bakken shales. These results demonstrate that, even in the very tight shales, the oil-containing pores are accessible for CO_2 permeation and oil production given sufficient contact time.

Geocellular models were created at the plug, core, near wellbore, and reservoir scales. Plug scale models were used to history-match the permeation and oil extraction tests. Simulations at the plug scale showed that the two most important variables correlating with oil recovery in the nonshale reservoir rocks are pore throat radius and water saturation, with porosity having a minimal effect. In the shales, total organic carbon (TOC) and pore throat radius were observed to

have the greatest effect, with CO_2 in the higher TOC shale plugs appearing to absorb into the kerogen, suggesting that high TOC may translate into higher CO_2 storage capacity, depending on the type of organic material. This also suggests that organic-rich shales may not only serve as effective vertical seals because of their low porosity and permeability, but may also be highly effective traps for whatever CO_2 is able to permeate into them. Reservoir-scale simulations of EOR schemes indicate the presence of natural fracture networks could result in more favorable CO_2 and oil sweep efficiency. The EOR simulations also showed incremental oil recovery from the injection of CO_2 into a Bakken reservoir as high as 5.4% of original oil in place (OOIP). The North Dakota Department of Mineral Resources estimates the OOIP for the Bakken petroleum system to be 300 billion barrels. The modeling results, therefore, suggest that the use of CO_2 for EOR in the Bakken may yield between 1.8 billion and 16 billion barrels of incremental oil. Simulation results also suggest a CO_2 storage resource estimate ranging from 169 million to 1.5 billion tonnes for the Bakken petroleum system in the United States.

IMPROVED CHARACTERIZATION AND MODELING OF TIGHT OIL FORMATIONS FOR CO_2 ENHANCED OIL RECOVERY POTENTIAL AND STORAGE CAPACITY ESTIMATION

INTRODUCTION AND BACKGROUND

In recent years, the largest booms in oilfield development are in unconventional tight formations (<10 mD), such as the Bakken and the Eagle Ford Formations, where fluid flow is dominated by natural and artificially induced fractures. The tight oil resources in the United States are massive, with several hundreds of billions of barrels of oil in place in the Bakken petroleum system (a system that includes the Bakken and Three Forks Formations, but is hereby referred to as simply "the Bakken") alone (Energy Information Administration, 2013). The Eagle Ford resource appears to be of comparable magnitude, and emerging tight oil plays such as the Niobrara and Tuscaloosa further underscore the growing importance of unconventional oil production to America's energy portfolio. Given their size and broad geographic distribution, tight oil formations may be great opportunities to simultaneously store large amounts of CO_2 while increasing the recoverable reserves of oil by injecting CO_2 for enhanced oil recovery (EOR). Current methodologies for estimating the potential for CO_2-based EOR and CO_2 storage resource in oil reservoirs are based on knowledge gained over the last 40 years from commercial CO_2 EOR operations in moderate- to high-permeability conventional reservoirs (Jarrell and others, 2002; U.S. Department of Energy, 2008, 2010a, 2012; IEA Greenhouse Gas R&D Programme, 2009). However, there is a lack of understanding as to the CO_2 storage and EOR potential in unconventional tight formations which has thus far precluded them as primary targets for EOR or storage. The widespread exploitation of tight oil resources is a relatively recent development (within the last 8 to 10 years); thus the current level of knowledge of mechanisms and factors affecting oil production from, and injection of CO_2 into, tight formations is relatively low when compared to knowledge of conventional reservoirs. To address those knowledge gaps, a multidisciplinary research project called "Improved Characterization and Modeling of Tight Oil Formations for CO_2 Enhanced Oil" was conducted by the Energy & Environmental Research Center (EERC), with funding from the U.S. Department of Energy (DOE), the North Dakota Oil & Gas Research Program, and the North Dakota Lignite Energy Council. The methods, results, and key findings are presented and discussed in this report.

One of the primary goals of the project is to generate data to support the development of improved CO_2 storage capacity estimates for the Bakken Formation. When this project was initiated in 2014, there was no globally accepted method to describe and systematically estimate the CO_2 storage capacity, also commonly referred to as CO_2 storage resource, of a given geologic sink. Over the past decade, separate efforts to develop an overarching classification system for CO_2 storage have been conducted by the United Nations Economic Commission for Europe (UNECE) and the Society of Petroleum Engineers (SPE). The UNECE effort resulted in a section of the United Nations Framework Classification for Fossil Energy and Mineral Reserves and Resources 2009 (UNFC-2009) that addressed the assessment of CO_2 storage, while the SPE work resulted in the CO_2 Storage Resources Management System (SPE-SRMS) published in 2016 (SPE, 2016). To maintain consistency between the two systems, the SPE Carbon Dioxide Capture, Utilization, and Storage Technical Section is working with UNECE to ensure that key definitions

and approaches are globally accepted. According to the SPE-SRMS (2016), "capacity refers to those storable quantities anticipated to be commercially stored by application of development projects to known storable quantities from a given date forward under defined conditions. Capacity must further satisfy four criteria: they must be discovered, storable, commercial, and remaining (as of a given date) on the basis of the development project(s) applied." Based on this definition, estimates of CO_2 storage potential in the Bakken Formation have not yet met the threshold of being classified as "capacity" because, to date, there is sparse data from the field demonstrating that CO_2 can be stored in the Bakken and no data to support the commercial viability of such storage. The SPE-SRMS (2016) states that the term "resources" is "intended to encompass all storable quantities (accessible and inaccessible) within geologic formations – discovered and undiscovered…." Given the relatively early stages of determining the technical and economic viability of CO_2 storage in tight oil formations such as the Bakken, the findings and discussions presented in this report will, therefore, refer to CO_2 storage in the Bakken in terms of "resource" or "potential," rather than "capacity."

The Bakken is characterized by several distinctive lithofacies, each with its own unique properties that may (or may not) significantly affect the mobility and ultimate fate of CO_2 within the formation. The lithofacies of the Bakken can be broadly divided into two groups: the shale group, which includes the Upper and Lower Bakken Shale Members, and the nonshale group, which includes the many lithofacies of the Middle Bakken Member. The fine-grained clastics and carbonates of the Middle Bakken Member are representative of a tight, fractured reservoir rock that is capable of transmitting fluids once it has been hydraulically fractured. In North Dakota and Montana, the Middle Member typically comprises between three and seven distinctly different lithofacies that range from silty carbonates to calcite/dolomite cemented siltstones. In most areas of the Bakken Formation, the Middle Member of the formation is bounded above by the Upper Bakken Shale and below by the Lower Bakken Shale. Both shale members are organic-rich, typically oil-wet shales that are the source rocks for the productive areas of the Bakken (Figure 1). Some of the key challenges associated with characterization of the Bakken include low porosity (typically <10%), low permeability (typically <1 mD), very fine grain minerals (4 to 60 μm) and clay-size particles (<4 μm) that are hard to resolve both chemically and physically, and a high degree of rock heterogeneity. Figure 2 shows a series of photographs of slabbed core samples from the two shale members and key lithofacies of the Middle Member (designated L1–L5), illustrating the range of heterogeneity that can be present in Bakken Formation rocks in a single well. These factors directly influence the potential of tight oil formations to transport and store CO_2. They also affect the ability of the injected CO_2 to mobilize oil from the matrix into the fracture network and, ultimately, increase oil production. Inadequate identification of these features poses serious challenges to the development of effective injection and production strategies for CO_2 EOR and storage in tight, fractured reservoirs.

The viability of injecting CO_2 into the Bakken for simultaneous CO_2 storage and EOR has been the focus of previous research activities of the EERC. The results of that work suggest that 1) CO_2 does have the ability to mobilize oil from Bakken shale and Middle Bakken reservoir rocks; 2) diffusion of CO_2 appears to be an important mechanism for moving oil from the reservoir matrix into the fracture network; and 3) the oil production response of a Bakken reservoir to CO_2 injection may be delayed, but the increase in oil production rates could be as high as 50% (Kurtoglu and

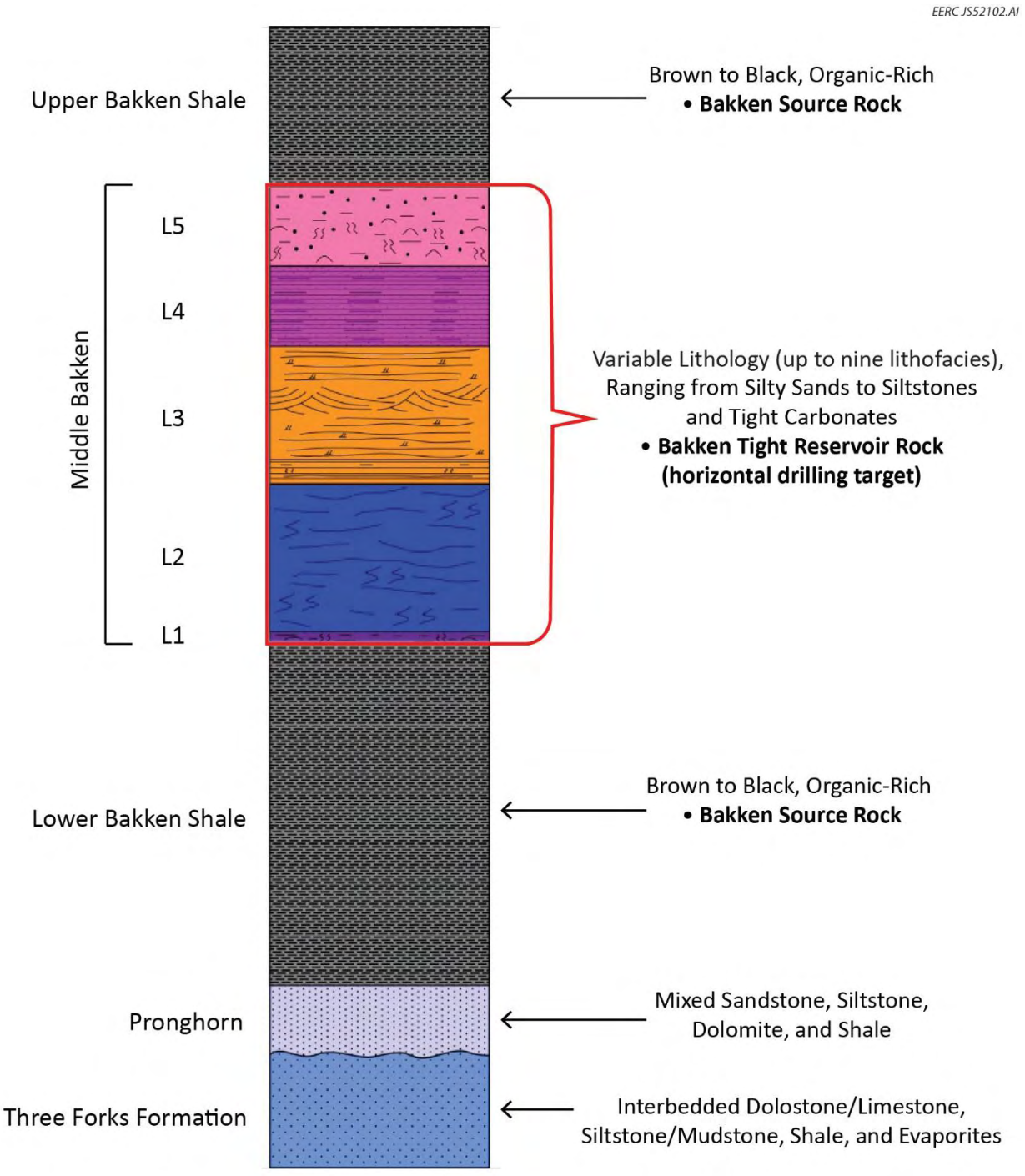

Figure 1. Major oil-producing lithofacies of the Bakken petroleum system. The system also includes the Lodgepole Formation (including the Scallion and False Bakken members) which overlies the Bakken Formation.

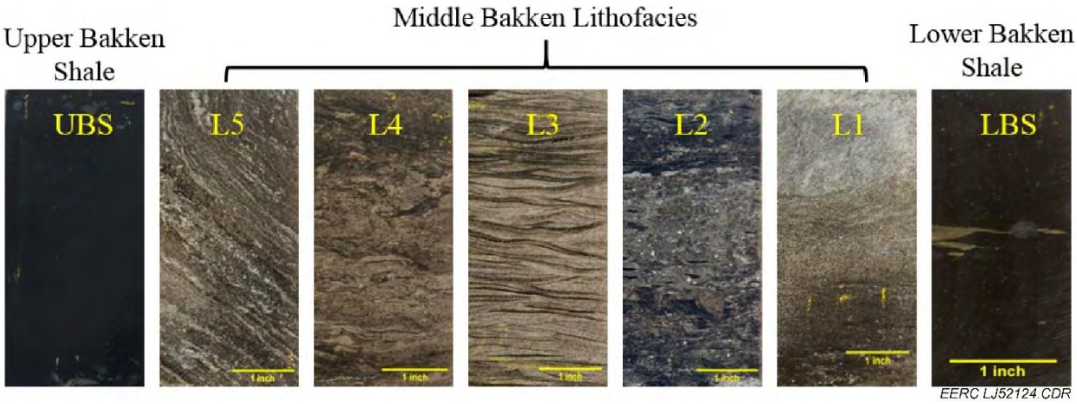

Figure 2. Photos of slabbed core from the Upper and Lower Bakken Shales and five distinct Middle Bakken lithofacies from a single well in McKenzie County, North Dakota (Jin and others, 2016).

others, 2013; Hawthorne and others, 2013; Sorensen and others, 2014). However, pilot-scale field injection tests using CO_2 have not yielded the results predicted by modeling (Sorensen and Hamling, 2016). The disparity between the laboratory and modeling results and the field tests reflects the large degree of uncertainty when it comes to understanding the mechanisms controlling fluid movement and phase behavior in the Bakken. This is due, in part, to significant data gaps in the identification and characterization of micro- and nanoscale fracture networks and porosity and in understanding the factors controlling CO_2 permeation and transport within the formation (Sorensen and others, 2015). With respect to CO_2 storage, the results of the EERC's previous efforts suggest that the storage potential of the Bakken ranges from over 160 Mt to as high as 3.2 Gt, with the large degree of uncertainty due, again, to the data gaps in the understanding of fluid-phase behavior in tight, organic-rich, fractured formations (Sorensen and others, 2014). A modeling-based study by the Colorado School of Mines revealed that multiphase fluid behavior and flow in fluid-rich shales vary substantially depending on the size of pore throats and that properties such as fluid viscosity and density are much different in nanoscale pores (mode of 2–3 nm) than in macroscale pores (mode of 11 µm) (Alharthy and others, 2013). Thus to better understand and model fluid permeation and transport within unconventional reservoirs, it is critical to understand the nature and distribution of nano-, micro-, and macroscale pores and fracture networks within the formation.

One of the key challenges in identifying and characterizing micro- and, especially, nanoscale fractures and pores in shales and other tight formations is a lack of analytical methods to detect and quantify these features and to scale them up from the microscale for application in geologic and simulation models. Past and ongoing work conducted at the EERC to better characterize small-scale fracture networks (Kurtoglu and others, 2013) supports recent literature (Josh and others, 2012; Erdman and Drenzek, 2013) highlighting the issues with using conventional analytical techniques, such as optical microscopy and scanning electron microscopy (SEM), to adequately characterize the micro- and, especially, nanoscale fracture networks, pore distributions, and other features of tight rocks. With this in mind, the use of advanced characterization techniques that are capable of resolving features at the nanoscale level are necessary to understand those flow pathways in both shale and nonshale rocks.

With respect to CO_2 mobility and oil mobilization in tight rocks, previous experimentation conducted at the EERC suggests that after pressurization of the fractures, CO_2 will begin to permeate into the unfractured rock matrix by (initially) pressure gradient and then by molecular diffusion. Although the low permeability of the Bakken reservoir rock may intuitively suggest that CO_2 permeation (and thus CO_2 EOR and storage) will be inhibited, laboratory experiments have shown that exposing apparently unfractured Middle Bakken samples to CO_2 can recover >95% of the oil from that rock (Hawthorne and others, 2013). Thus if the oil in the pores of the seemingly unfractured rock can be recovered by CO_2, CO_2 must be capable of permeating completely into the rock matrix. Furthermore, these experiments also suggested that CO_2 can extract more than 50% of the oil from the Upper Bakken shale, indicating substantial permeation into that even tighter rock, although this process was orders of magnitude slower than in the Bakken nonshale reservoir rock (Hawthorne and others, 2013). The big unknown with the previous experiments conducted at the EERC was the degree to which nano- and/or microscale pores and fractures affected CO_2 and oil mobility. It is clear that the use of advanced analytical techniques may be able to adequately identify and characterize the nano- and microscale pore spaces and fracture networks within the various Bakken lithofacies. The results of previous efforts highlighted that truly understanding the EOR and CO_2 storage potential in tight rocks will require integrated, advanced laboratory studies. With that in mind, a scope of work was designed and executed to 1) determine the permeation rate of CO_2 into, and oil out of, Bakken core samples and 2) couple the permeation rate data with extensive advanced characterization of the rock, including quantifying the presence or absence of micro- and nanoscale fracture networks and geochemical, geomechanical, and petrophysical properties.

The effects that kerogen and bitumen may have on CO_2 storage and EOR in the shales are also not well understood. Because the kerogen–bitumen content of some Bakken shales are in the range of 10 to 15 wt% (up to 50 vol%), it is important to understand their potential interactions with CO_2 and how that may affect CO_2 storage and EOR. In particular, kerogen and bitumen may act as a chemical sorbent phase that could significantly increase the CO_2 storage potential of the shales over what would be expected based only on a volume/pressure basis.

The aforementioned data gaps obviously impact the accuracy of geologic models and the ability of simulation models to predict CO_2 storage and EOR potential in both the shale and nonshale lithofacies of tight oil formations. Improvements needed in geologic models include better petrophysical analysis of well log data in tight, naturally fractured reservoirs and greater understanding of the distribution of macro-, micro-, and nanoscale fracture networks. Conventional analytical challenges in well log interpretation arise because of the heterogeneity of these reservoirs, causing a lack in accuracy and the need for improving well log correlations based on changes in lithology. Challenges arise in accurately determining these parameters unless laboratory data are available to calibrate the results. While general assumptions can be made, a better understanding of in situ reservoir matrix properties is needed. Ineffective assumptions can lead to the miscalculation of fracture permeabilities and inaccurate predictions of CO_2 transport, CO_2 storage potential, and incremental oil recovery. With that in mind, the integration of advanced characterization data and CO_2 permeation/hydrocarbon extraction rate data can lead to more accurate static and dynamic modeling efforts to better understand tight oil formations and how to properly assess their CO_2 EOR and storage potential. The application of advanced techniques to characterize pore throat networks and an improved understanding of the mechanisms and

magnitude of CO_2 transport and oil mobility in tight oil formations is critical to the development of geologic and simulation models that help meet the overall goals of the DOE National Energy Technology Laboratory's (NETL's) Carbon Storage Program.

GOALS AND OBJECTIVES

The goal of the overall project is to better assess and validate CO_2 transport and fluid flow in fractured tight oil reservoirs of the Bakken. The project is also designed to generate data to further illuminate the roles that the shale members may play with respect to CO_2 storage, containment, EOR or, possibly, even all three. The project has been organized into two distinct phases, each with its own set of activities, with the knowledge gained in Phase I being directly applied to the Phase II activities.

Phase I of the project entailed a variety of activities to improve understanding of natural and artificially induced fracture and pore networks within the Bakken Formation. The primary goal of the Phase I activities was the identification and characterization of macro-, micro-, and nanoscale fracture networks and pore spaces within the Bakken samples. Key activities conducted under Phase I included the following:

- Generation of baseline data on petrophysical, geochemical, and geomechanical properties of the collected Bakken rock samples using standard techniques.

- Application of advanced microscopy and other technologies to better detect and characterize the macro-, micro-, and nanoscale fracture networks and pore characteristics using samples collected from the Bakken shales and nonshale reservoir rocks.

- Identification of correlations between fracture network characteristics and the petrophysical properties of Bakken rock samples that can be identified using well log data to predict the presence and characteristics of fracture networks.

- Examination of the roles that kerogen and bitumen may play in determining the roles that shales may play with respect to CO_2 storage, containment, and EOR.

Phase II of the project included laboratory-based experimental activities and modeling exercises to examine interactions between CO_2 and the shale and nonshale rocks of the Bakken Formation. The primary goals of Phase II activities were to determine CO_2 permeation rates and hydrocarbon extraction rates and develop insight regarding the mechanisms controlling CO_2 storage and EOR in tight organic rich shales and tight nonshale rocks. Key activities under Phase II included:

- Determination of CO_2 permeation rates and oil extraction rates within the matrix of Bakken nonshale reservoir samples and within samples of Bakken shale using static exposure testing and flow-through testing.

- Correlation of well log data to Phase I core characterization data using multimineral petrophysical analysis (MMPA).

- Construction of static geocellular models at the core plug, whole core, near-wellbore, and reservoir scales.

- Design and execution of dynamic simulation modeling exercises at different scales.

- Development of a best practices manual (BPM) on the characterization and modeling of tight oil formations for CO_2 EOR and storage. The BPM is included as a section of this report.

This report presents the approach and highlights of the activities and key results of the Phase I and Phase II activities that are thought to likely have the most impact on advancing the science of CO_2 storage and EOR in tight oil formations. A more exhaustive compilation of the raw data is provided in the form of data sheets in Appendix A. Manuscripts for papers that have been presented at technical conferences or submitted for publication in peer review journals are provided in Appendix B. Additional data and results in PowerPoint presentations that were provided to DOE over the course of the project are included in Appendix C.

LABORATORY HYDRAULIC FRACTURING INVESTIGATIONS

Hydraulically stimulated fractures serve as the primary fluid flow pathways in a Bakken reservoir. However, the geometry and distribution of those induced fracture networks are poorly understood. Because of that lack of understanding, fracture networks in models are typically represented by patterns of straight lines that are either regularly spaced or randomly spaced with little basis in real-world data. To determine the effects of rock and fluid properties on the size distributions of fractures produced during hydraulic fracturing of rock, laboratory procedures were developed to hydraulically fracture rock core plugs and carry out testing to develop data-driven insight on the geometry and distribution of induced fracture networks.

In order to obtain samples of hydraulically fractured reservoir rock in which detailed analysis of fracture networks could be performed, a laboratory system for fracturing rock core plugs was built and tested. To hydraulically fracture rock, fluid must be pumped into a borehole at a rate higher than the formation can accept it, causing the pressure in the hole to rise until it reaches the breakdown pressure of the rock. At this point, the rock fractures perpendicularly to the direction of the least principle stress. In a tectonically stable basin, such as the Williston Basin, the least horizontal stress is usually less than the overburden stress, so the fractures typically occur in a vertical plane relatively perpendicular to the bedding planes of the rock (Hubbert and Willis, 1957). In order to be able to identify which fractures were caused by hydraulic stress and which fractures were already present in the plugs, a one-part epoxy with a viscosity of 8000 centipoise was used as the fracture fluid. To ensure that the fractures made in the laboratory system would be similar to those that occur in the field, scaling laws were used to determine the flow rates of the fracturing fluid. Correct scaling ensures that the physics of the fracturing processes in the field are accurately reproduced in the laboratory, assuming simple planar fracture propagation. In order to scale the

laboratory experiments, DePater and coworkers (1994) have performed a dimensional analysis of hydraulic fracturing processes to select an appropriate set of variables that were used to algebraically derive a set of dimensionless groups with values that should be similar between the hydraulic fracturing conditions in the field and in the laboratory. In order to easily manipulate the relatively complex scaling factors, a spreadsheet was developed that is similar to the one used by Casas (2005). Values for shale rock properties and field fracturing parameters found in the literature and through discussions with a hydraulic fracturing engineer operating in the Bakken oil field were entered into the spreadsheet which was used to calculate the values of the relevant dimensionless groups, and then values for the laboratory fracturing conditions were chosen to provide similar values for those dimensionless groups.

Core Plugs

Four plugs 1.185 in. in diameter were removed from a Middle Bakken core collected from North Dakota Industrial Commission (NDIC) Well #8709, with the bedding planes parallel to the axis of the plug so that fractures occurring perpendicular to the axis would also be perpendicular to the bedding planes. Plug samples used in EERC studies are assigned sample tracking and reporting (STAR) numbers so results of one experiment on a rock sample can be correlated to other data associated with that sample. STAR #116219 was taken from the Middle Bakken Lithofacies 5, STAR #116220 was taken from Middle Bakken Lithofacies 4, and STAR #116221 and STAR #116222 were taken from the Middle Bakken Lithofacies 3, which is targeted for drilling and hydraulic fracturing operations. The STAR numbers are used for internal tracking by the EERC. The ends of the samples were faced flush for a total sample length of 2.5 in. A ¼-in. borehole was cored out of the center of each sample 1.90 in. deep. A ¼-in. drill bit was used to smooth and finish the bottom of the hole. A groove was machined in the hole at the middle of the plug to provide a stress concentration zone similarly to how perforation charges are used to concentrate stresses for downhole hydraulic fracturing activities. The grooves are machined approximately 0.06-in. deep. Figure 3 provides details for the machined sample geometry.

A stainless steel injection port with 0.25-in. outside diameter and 1/8-in. injection tube was glued into the ¼-in. hole using two-part epoxy. Teflon disks 1/16 in. thick with a width equal to the plug diameter were used to provide additional sealing against the injection shaft, the core face, and the platen. These disks also allowed some compliance to help reduce end effects. Copper foil and two matched pairs of resistive strain gauges were applied to the sample to monitor local deformation. These leads were run along the epoxy injection line and outside of the cell to protect them from damage.

Micro-computed tomography (CT) analyses were used to provide information on core integrity before and after testing. The views of the CT scans were concentrated at the center 1 in. of sample length to provide the best resolution possible for the area of interest near the machined notch. A voxel size of approximately 36 µm was achieved. The CT signal from a point in the sample depends on the energy of the x-ray source and the linear absorption coefficient of the material at that point. Most epoxies have a low linear absorption coefficient (µ). Therefore, in order to better differentiate injected epoxy from other low-µ phases, iodoform was mixed with the epoxy at a concentration of 5%. This mixture was calculated to have a µ between air and quartz.

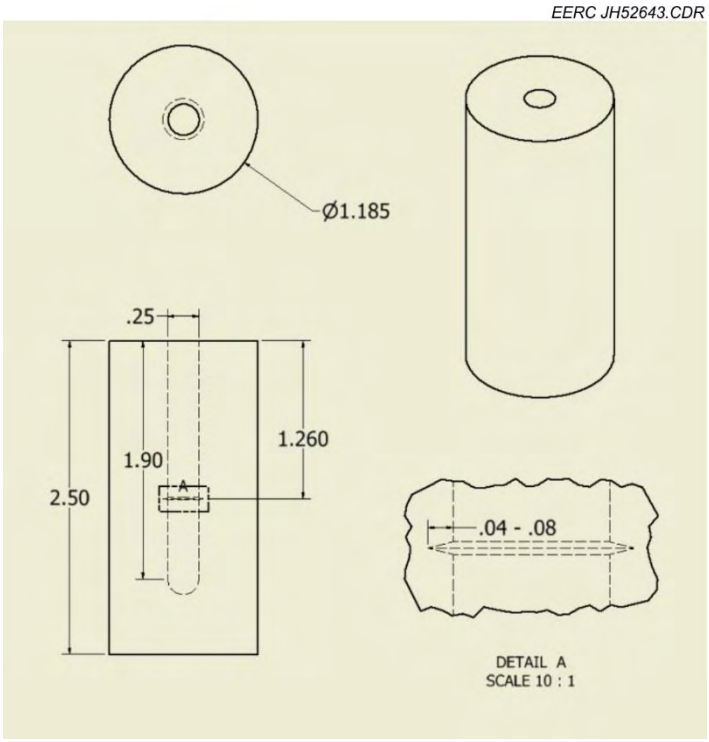

Figure 3. Geometry for machining of hydraulic fracturing sample.

Preparation of the Sample Assembly

The sample assembly, which is shown in Figure 4, consists of the following from top to bottom:

- Top epoxy injector head with injector O-ring seal
- 0.5-in.-thick Teflon thermal spacer with stainless antiextrusion ring
- Top platen with injector feed-through
- Top thin Teflon disk
- Sample with injector port
- Bottom thin Teflon disk
- Bottom platen
- 0.5-in. bottom thermal spacer with stainless antiextrusion ring

The sample assembly was wrapped with two layers of clear heat shrink tubing. This allowed the assembly to be more easily handled without damage, protected the strain gauge leads, maintained the alignment of components, made it easier to insert and remove the sample from the core holder, and added an extra sealing layer. The sample assembly was inserted into a RocTest 10,000-psi Hoek cell with a specially made gasket to allow testing at elevated pressures and temperatures. The Hoek cell was then installed in the load frame and connected to the confining and injection ports, as shown in Figure 5. Figure 6 shows a schematic of the laboratory hydraulic fracturing equipment.

(a) (b) (c)

Figure 4. a) Sample injection port after removal from sample, b) sample assembly components before testing with top injection head, and c) Hoek cell with sample assembly inserted and top injection head.

Testing – Mechanical Loading Description

The following loading descriptions represent the process used to apply stresses to the sample during testing. The numbered steps are represented visually as stress vs. time and labeled in Figure 7:

1. Once the Hoek cell is loaded and the top injection head is attached, it is centered with the top platen and loaded to a seating axial load of 500 lbf.

2. After the axial load stabilizes, a radial confining pressure of 500 psi is applied to seal the sample and cell.

3. A vacuum is pulled on the system below 30 torr to remove the bulk of the air from the sample and system, but to avoid affecting the epoxy, the duration of vacuum application is very brief.

4. The vacuum valve is closed, and epoxy is injected into the system at 200 psi until a stable pressure is reached.

Figure 5. Hoek cell and sample assembly inserted into compression load frame and connected to the system.

A purpose-built load control program is used to bring the system pressures up to desired levels and log system conditions.

Load is increased under computer control according to the following conditions:

- Radial stress is set to mirror axial stress (radial stress = axial stress).
- Axial stress is set to lead injection pressure by 500 psi (axial stress = injection pressure + 500 psi).
- An initial injection flow rate of 0.2 mL/min is used to bring the system pressures up to starting conditions.

At this point, an additional load condition is set that requires that radial stress must exceed injection stress by at least 500 psi so the system will automatically compensate if the 5000-psi radial stress threshold is exceeded by the injection pressure but will not decrease when the sample fractures and injection pressure falls.

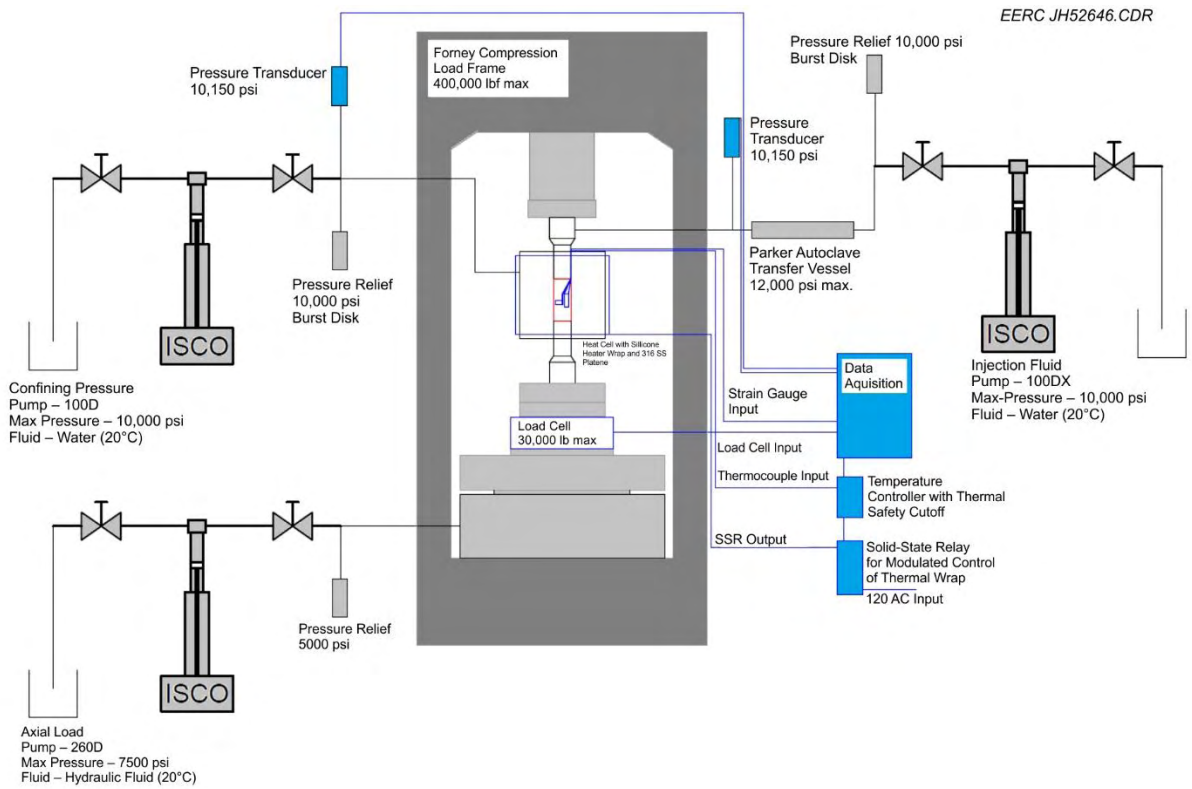

Figure 6. Schematic of the hydraulic fracturing system.

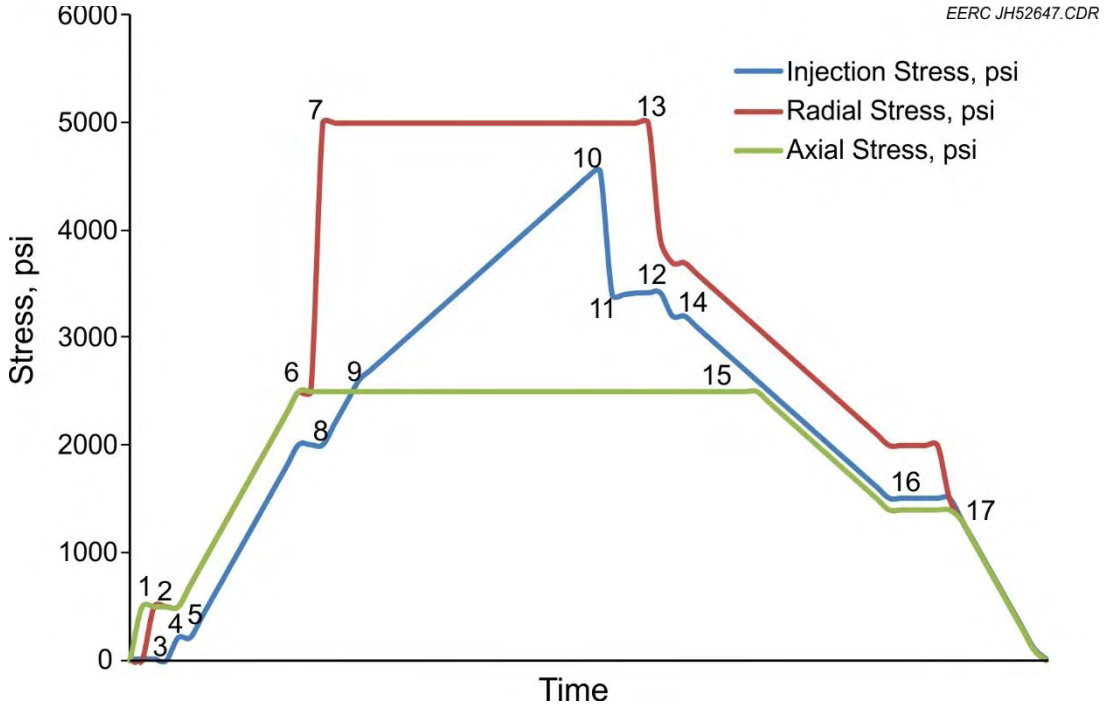

Figure 7. Hydraulic fracturing test sample stress-loading diagram.

5. Injection flow is started at a rate of 0.2 mL/min until 2500-psi radial and axial stresses are reached, with an injection stress of 2000 psi.

6. Once 2500-psi axial and radial stresses are reached, the injection flow is stopped and the system is set to maintain constant axial stress of 2500 psi.

7. The radial stress = axial stress condition is turned off, and radial stress is increased to 5000 psi.

8. Injection rate is then increased at 0.2 mL/min until injection pressure matches axial stress.

9. Injection rate is reduced to the test rate of 0.018 mL/min as determined by scaling equations to match field-scale flows and viscosities to lab-scale testing.

   Injection continues until either a fracture is observed or the maximum system pressures are reached. Because of the extremely low compressibility of the epoxy, fracture initiation is observed as a loss of injection pressure. This should also correlate with other indicators such as increased axial sample strain.

10. Once fracture initiation is observed, the injection pump volume is recorded.

11. Injection is continued until either an additional 4.48 mL of fluid is injected or axial pressure rate of change begins to match injection pressure rate. This is an indicator that the fracture cross section is a large proportion of the sample cross section.

12. Injection is stopped after 4.48 mL of fluid is injected or fracture cross section is estimated at greater than 75% sample cross section.

13. Radial stress is set to trail injection stress (radial stress = injection stress + 500 psi).

14. Injection pressures are reduced slowly at approximately 0.1 mL/min flow rate.

15. Axial stress is set to lead injection pressure if the axial stress = injection stress – 100 psi. This allows the fracture to remain propped open while the sample is unloaded to acceptable pressures for heating.

16. Once an injection pressure of approximately 1000 psi is reached, the system is allowed to maintain constant stresses of:

    - 2000-psi radial pressure.
    - 1500-psi injection pressure.
    - 1400-psi axial pressure.

Testing – Heating the Sample

Stress control on the sample is maintained throughout the heating and cooling processes to lock the sample in its current state with the fracture propped open. The sample is heated to 110°C overnight to allow proper curing of the epoxy.

Once the internal temperature of 110°C is reached for an acceptable curing duration, the heat is removed to allow the sample to cool at pressure.

17. Pressures are uniformly decreased until a zero load condition is achieved.

The sample is then removed from the cell and wrapped with a layer of thick Teflon heat shrink to help maintain sample integrity, as shown in Figure 8.

The injector is removed from the sample by applying heat to the shaft with a heat gun or similar heating source to weaken the two-part epoxy. The sample is then submitted for posttest micro-CT analysis.

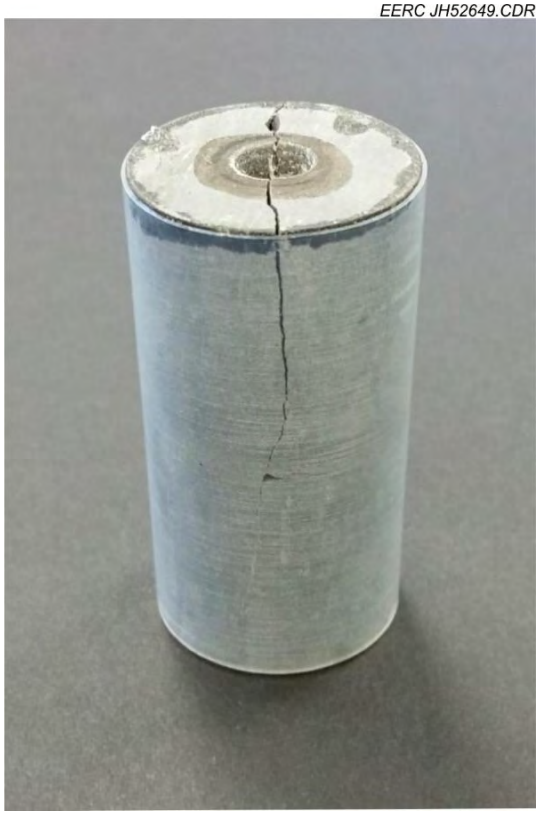

Figure 8. Sample 116219 posttest with injector removed.

Micro-CT Analyses of Fractured Samples

Micro-CT data were collected using a GE v|tome|x system. Scans were acquired using an energy of 180 kV. Voxels are isotropic, and voxel resolution is around 36 μm. Pre- and postfracturing micro-CT scans were performed on the middle third of each sample, resulting in eight sets of data. Each data set was composed of 1000 slices where each slice is a 16-bit tiff-formatted image. The top and bottom 50 slices of each end were removed because of artifacts resulting from the cone beam geometry.

DISCUSSION OF HYDRAULIC FRACTURING LABORATORY TEST RESULTS

In general, samples were loaded according to the hydraulic fracturing load diagram, although certain adjustments were made, as required, to correct for any unexpected condition during testing, such as a gasket leak, or negative effects on the sample assembly observed through bulk displacement monitoring. Data for the Middle Bakken 5 plug, 116219, are discussed here in detail. Similar data were collected for the other samples but will not be discussed in detail because, ultimately, none of them were successfully hydraulically fractured because of operator error or equipment failure.

Sample 116219 contained one significant vertical fracture prior to testing. This fracture was larger in the posttest and in line with a vertical fracture on the opposite side of the bored hole. This sample is the only one to exhibit a fracture originating from the notch machined inside the hole. The resulting fracture network was relatively simple, consisting of a vertical fracture along the core and a horizontal fracture from the notch. This sample was not fractured during stress application because no pressure drop occurred during epoxy pressurization. Instead, the existing vertical fracture was expanded because of the loss of confining pressure during the end of the heating cycle once a large portion of the epoxy was already hardened.

Figure 9 shows the stress application data for the attempted hydraulic fracturing of Sample 116219. As can be seen in the data, injection and radial pressures reached the maximum pressure conditions for the system with no sign of fracture (9100-psi radial and 8900-psi confining). The sample was then set up at reduced stresses for heating at around 12:01 a.m. on May 17, 2016. At approximately 4:30 a.m., the Hoek cell gasket failed, resulting in a loss of confining pressure. The release of hot water also triggered the overtemperature limit on the temperature controller.

Analysis of Hydraulic Fracturing Testing on Sample 116219

An analysis of micro-CT data for Sample 116219 was performed to compare the pre- and posttest gray-scale measurements to identify the gray value of the epoxy when compared to air and rock materials. This relationship is shown in Figure 10.

A detailed 3-D rendering was performed by filtering out higher-intensity data to isolate the air and epoxy values. Figure 11 shows this rendering of the fracture planes induced by a loss of

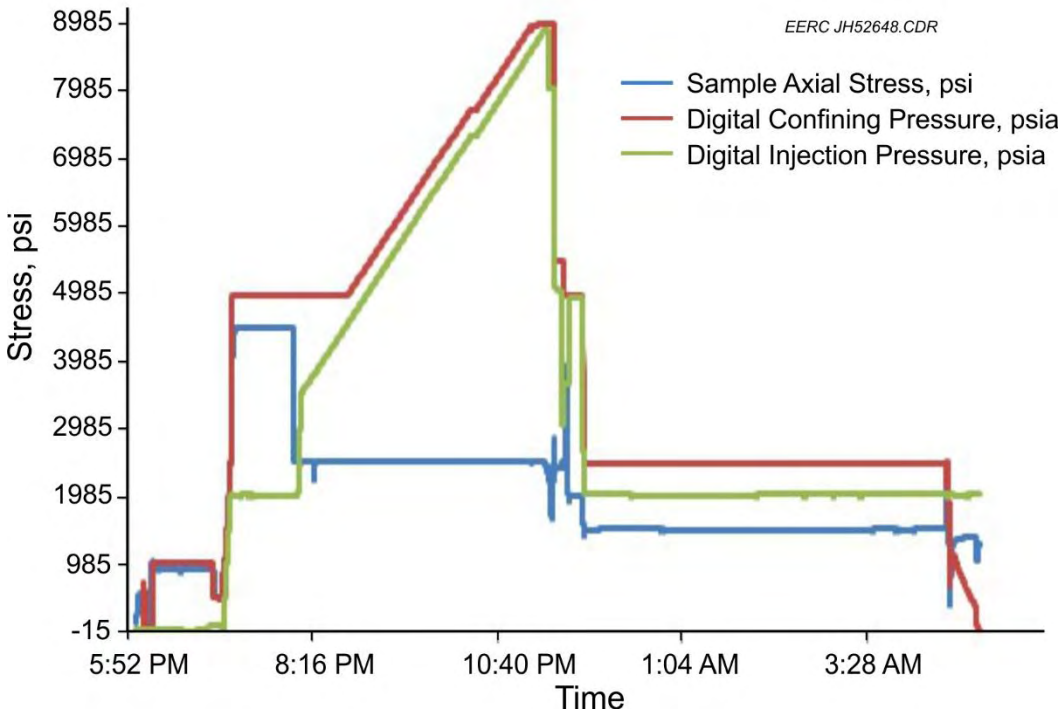

Figure 9. Stress loadings vs. time for Sample 116219.

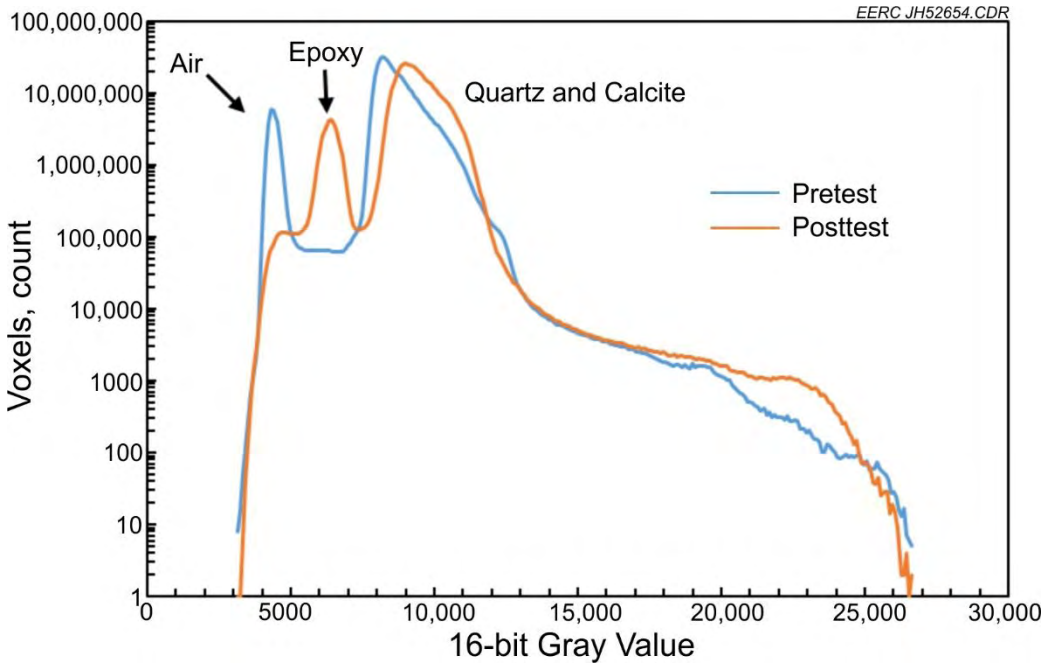

Figure 10. Histograms for pre- and posttest image stacks for Sample 116219.

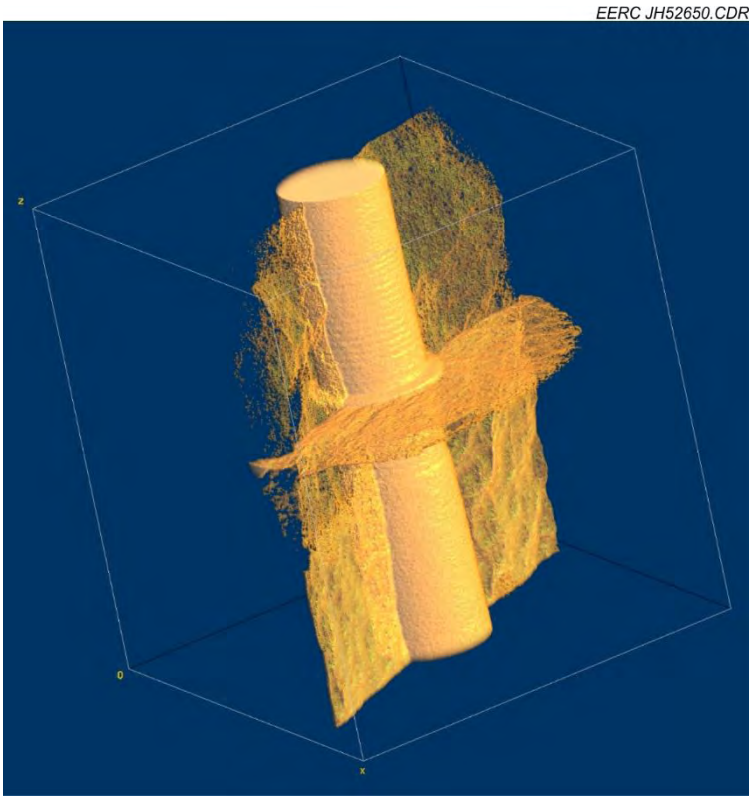

Figure 11. Volume rendering of the posttest fracture network generated in Sample 116219 from the loss of confining pressure with an injection pressure of 2000 psi.

confining pressure while injection pressure was maintained. The vertical fractures appeared to initiate along existing fracture planes parallel to the bedding planes of the plug which propagated through the sample. These fractures were created as the maximum hoop stress exceeded the tensile strength of the sample.

Figures 12 and 13 show projections of the plug pre- and posttest with an attached color scale. These images show the density variation throughout the sample and are a good means of comparing the pre- and posttest sample integrity. A long vertical fracture parallel to the bedding planes is evident in the sample before testing, and the posttest analysis shows that the fracture was propagated along this existing fracture plane.

A horizontal fracture propagated out of the machined groove similar to the effect we were trying to create through hydraulic fracturing. However, this fracture was created after the epoxy in the sample had already hardened. Figure 14 shows a cross section of the machined notch pre- and posttesting. The posttest image shows a distinct contrast between the epoxy and air. Air is darker in color. There is a slight separation of the epoxy from the wall of the sample which may be due to shrinkage during final curing. The lack of epoxy within the fracture indicates that it was not fractured during epoxy pressurization. Upon removal of the sample, it was noted that the epoxy closest to the injection port was not fully hardened. This epoxy may have exerted some fluid

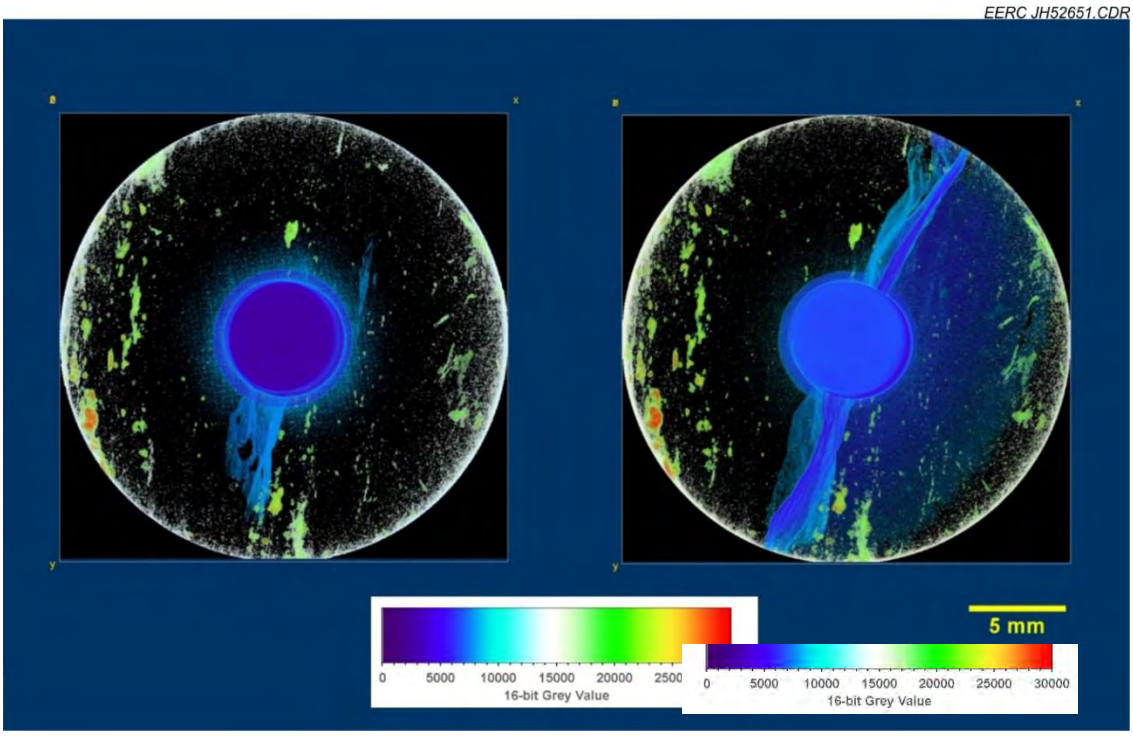

Figure 12. XY projection of Sample 116219 pre- and posttest.

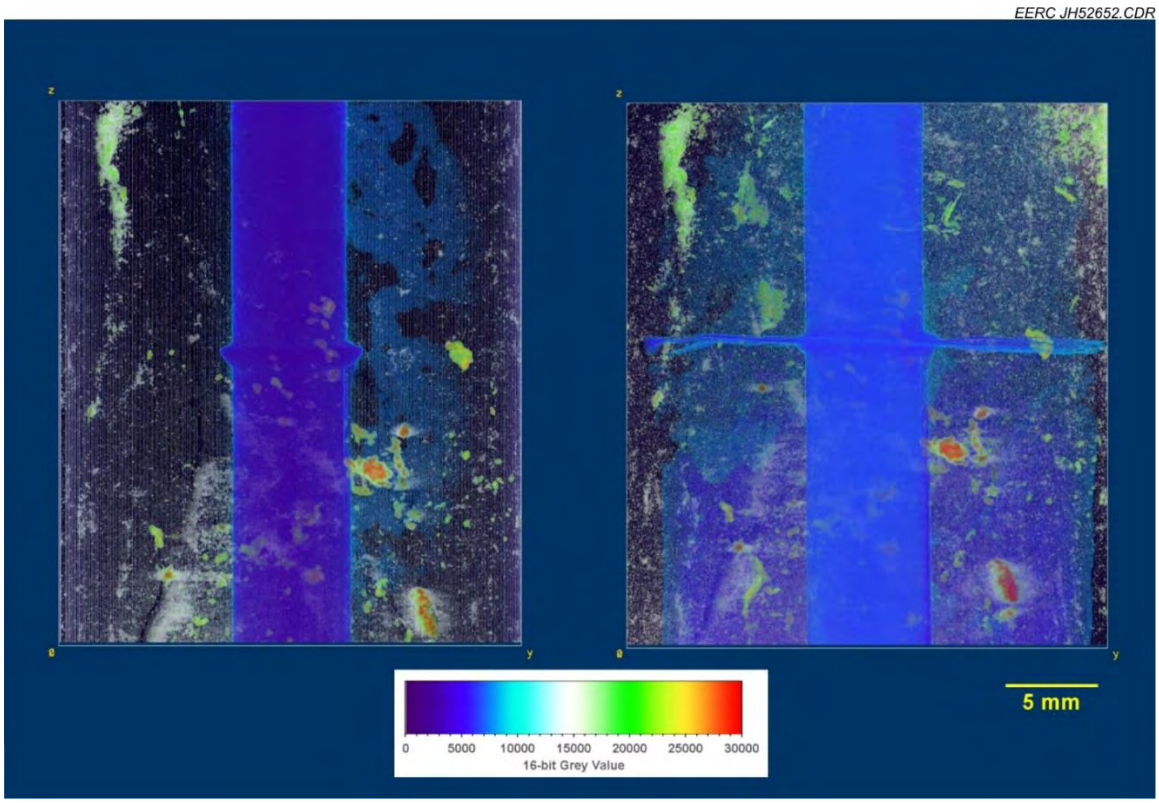

Figure 13. YZ projection of Sample 116219 pre- and posttest.

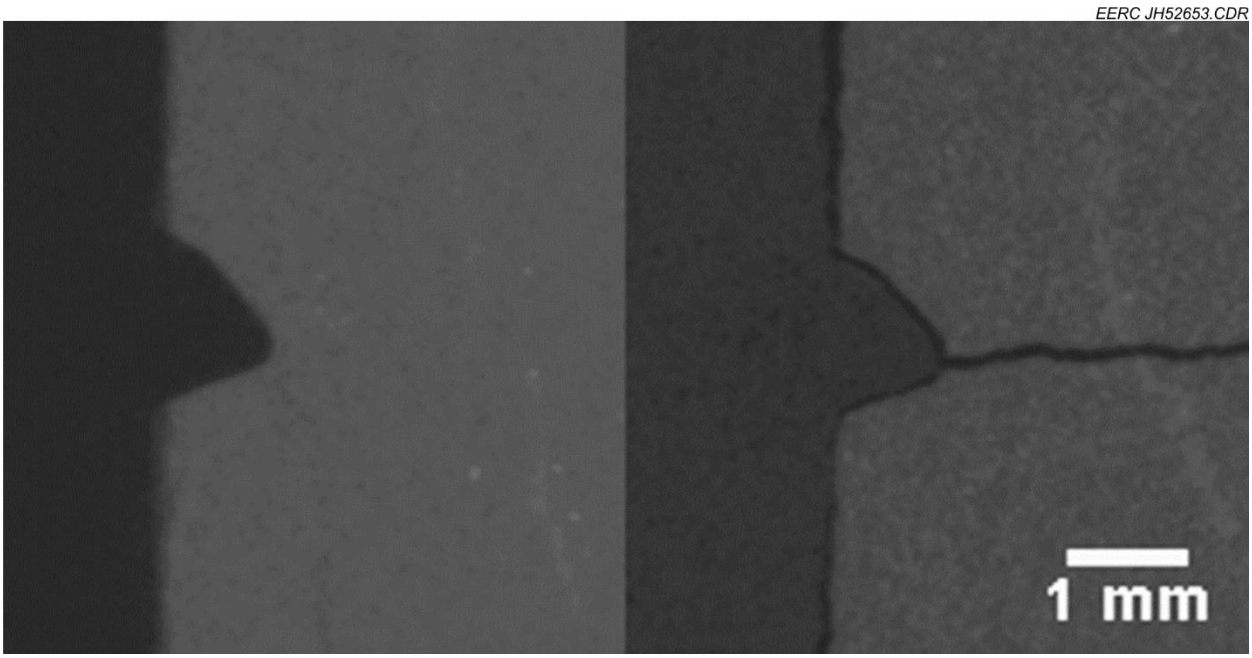

Figure 14. Close-up view of the notch pre- and posttest on Sample 116219.

pressure on the top portion of the sample, inducing a bending moment with the loss of confining pressure that induced the horizontal fracture at the notched stress concentration. To finish curing the epoxy, the plug was placed in an oven at 110°C for 3 hours after depressurization. It is evident in Figure 14 that epoxy shrank away from the plug surfaces during curing.

Sample 116220 showed no sign of fractures pre- or posttest. The sample is very homogeneous, and some air was seen inside of the core epoxy, possibly due to epoxy shrinkage. During testing, it appeared that the sample had been fractured during injection stress loading at approximately 4400 psi as indicated by a drop in epoxy pressure, and the test was treated as such. However, during setup for heating, it was found that epoxy was visible along the top platen from the outside of the cell, indicating a leak between the injection port and the sample had occurred because of improper sealing by the additional Teflon insert.

Sample 116221 was a control test used to determine if any fracturing occurred as a result of drilling of the borehole. An injection pressure of only 100 psi greater than the axial stress was used. The sample was highly banded, with some preexisting fractures parallel to the band layers. Posttest analysis showed that no fracturing had occurred as a result of sample preparation.

Sample 116223 contained preexisting fractures along a bedding plane. Also, high-density burrowing was also seen that crossed bedding planes. This sample showed the largest amount of pretest fracturing in a complicated network. Similar to Plug 116219, no pressure drop occurred during epoxy pressurization, indicating that it was not hydraulically fractured even at the maximum possible epoxy pressure. However, the sample failed the posttest because of an error setting up the axial pressure for maintenance overnight. The pump applied a steadily increasing

load until the sample failed axially and the pump capacity was exhausted. These fractures were mechanically induced, not hydraulically induced. The sample was crushed.

CONCLUSIONS OF HYDRAULIC FRACTURING LABORATORY TESTS

Hydraulic fracturing tests were completed with varying degrees of success. The process for loading and testing was extremely complex but was aided by the use of computer-controlled systems. There are multiple improvements that could be made to the system to achieve the desired results, including increasing the depth of the notch or increasing the upper pressure limits on the system.

The Middle Bakken 5 plug produced fractures that were induced hydraulically during curing but not through controlled means with pressurized epoxy. No hydraulically induced fractures occurred in any of the samples even at the maximum epoxy pressure possible in the existing system. Therefore, although this type of hydraulic fracturing application in the laboratory shows promise, it will require more development to fully replicate conditions in real-world hydraulic fracturing operations and yield results that are representative of fracturing behavior in Bakken reservoirs.

EVALUATION OF FLOW PATHWAYS IN SHALE AND NONSHALE BAKKEN ROCKS

Samples from key lithofacies of the Bakken shales and Middle Member of the Bakken were collected from four wells in productive areas of North Dakota (Figure 15). Study wells from which core samples were obtained for this project are referred to as D, G, MW, and MT. Of these four wells, core samples from the D, G, and MW were characterized in detail for fractures and pore networks at the macro-, micro-, and nanoscales using advanced characterization techniques. Core samples from the MW well were analyzed for geomechanical properties. Baseline petrophysical characteristics of samples representing all of the key Bakken rock types from all four wells were determined using conventional rock analytical techniques. The specific baseline petrophysical tests that were conducted are listed in Table 1, and the results of those baseline analytical activities were compiled into an extensive collection of data sheets that were provided to DOE in 2015. An example of a set of data sheets for a single sample is provided in Appendix A.

Conventional SEM techniques were applied to the samples that were used in the baseline analytical activities in an effort to identify and characterize induced and natural macro- and microscale fractures in each of the key lithofacies. The approach used in these fracture characterization activities was the same as that used in previous EERC Bakken studies and described in Sorensen and others (2015). The results from these conventional SEM fracture studies are included in the data sheets and were also compiled into a deliverable document in the form of a PowerPoint presentation that served to compare and contrast the various fracture characterization techniques that were used during Phase I. That PowerPoint presentation served as the basis for the go/no-go decision point for DOE approval of Phase II.

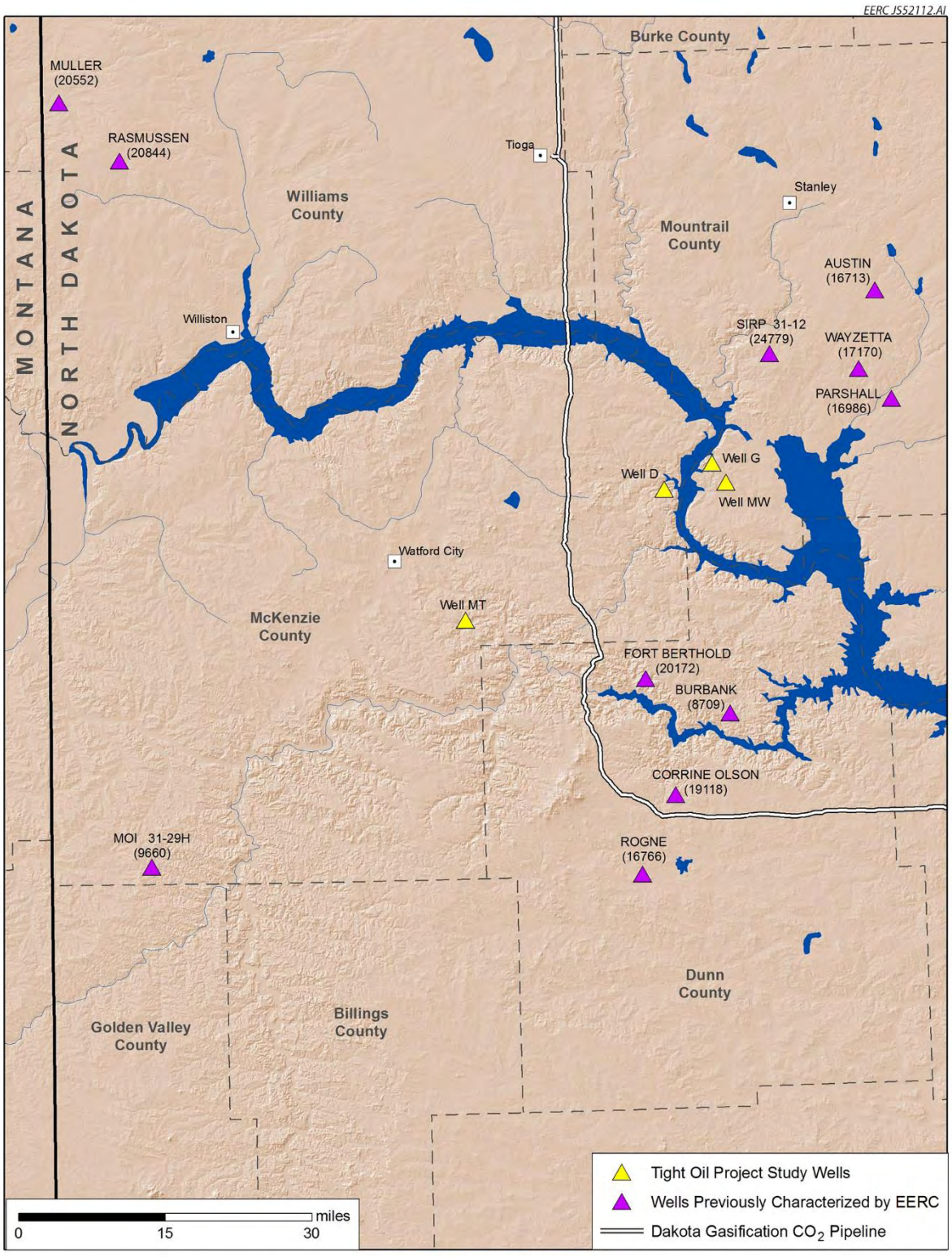

Figure 15. Map showing locations of study wells used in this project ("Tight Oil Project Study Wells").

Table 1. Suite of Analyses for Bakken Reservoir and Shale Rock Samples

Analysis Type	Information Derived
Breakthrough Pressure Test	Entry pressure for select fluid injection
Mercury Injection Capillary Entry Pressure Test	Pore throat size and distribution
Porosity/Grain Density	Rock porosity
X-Ray Diffraction (XRD)	Bulk mineralogy
X-Ray Fluorescence (XRF)	Bulk chemistry
SEM–Energy-Dispersive Spectroscopy (EDS)	General sample morphology, elemental distribution, and inferred mineralogy
Optical Petrographics	Mineral phases, grains, macrofracture characteristics, depositional environment
Geomechanical Testing	Peak strength, Young's modulus, Poisson's ratio

RESERVOIR CHARACTERIZATION

Rock Characterization

Dozens of core plugs were collected from four wells in North Dakota that penetrate through the entire Bakken Formation. Figure 2 shows white light photographs of slabbed core samples of the major lithofacies that occur in the Bakken in those four wells. The major lithofacies in the study area are, from bottom to top, the Lower Bakken Shale (LBS), Middle Bakken Lithofacies 1 (MB-L1), Middle Bakken Burrowed Lithofacies (MB-L2), Middle Bakken Laminated Lithofacies (MB-L3), Middle Bakken Packstone Lithofacies (MB-L4), Middle Bakken Lithofacies 5 (MB-L5), and the Upper Bakken Shale (UBS). Figure 2 illustrates the high degree of heterogeneity that exists within the different Middle Bakken lithofacies with respect to matrix characteristics, particularly in regard to depositional features and mineralogy distribution. Detailed evaluation of rock properties was conducted using photomicrography, SEM, XRD mineralogical analysis, and XRF analysis to determine the rock composition and chemical elements in the Bakken lithofacies.

Thin-section samples of the key Bakken lithofacies were analyzed and photographed using a petrographic microscope. Mineralogical assemblages and prevalence were determined and estimated through the use of standard optical techniques. Photomicrographs were produced at 20× magnification with plane-polarized light as shown in Figure 16. The photomicrographs clearly show the variation of mineralogy and grain size between the Bakken lithofacies.

Thin-section slides used for petrographic optical microscopy analysis were also used for SEM analysis. Backscattered electron (BSE) images were obtained on the samples to characterize textural and structural features of the different minerals found in the samples. X-ray signals obtained using EDS were used to identify the chemical composition of the different mineral grains. Finally, the combination of textural and structural features observed from BSE images with the chemical elemental composition obtained from EDS analysis were used to determine the mineral composition of the sample. Figure 17 shows the distribution of mineral components in the Upper Bakken Shale matrix, including grains such as quartz, dolomite, feldspar, pyrite, and albite

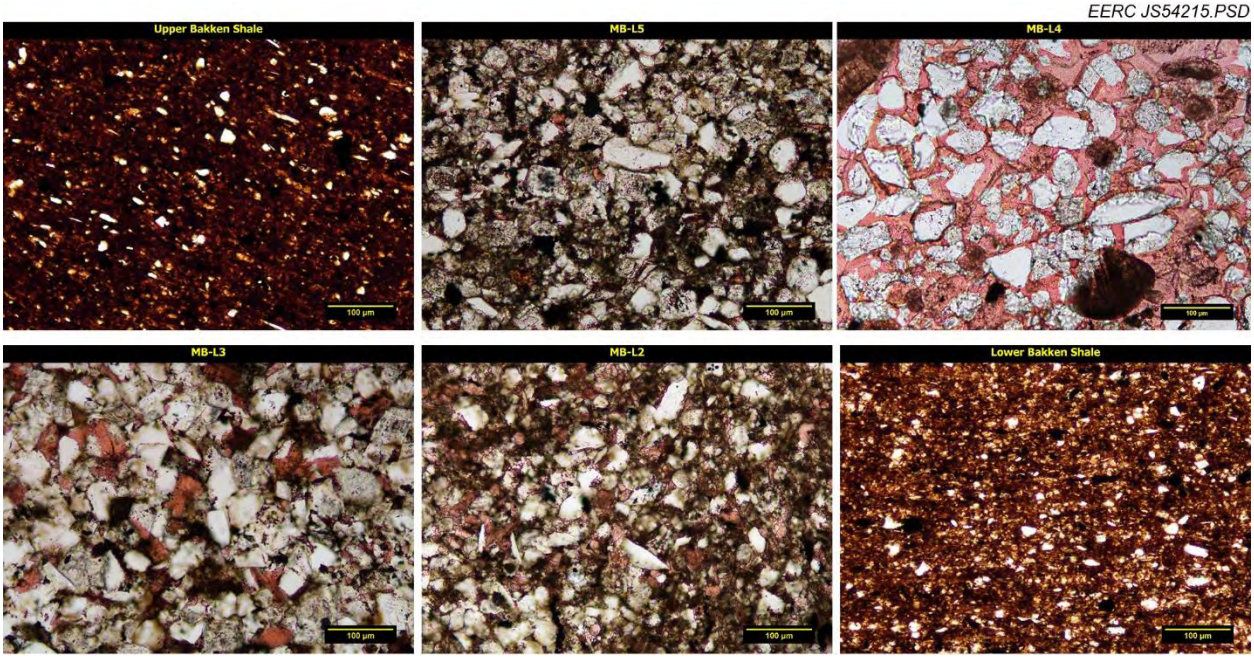

Figure 16. Photomicrographs for selected Bakken samples.

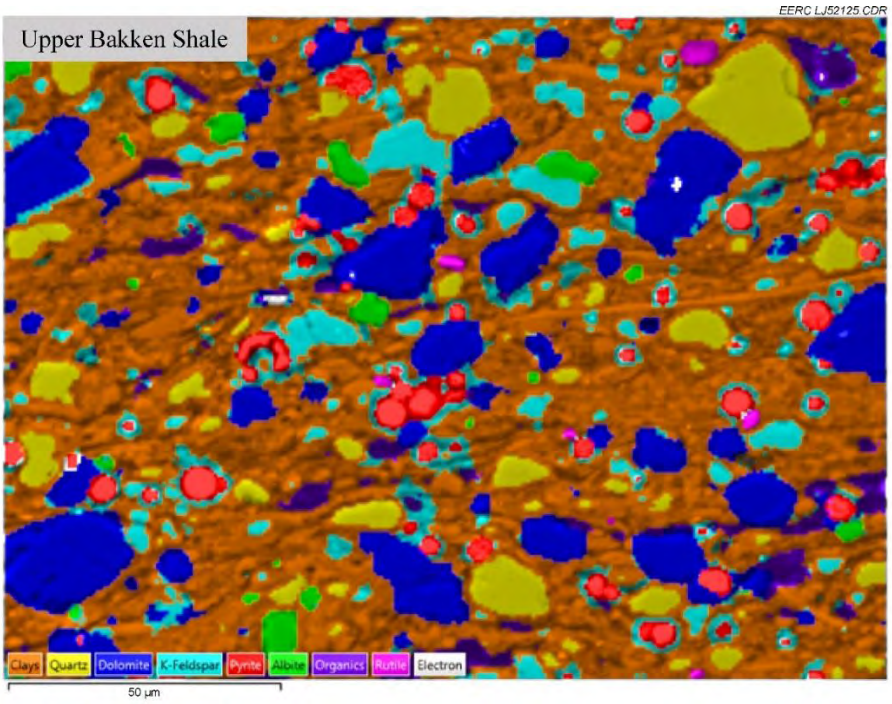

Figure 17. Mineral composition of the Upper Bakken Shale determined by SEM (Jin and others, 2016).

surrounded by a clay-rich matrix and occasional organics. The Lower Bakken Shale has a similar mineral composition to the Upper Bakken Shale, while Middle Bakken samples have significantly more dolomite and quartz than clays, which indicates the lithology of the unit is a mix of sandstone and limestone. An example of a combined BSE image and mineral map of a Middle Bakken (MB-L3) sample is provided in Figure 18.

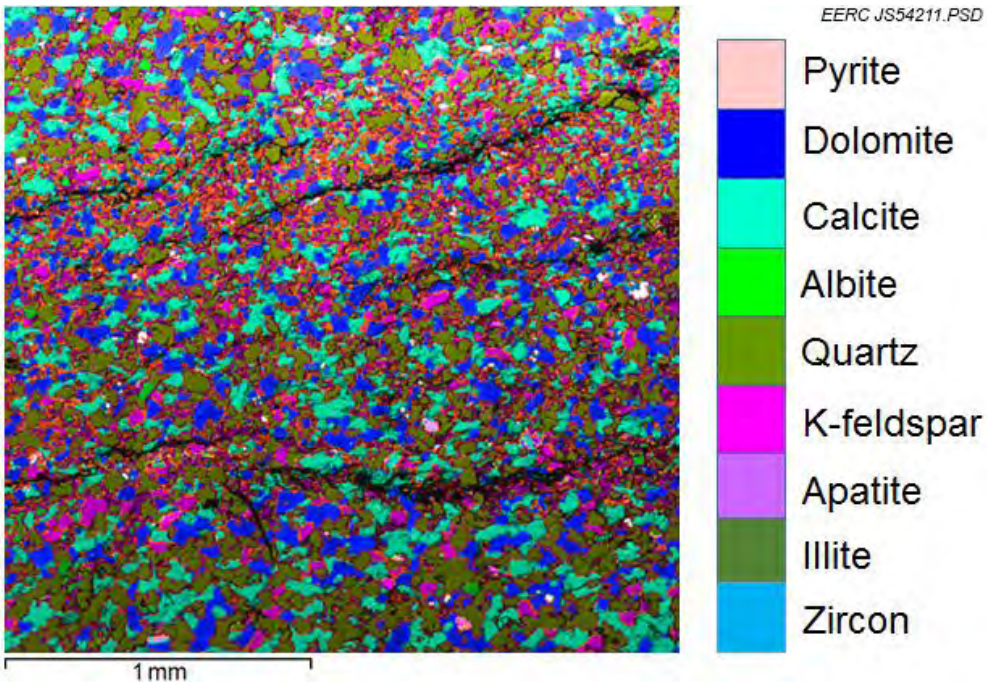

Figure 18. Mineral map combined with backscatter SEM image from a sample of Middle Bakken – laminated lithofacies (MB-L3). Black represents porosity, which is dominated by microfractures, and the colors represent different minerals (Sorensen and others, 2017).

XRD mineralogical analysis was conducted to quantify the bulk mineral composition of the samples using the Rietveld refinement method (Bish and Howard, 1988; Mittemeijer and Welzel, 2013). The XRD results, summarized in Figure 19, show that quartz, carbonate minerals (i.e., calcite and dolomite), clays, and alkali-feldspar are the dominant mineral components in the Bakken Formation; however, there are more organic-rich clays than carbonates in the Upper and Lower Bakken Shales, while there is very little organic matter in the Middle Bakken.

Mercury capillary entry pressure testing was also done on samples of each of the major lithofacies to determine the pore throat size distribution. Figure 20 shows pore throat size histograms for a Lower Bakken Shale sample and two Middle Bakken samples. The pore throat size distributions are typical of what were observed and show that the matrix of the shales and Middle Bakken lithofacies are dominated by nanoscale pore throats. Previous work by Sorensen and others (2015) showed that macro- and microscale fractures provide a majority of the naturally

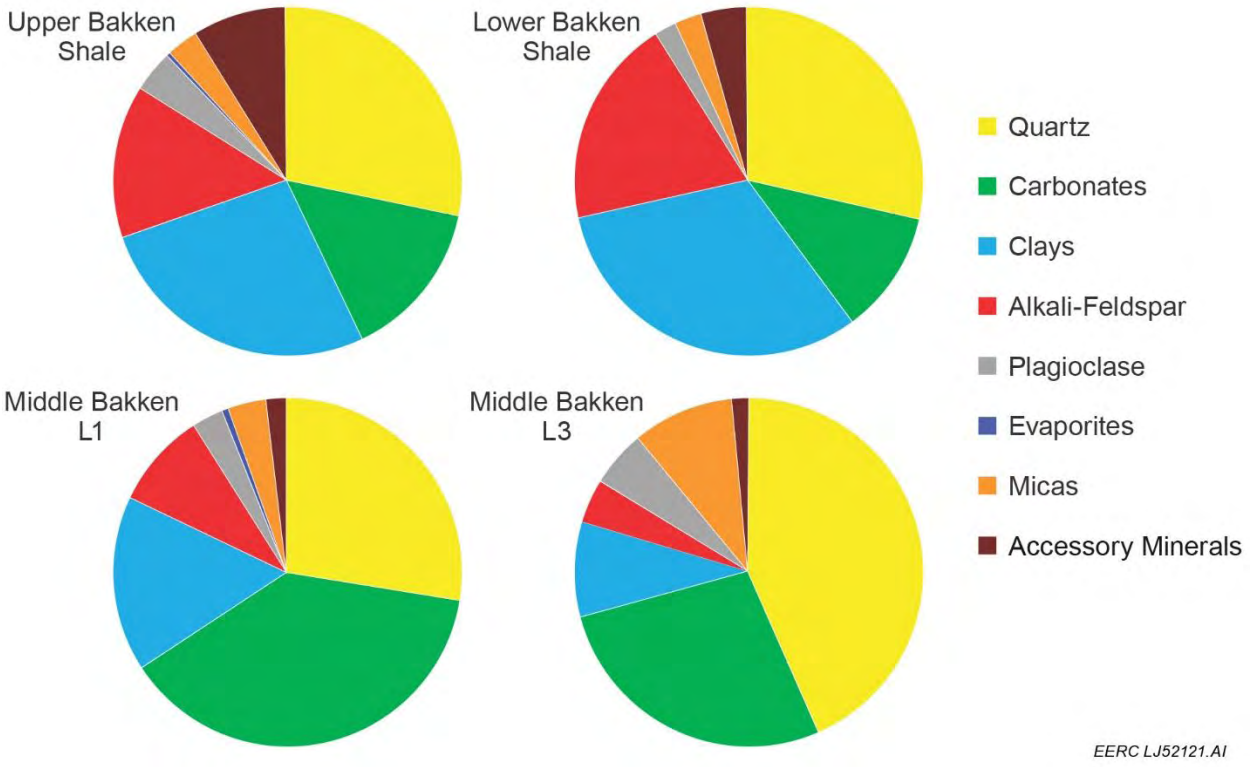

Figure 19. XRD analysis for the selected Bakken samples (Sorensen and others, 2017).

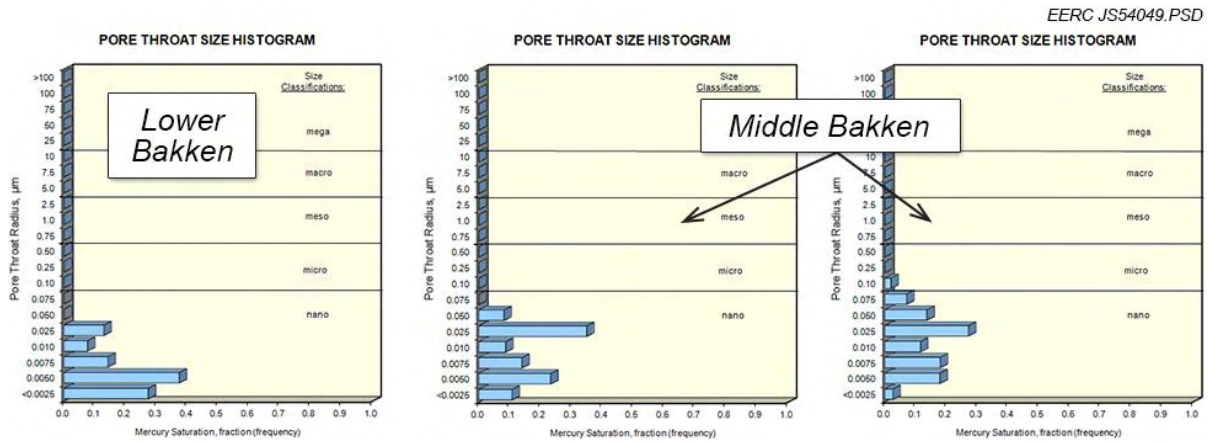

Figure 20. Pore throat size distribution based on mercury capillary entry pressure testing (Sorensen and others, 2017). Images courtesy of Core Laboratories, Inc., modified.

occurring fluid flow pathways in the most oil-productive zones of the Middle Bakken. The multiple scale levels of porosity and permeability within the various lithofacies, combined with the effects of scale on fluid-phase behavior in tight formations (Alharthy and others, 2013), serve to complicate the ability to model and predict CO_2 permeation and oil mobilization rates within unconventional tight oil formations such as the Bakken.

Advanced Core Characterization

Knowledge of the bulk porosity, permeability, and mineralogy of the various Bakken lithofacies derived from conventional analytical methods provides the context to evaluate macro- to microscale formation attributes such as depositional environment. However, the dominance of low end micro- to nanoscale pore throat sizes suggests that detailed knowledge of nanoscale pore throat networks is necessary to accurately predict fluid-phase behavior. That knowledge, in turn, is needed to determine the mechanisms controlling CO_2 permeation and storage in the Bakken, as well as attendant hydrocarbon mobilization that can lead to EOR. To improve upon the shortcomings of conventional analytical techniques to identify critical features of tight rocks (Josh and others, 2012; Erdman and Drenzek, 2013), a combination of advanced imaging and microscopy techniques, including whole-core and micro x-ray computerized tomography (CT and micro-CT) imaging, field emission scanning electron microscopy (FESEM), and focused ion beam scanning electron microscopy (FIBSEM), were used to characterize samples in terms of several parameters, including naturally occurring fracture apertures, intensity, and orientation; pore throat mineralogy and connectivity; and rock matrix characteristics, mineralogy, and organic content. Whole-core CT and micro-CT scanning, FESEM, and FIBSEM were conducted on core samples from three wells representing the major Bakken lithofacies types.

Fracture networks were first identified at the macroscale through visual core descriptions and whole-core CT scanning. CT imaging provides a noninvasive way of generating detailed information on the occurrence of fractures, bedding planes, fossils, and bioturbation in core from shales and tight formations (Walls and Armbruster, 2012; Erdman and Drenzek, 2013; Wargo and others, 2013). CT imaging using x-rays produced at different energy levels allows for continuous whole-core scans that can be calibrated to produce images of bulk density and photoelectric factor distribution, which can be used to interpret porosity, organic content, and mineralogy. Figure 9 shows an example of how whole-core CT scanning data can be processed to provide unique insight regarding the three-dimensional distribution of features that may affect fluid flow. In this case, Figure 21 shows the distribution of fossil worm burrows and brachiopods within a section of the Middle Bakken burrowed lithofacies (MB-L2).

The visual descriptions and CT scanning results were used to select locations for further analysis. One-inch-diameter plugs were collected from those locations within the whole core and then evaluated using micro-CT scanning, optical microscopy of thin sections, SEM, and SEM–EDS imaging to better characterize macro- and, possibly, microscale features. The micro-CT scanning process was followed by FESEM analysis of ion-milled samples to determine porosity and organic matter volume fraction for multiple samples. Finally, FIBSEM imaging techniques were used on portions of selected 1-inch plugs to characterize areas of interest identified in the initial FESEM results. The goal of the FESEM and FIBSEM work was to evaluate connective fractures and pore networks down to the smallest apertures that present technology can determine. FESEM is capable of 1,000,000× magnification with a spatial resolution of 1.2 nm with proper conditions and sample preparation (JEOL-USA, 2013). This analytical technique was used for characterization of nano- and microscale features, such as determining fine-grain mineral (i.e., clay) occurrence and grain geometries, nanoscale pore visualization, micropore and pore throat mineralogy, and nano- and microfracture imaging and analysis (aperture, intensity, orientation).

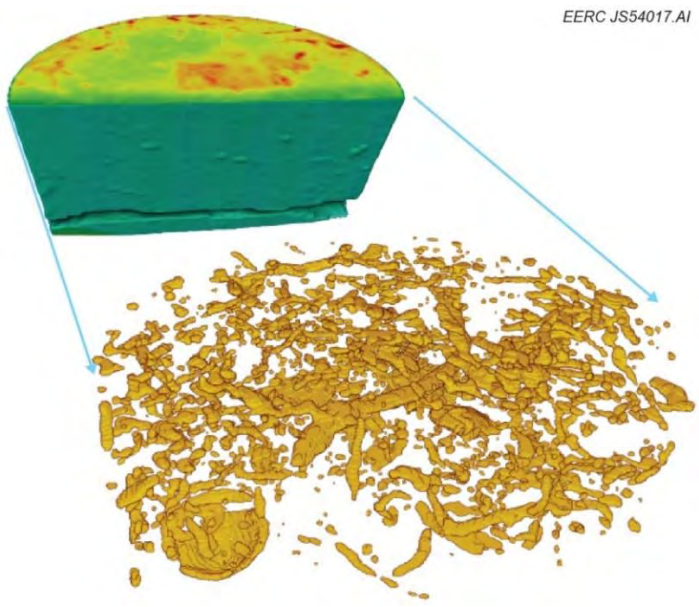

Figure 21. CT scan of a 4-inch-diameter core of Middle Bakken burrowed lithofacies (MB-L2). The CT data have been processed to highlight the three-dimensional distribution of burrows and a brachiopod fossil that are within the core sample (Sorensen and others, 2017).

FIBSEM is a technique that couples FESEM with a focused ion beam (FIB) into a single instrument that can be used to mill away very thin layers of the sample surface, leaving a fresh, highly polished surface of the sample that can be imaged and analyzed. The images are then stacked to reconstruct a 3-D image of the sample area of interest for enhanced understanding of the properties of the tight rock sample such as fracture networks, porosity and pore-size distribution, connected versus isolated porosity, and distribution of organics and mineral phases. By using the very high resolution imaging techniques available with these advanced methods, detailed knowledge of the ultrafine fractures and pore networks was determined. To the best extent possible, the micro- and nanofracture characteristics, such as aperture, were inventoried. This report focuses on the identification and characterization of micro- and nanoscale fractures and pores using whole-core CT and micro-CT scanning, 2-D SEM, FESEM, and FIBSEM techniques.

Figures 22–24 show CT-derived images of sections of whole core from the same well. The four tracks shown in these three figures represent different methods for processing the CT data to highlight the key properties of bedding features, matrix density, and fracture intensity. From left to right, Track 1 is the original CT image. Track 2 is processed in such a way as to highlight bedding features. Track 3 is a log histogram of fractures (left peaks) and high-density matrix (right peaks). Track 4 is CT data processed to show just the fractures. Figure 22 shows a section of whole core representing the Upper Bakken Shale. Macrofractures (vertical and horizontal) observed here are most likely induced by the core collection and handling process. Occasional bright spots and bright bands in largely similar matrix suggest potential areas of microfractures, although their proximity to induced macrofractures suggests that they may also be induced by the core collection and handling process. However, some swarms of fractures, such as those seen just below the

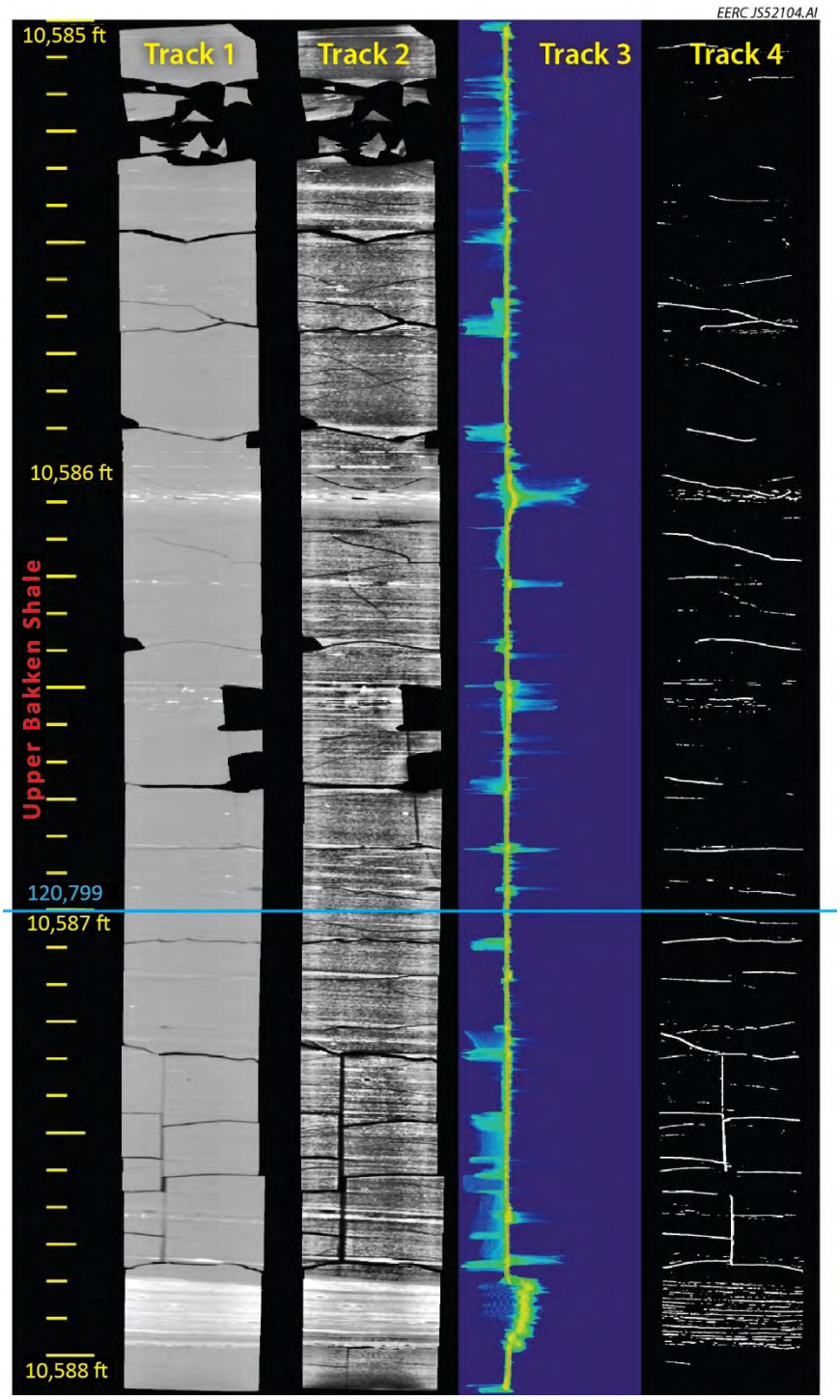

Figure 22. Upper Bakken Shale imaged using whole-core CT scanning data. The four tracks depict different means of processing the CT data. The blue line shows where a plug sample was collected for additional analyses. The contact between the shale and the Middle Bakken occurs at a depth of 10,587 ft and 10 inches (Sorensen and others, 2016) Images from Ingrain Inc. were processed by the EERC.

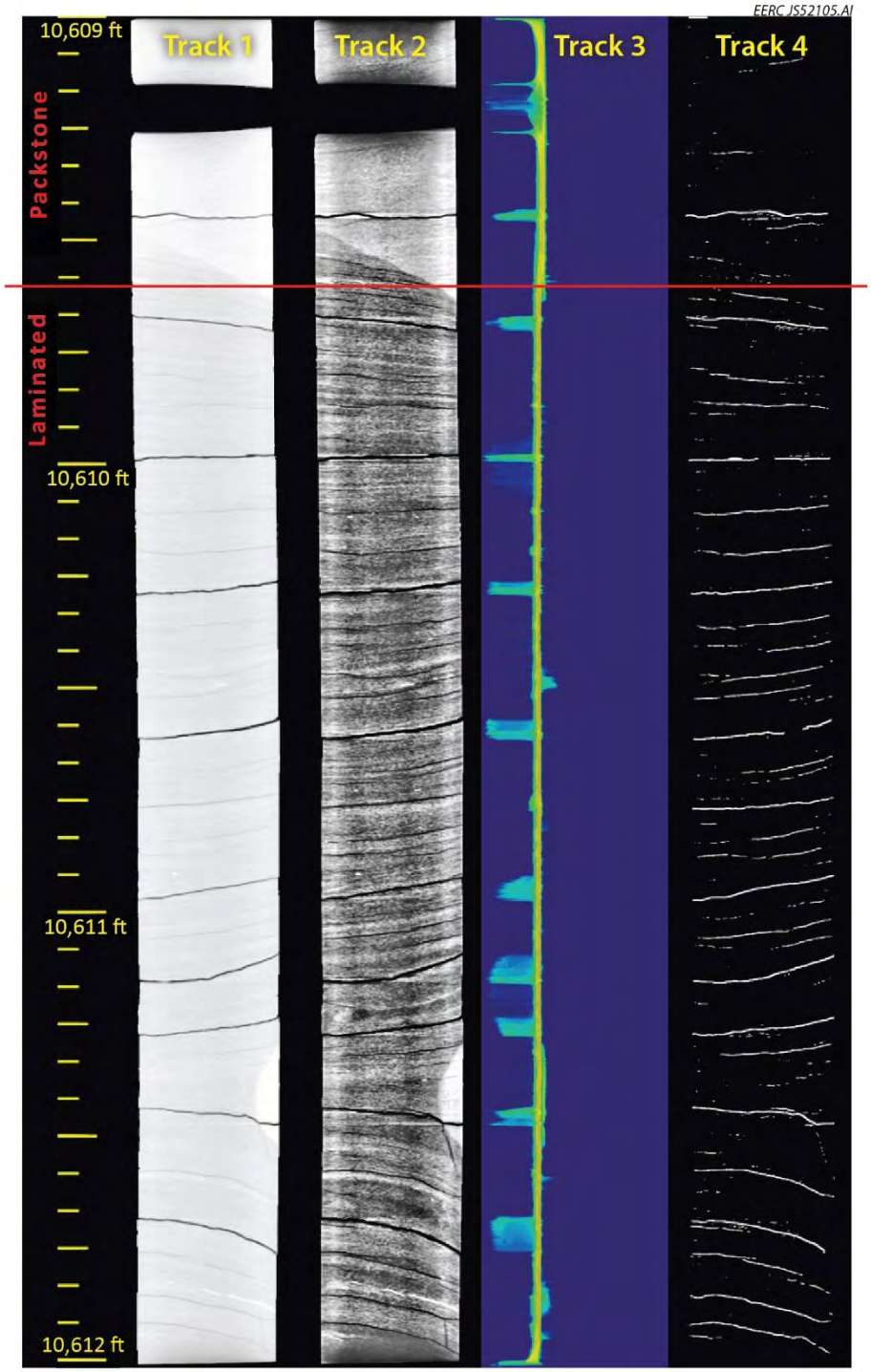

Figure 23. Portions of two Middle Bakken lithofacies, the packstone and the laminated, from one of the study wells imaged using whole-core CT scanning data. The contact between the two Middle Bakken lithofacies is shown by the red line (Sorensen and others, 2016). Images from Ingrain Inc. were processed by the EERC.

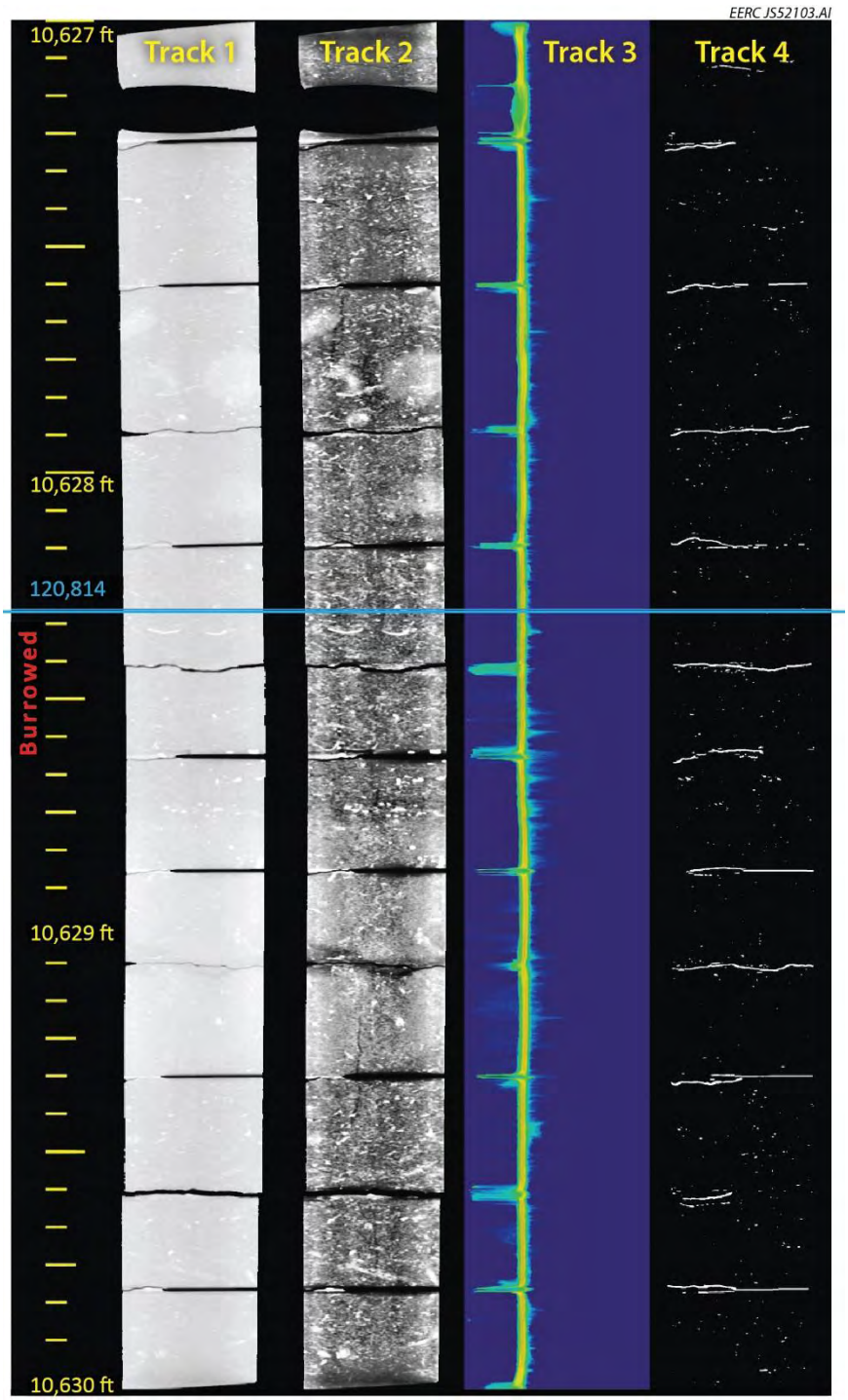

Figure 24. A section of the burrowed lithofacies of the Middle Bakken from one of the study wells imaged using whole-core CT scanning data. The blue line shows a plug-sampling location (Sorensen and others, 2016). Images from Ingrain Inc. were processed by the EERC.

10,586-ft depth marker in Figure 22, also appear to coincide with areas of high-density matrix and may be naturally occurring. The bottom 2 inches of the Figure 10 image shows the top 2 inches of the Middle Bakken, which is clearly identified by the changes in both matrix density and fracture intensity.

Figure 23 shows a section of whole core from the same well that includes portions of the packstone and laminated lithofacies, and the contact between the two, in the Middle Bakken reservoir. Of interest in Figure 23 is that the contact between the packstone and laminated lithofacies is not readily obvious in Tracks 1 and 3, but Track 2 clearly shows an abrupt change in bedding features that signifies the contact. Also, Track 4 clearly shows the laminated zone to have a much higher fracture intensity as compared to the packstone. While many of the laminated zone fractures shown in Track 4 are likely induced, the lack of similar fractures in the packstone suggests that the laminated zone is a more brittle zone and may be more prone to having more natural microfractures. This supports previous observations presented in Kurtoglu and others (2013) and Sorensen and others (2015). It also is congruent with the fact that the laminated lithofacies is often the target for horizontal drilling in the Bakken.

Figure 24 is a set of the same types of CT-based images for the burrowed lithofacies of the Middle Bakken. Track 2 clearly shows the high number and distribution of fossil burrows for which the lithofacies is named. Track 4 also shows the relative lack of fractures as compared to the other Middle Bakken lithofacies, suggesting it is geomechanically more competent and likely less prone to contain microfractures. This is also consistent with the industry consensus that the burrowed lithofacies is typically less productive than the overlying laminated and packstone lithofacies.

Using the whole-core CT scanning results, locations along each core were selected for the collection of 1-inch-diameter plug samples. For each well, at least one plug sample was taken from both of the shales, each of the major lithofacies in the Middle Bakken, and near the shale–Middle Bakken contacts to represent the transitional zone. The plugs were then scanned using micro-CT to identify zones of microfracturing and to choose locations for analyses by FESEM and FIBSEM. Figure 25 shows an example of a micro-CT image of a plug, oriented horizontally, collected from the Middle Bakken laminated lithofacies. The micro-CT image shows faint lamination with a few apparent microfractures. Horizontal, vertical, and angled microfractures are apparent. The red box indicates the area of the plug sampled for FIBSEM and FESEM analyses. The blue line on the red box indicates the location of FESEM analysis.

Figures 26–28 show results from FESEM analyses and FIBSEM images, all from the same portion of the laminated (MB-L3) lithofacies plug sample shown in Figure 23. Collectively, the results of the advanced analyses on this sample showed that very little (<1%) organic material was present. Porosity was associated with both microfractures and intergranular matrix porosity, although matrix porosity appeared to be dominant. The infill material within the micro- to nanoscale pore networks shown in Figure 27 suggests that they are naturally occurring. The FESEM and FIBSEM images in Figures 27 and 28, respectively, show clay-filled micro- to nanoscale pore networks. The FIBSEM images in Figure 29 are colored to differentiate between organics, connected porosity, and unconnected porosity. The Figure 29 image shows that, for this

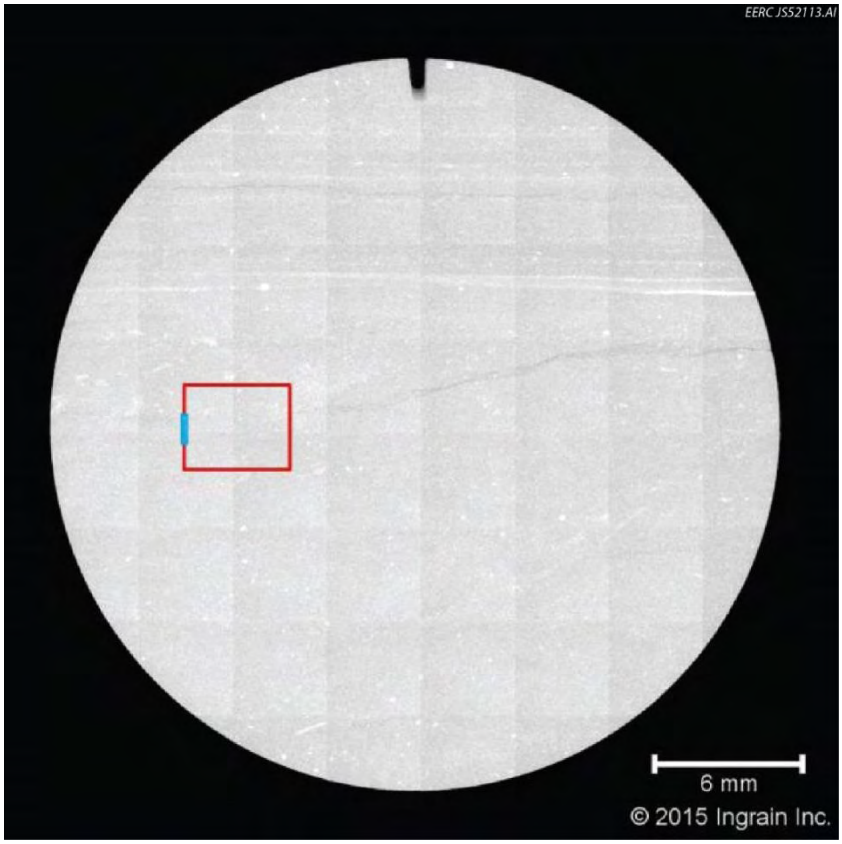

Figure 25. Micro-CT of a 1-inch plug, oriented horizontally, from the Middle Bakken laminated lithofacies (Sorensen and others, 2016). Courtesy of Ingrain Inc.

sample of laminated Middle Bakken, very little organic material is present. It also indicates that although the aperture of the pore network is at the nanoscale, much of the porosity does appear to be connected.

Figure 26 shows an example of the image and associated analytical data generated by the FESEM analysis conducted by Ingrain on the part of the laminated Middle Bakken sample depicted by the blue line in Figure 25. Figures 26 and 27 show an FESEM image, and Figures 28 and 29 show FIBSEM images of the same sample processed differently to show different properties. The shale members of the Bakken Formation are known to be organic-rich, serving as the source rock for hydrocarbons in the Bakken petroleum system. The organic-rich nature of the shales was confirmed by the FESEM analysis of samples of both Upper and Lower Bakken Shales, an example of which is shown in Figure 30. Figure 31 shows two FIBSEM images of the same Upper Bakken Shale sample: one that uses gray scale to illustrate the distribution of organics, minerals, and porosity and another that uses colors to illustrate the distribution of connected and unconnected porosity as well as organics. Figure 31 not only shows that the Upper Bakken Shale is dominated by organics, as expected and already quantified by the FESEM, but also appears to have more connected nanoscale porosity than unconnected. This observation suggests that this nanoscale pore network may be the means by which CO_2 can permeate the Bakken shale and mobilize hydrocarbons, as observed by Hawthorne and others (2013).

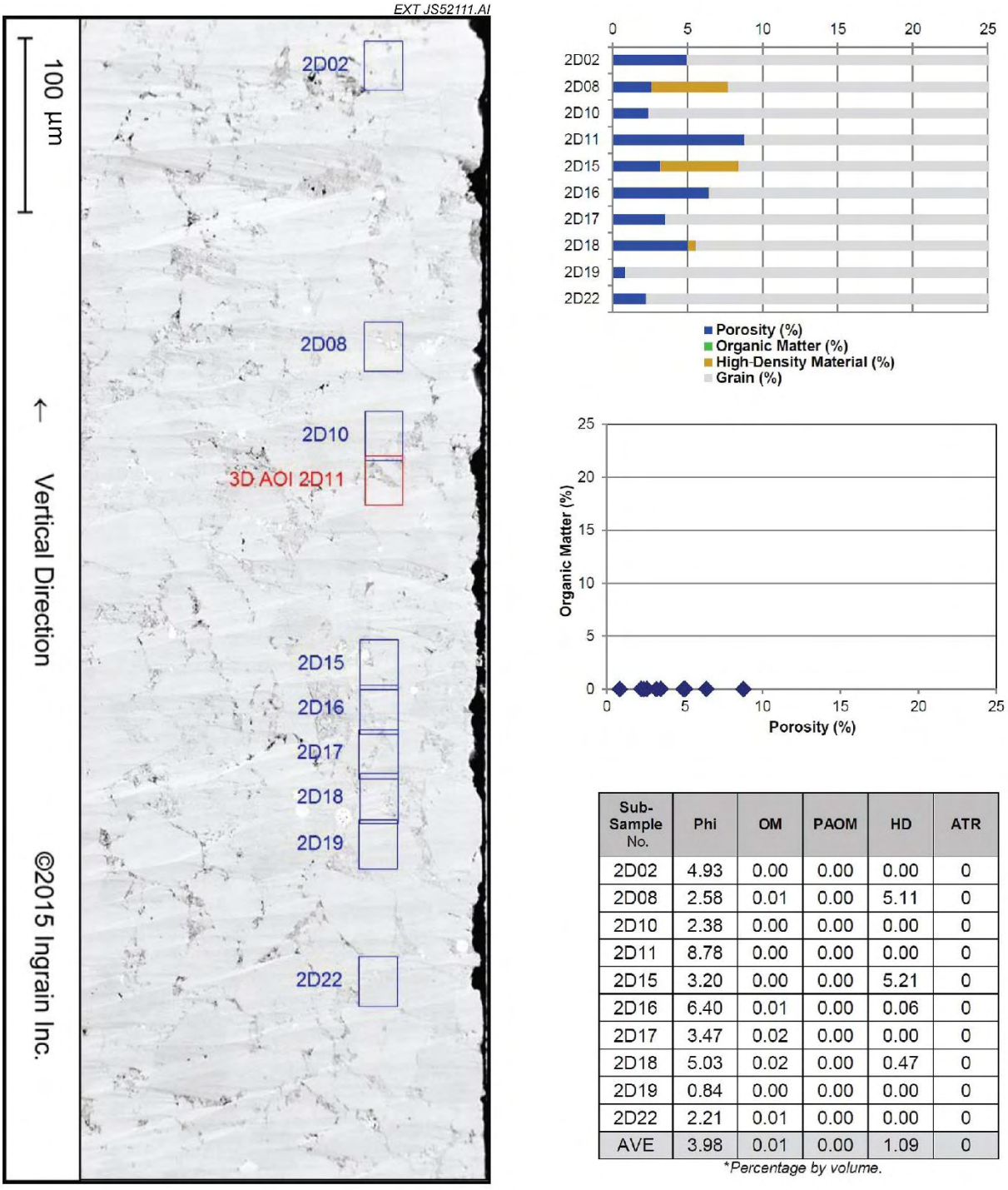

Sub-Sample No.	Phi	OM	PAOM	HD	ATR
2D02	4.93	0.00	0.00	0.00	0
2D08	2.58	0.01	0.00	5.11	0
2D10	2.38	0.00	0.00	0.00	0
2D11	8.78	0.00	0.00	0.00	0
2D15	3.20	0.00	0.00	5.21	0
2D16	6.40	0.01	0.00	0.06	0
2D17	3.47	0.02	0.00	0.00	0
2D18	5.03	0.02	0.00	0.47	0
2D19	0.84	0.00	0.00	0.00	0
2D22	2.21	0.01	0.00	0.00	0
AVE	3.98	0.01	0.00	1.09	0

*Percentage by volume.

Figure 26. Example of FESEM analysis results for a sample of Middle Bakken laminated lithofacies (Sorensen and others, 2016). Courtesy of Ingrain Inc.

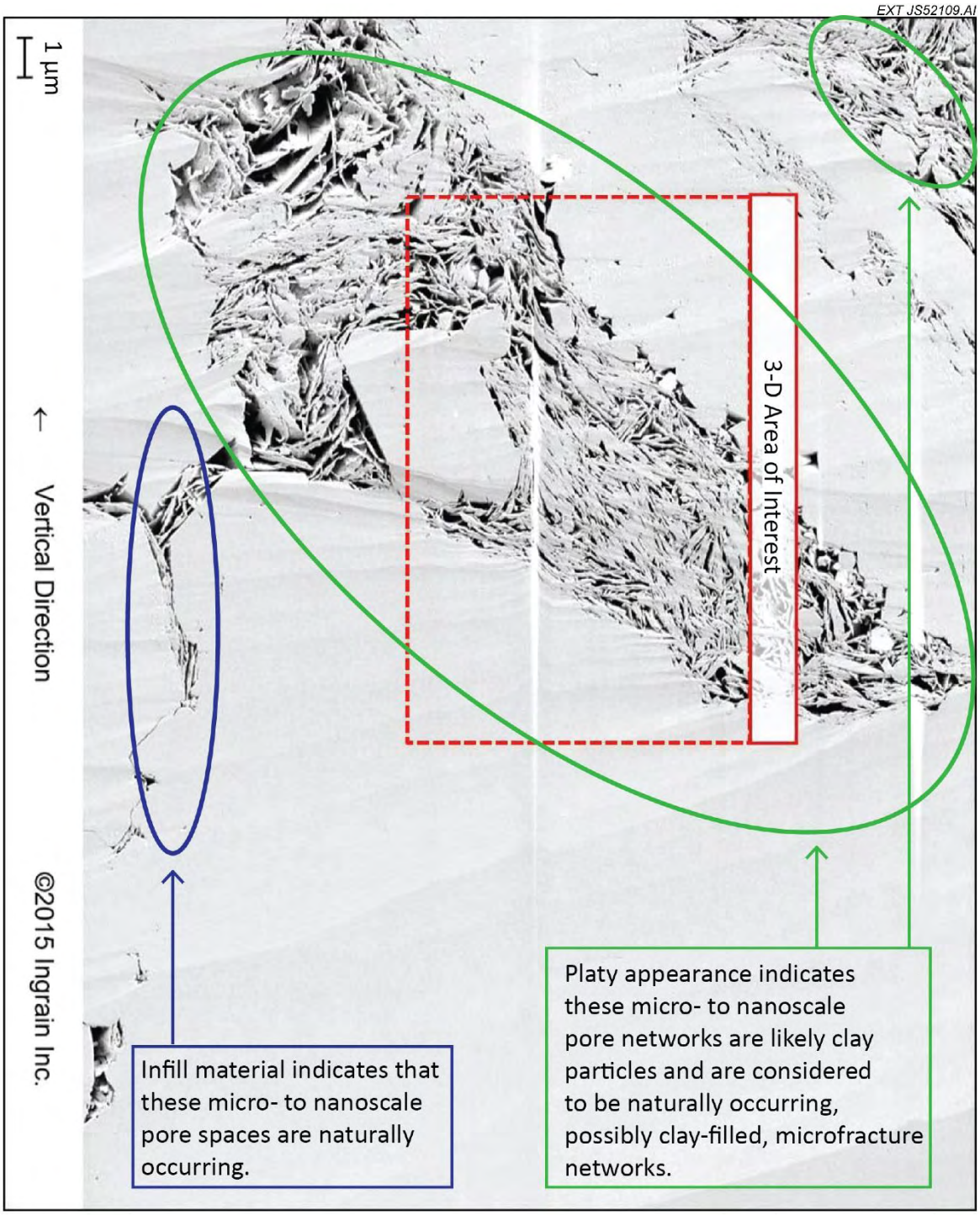

Figure 27. Example of FESEM analysis of a sample of Middle Bakken laminated lithofacies. This image is of the area identified as 3-D AOI 2D11 in the FESEM shown in Figure 14 (Sorensen and others, 2016). Courtesy of Ingrain Inc., modified.

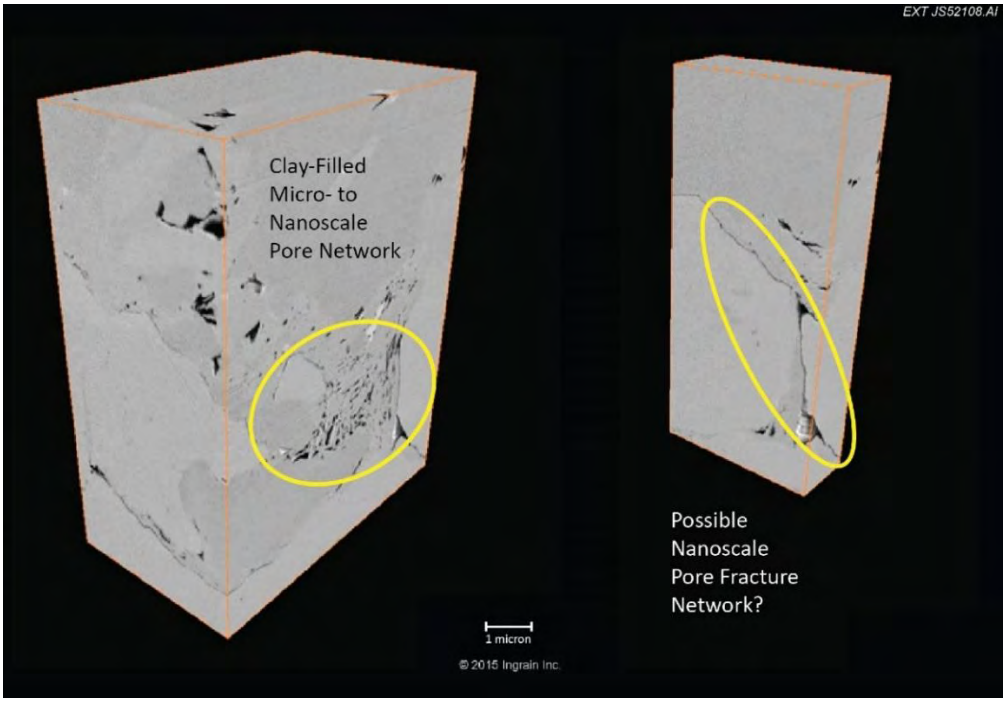

Figure 28. Example of FIBSEM analysis of a Middle Bakken laminated lithofacies (Sorensen and others, 2016). Courtesy of Ingrain Inc., modified.

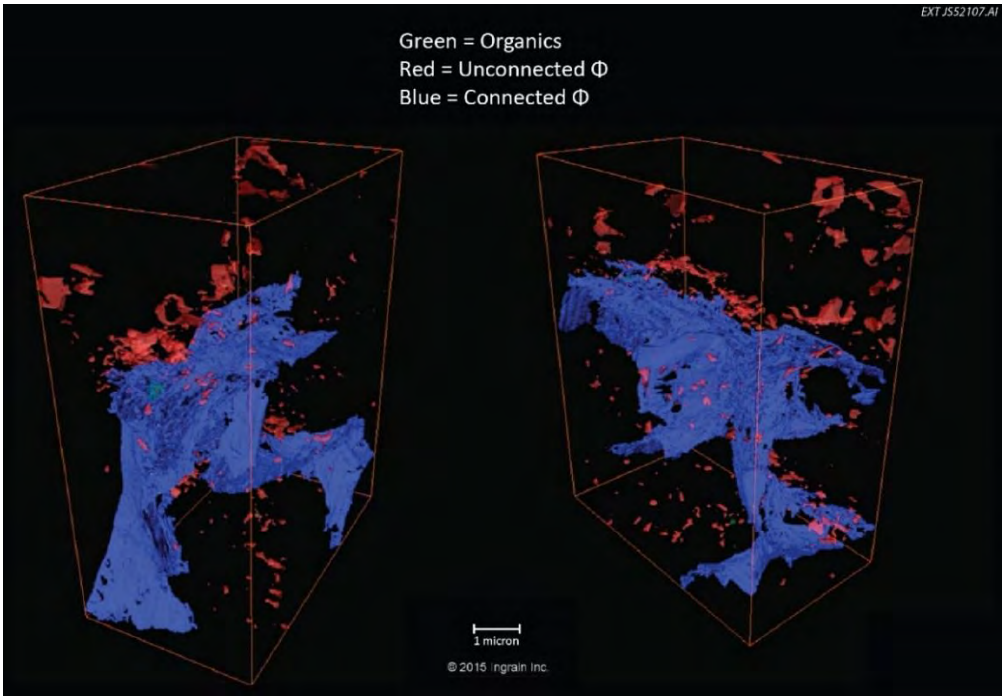

Figure 29. Example of FIBSEM analysis of a Middle Bakken laminated lithofacies (Sorensen and others, 2016). Note the limited organics presence appearing near the vertical center in the left image. Courtesy of Ingrain Inc.

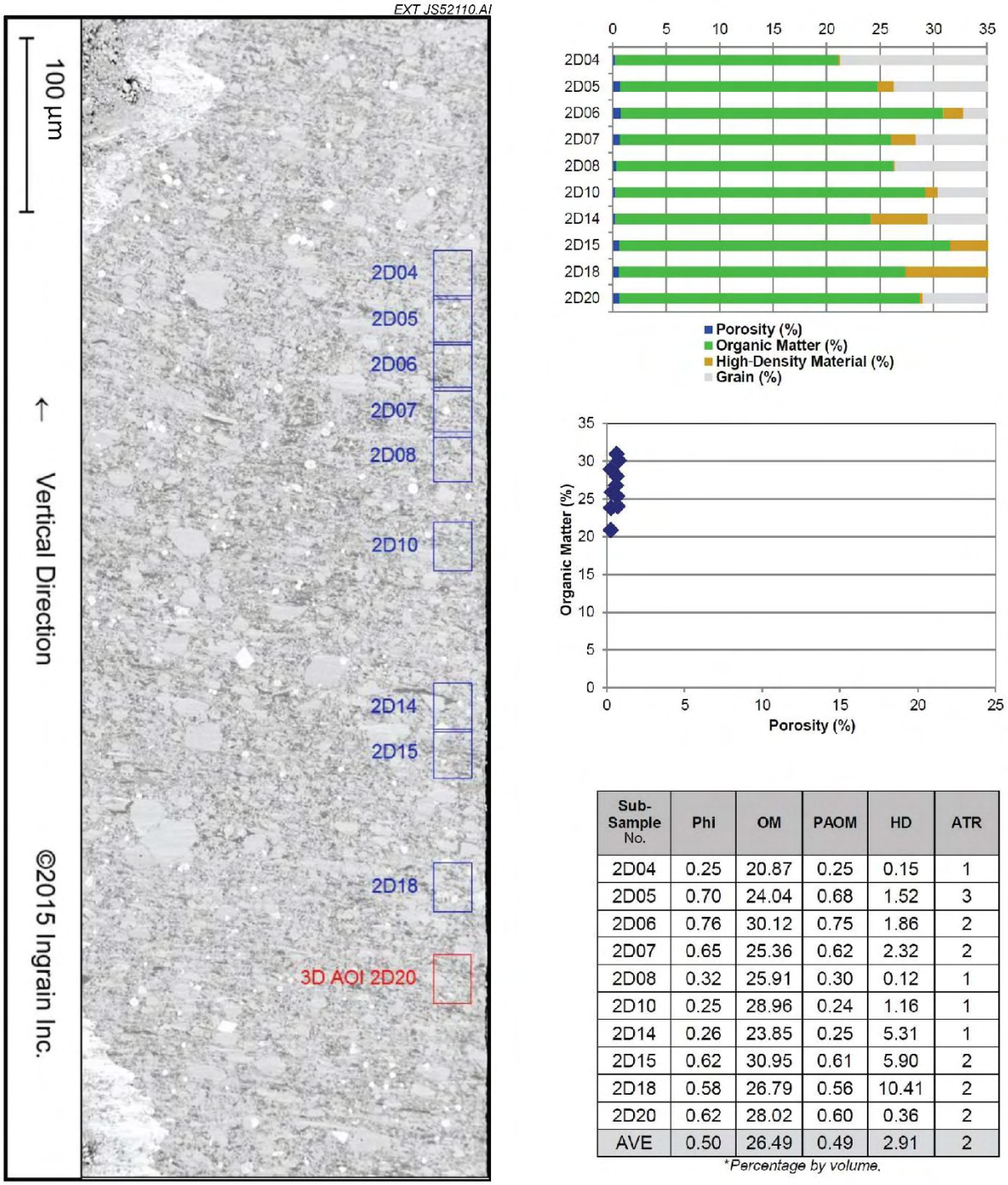

Sub-Sample No.	Phi	OM	PAOM	HD	ATR
2D04	0.25	20.87	0.25	0.15	1
2D05	0.70	24.04	0.68	1.52	3
2D06	0.76	30.12	0.75	1.86	2
2D07	0.65	25.36	0.62	2.32	2
2D08	0.32	25.91	0.30	0.12	1
2D10	0.25	28.96	0.24	1.16	1
2D14	0.26	23.85	0.25	5.31	1
2D15	0.62	30.95	0.61	5.90	2
2D18	0.58	26.79	0.56	10.41	2
2D20	0.62	28.02	0.60	0.36	2
AVE	0.50	26.49	0.49	2.91	2

*Percentage by volume.

Figure 30. Example of the data generated by FESEM analysis of an Upper Bakken Shale sample (Sorensen and others, 2016). Courtesy of Ingrain Inc.

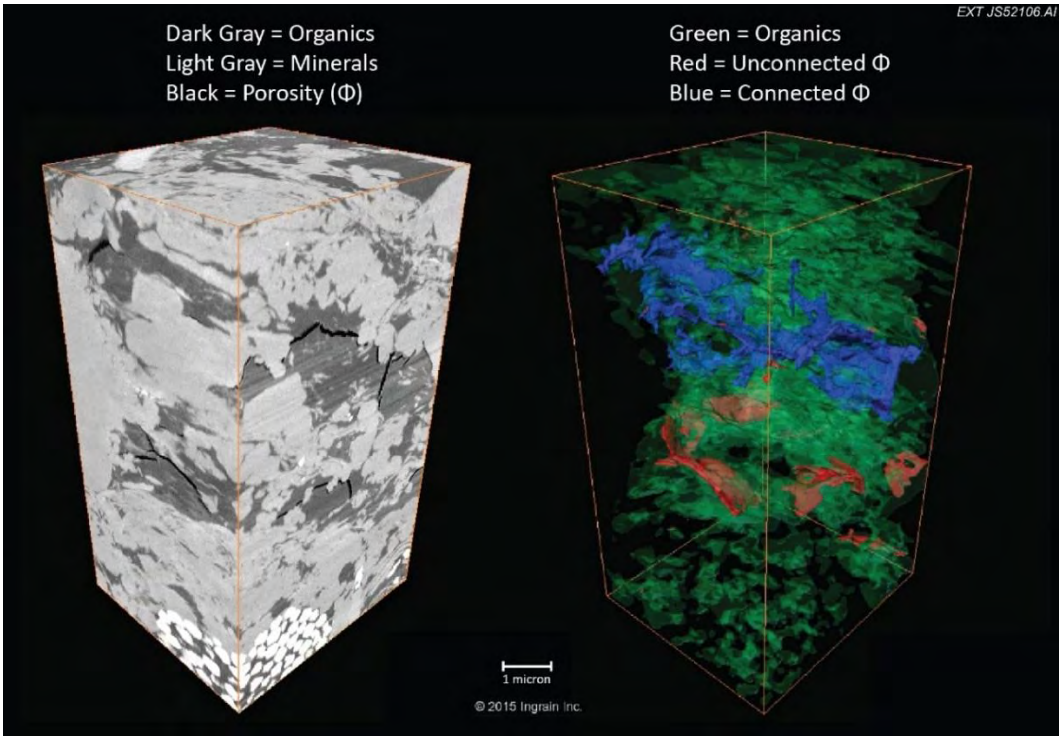

Figure 31. Example of FIBSEM analysis of an Upper Bakken Shale sample. Note that connected porosity is in the organic material (Sorensen and others, 2016). Courtesy of Ingrain Inc.

EXAMINATION OF POROSITY AND PERMEABILITY

The advanced FESEM and FIBSEM data generated by Ingrain were used to examine porosity and permeability of samples of the Middle Bakken and Bakken shales from the D, MW, and G Wells. The selected 2-D SEM locations were extracted and polished at Ingrain's Digital Rock Physics lab with a precision ion polishing system. After precision ion polishing, approximately ten locations per sample were imaged with Carl Zeiss SEM systems that employ simultaneous energy selective backscatter electron (ESB) and secondary electron (SE2) detectors at resolution of approximately 10 nm/pixel. Each resulting image was processed to determine the total volume percentage of porosity, permeability, organic matter, and high-density minerals. Those data are compiled and presented in the Ingrain analytical reports provided in Appendix B.

POROSITY BASED ON SEM AND FIBSEM

Porosity readings were calculated by Ingrain via averaging 2-D SEM images, with a porosity associated with organic material (PAOM) reading also being provided. The porosity values calculated from those images of shale samples ranged from 0.35% to 0.75%, while the PAOM ranged from 0.17% to 0.54%. The 2-D SEM-based porosity measurements for the nonshale samples were significantly higher, ranging from 0.89% to 7.53%. However the estimates of PAOM in the nonshales only ranged from <0.01% to 0.08%, significantly lower than the PAOM of the shales.

Ingrain also provided porosity readings from fewer samples via 3-D focused FIBSEM images at 15 nm/voxel. Those readings showed porosity in the shales ranging from 0.47% to 0.92%, with PAOM of the shales ranging from 0.42% to 0.92%. These values suggest that a bulk of the porosity in the shales is associated with the organic matter. The nonshale porosity values calculated from FIBSEM images range from 2.0% to 12%, with PAOM values of 0.01% or less. These data show that while the porosity of the Bakken shales is an order of magnitude lower than the nonshale rocks of the Middle Bakken, a bulk of the shale porosity, typically more than half, is associated with organic matter such as kerogen and/or bitumen. In sharp contrast, the data also show that while the nonshale Bakken rocks are much higher in porosity, they have very little porosity associated with organic matter. This suggests that detailed understanding of the organic matter is important in determining the mechanisms affecting fluid movement in organic-rich shales.

PERMEABILITY BASED ON FIBSEM DATA

Ingrain provided calculations of absolute permeability (measured in nanodarcies, or nD) via the same 3-D FIBSEM images for all three cores. Absolute permeability was computed using measurements of connected porosity in the horizontal and vertical directions. The calculated absolute permeability values for the shales ranged from <1 to 32 nD, while the nonshale absolute permeability values ranged from 60 to 366,000 nD, with most values ranging from 500 to 9000 nD. It is important to note that because of the extremely small sample size, the FIBSEM images should not be considered representative of the permeability of the larger core sample or reservoir as a whole. In the case of the nonshale Middle Bakken rocks, the FIBSEM images typically represent areas of the larger rock sample that were selected to investigate the nature of microfractures. This means that for many of the nonshale samples the permeability values associated with those FIBSEM images largely reflect the contribution that microfractures make to the overall permeability of that particular lithofacies. With respect to the shales, the use of only connected porosity to calculate absolute permeability means that any permeability associated with the organics, which tend to have relatively high PAOM values, is not accounted for; therefore, the values derived from the FIBSEM images may underpredict the actual permeability of the shales to gases such as CO_2. However, in a broad sense, these data do confirm that permeabilities in the matrix of the Middle Bakken lithofacies are several orders of magnitude higher than those of the Upper and Lower Bakken Shale matrix.

KEROGEN AND BITUMEN STUDIES

Organic Matter

Ingrain used the same 2-D SEM and 3-D FIBSEM to calculate percentages of organic matter present in Bakken shale and nonshale Middle Bakken samples. The range of organic matter in the shales ranged from 9% to 27% by volume, while the nonshale samples ranged from 0.01% to 0.20% organic matter by volume. These data point to all three wells having more porosity in the nonshale Middle Bakken than in either the Upper Bakken Shale or the Lower Bakken Shale. It

also establishes that both 2-D and 3-D data show that there is more PAOM associated with the organic-rich shales than in the more porous, organic-poor, nonshale Middle Bakken.

The Middle Bakken lithofacies have higher overall porosity, but the PAOM data demonstrate evidence of microporosity in the shale units (Figure 32). The PAOM data demonstrate that the microporosity in the organic matter of the shales is relatively significant. While overall porosity is low in the shales, there is still pore space present. One thing that may be a point of further interest is whether or not that microporosity is seen only in distinct organic matter grains (i.e., kerogen or bitumen) or whether it exists in intermixed clay-organics in the shales.

While previous EERC efforts have provided insight on the effect that CO_2 has on removing hydrocarbons from the Bakken shales, the effects that kerogen and bitumen may have on CO_2 storage and EOR in the shales are not well understood. Because the kerogen–bitumen content of some Bakken shales is in the range of 10 to 15 wt% (up to 30 vol%), it is important to understand their potential interactions with CO_2 and how that may affect CO_2 storage and EOR. In particular, kerogen and bitumen may act as a chemical sorbent phase that could significantly increase the CO_2 storage potential of the shales over the potential that would be expected based only on a volume/pressure basis. A series of laboratory experiments under reservoir temperature and pressure conditions were conducted on samples of Bakken shale from the four study wells to examine those effects. The studies of kerogen and bitumen in the Bakken, and their relevance to CO_2 storage and EOR, used a combination of techniques, including standard pyrolysis-based analysis known as Rock Eval, a slow-heating variation of the Rock Eval technique, and vitrinite reflectance measurements.

Organic Petrology – Vitrinite Reflectance

A long-standing, widely accepted technique used by organic petrographers for aiding in the determination of thermal maturity in petroleum sources rock is vitrinite reflectance measurement. The vitrinite maceral in sedimentary rocks is the organic matter remaining from the chemical alteration of woody material experienced during diagenesis, catagenesis, and metagenesis (Taylor and others, 1998). Vitrinite reflectance increases systematically with increasing maturity and depth of burial, which makes this characteristic a key measurement in determining thermal maturity of rock strata in sedimentary basins (Mukhopadhyay and Dow, 1994).

For determining vitrinite reflectance measurements, whole rock or coarsely ground samples are mounted in epoxy, polished, and viewed under reflected white light with oil immersion using a microscope-photometer system that has been calibrated with known reflectance standards. Ideally, a minimum of 20 random measurements are made and the numbers averaged and reported as percent reflectance (% VRo) (ASTM Method D7708-14).

In marine shales like the Bakken, where the majority of the organic matter is derived from marine algal matter and not woody plants, the more predominant maceral used for reflectance measurement is solid bitumen. Solid bitumen in shale is visually similar to vitrinite in reflected white light and typically occurs as amorphous or void-filling accumulations. Reflectance

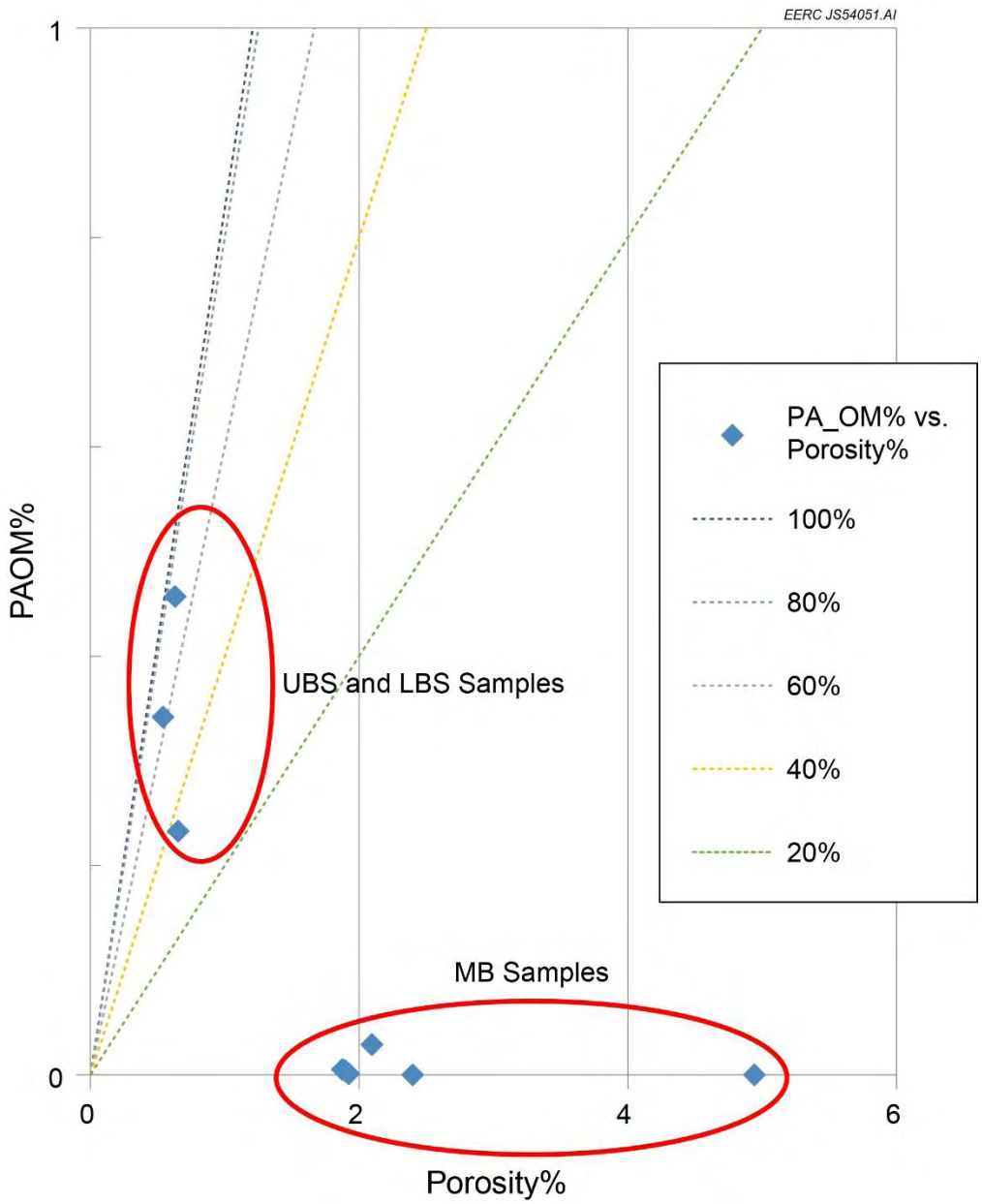

Figure 32. Porosity plotted in relation to PAOM. The low-porosity Upper Bakken Shale and Lower Bakken Shale samples have higher PAOM readings than the higher-porosity MB samples. These data are from the Well MW core. Courtesy of Ingrain Inc., modified.

measurements of this maceral are reported as %BRo and can be converted to vitrinite equivalent values (VRo_{eq}) using the following equation (Bertrand, 1990):

$$VRo_{eq} = (BRo + 0.03)/0.96 \quad \text{[Eq. 1]}$$

The upper and lower shale samples from the three study wells were mounted in epoxy and polished according to standard methods and submitted to two different laboratories for reflectance measurements: the University of North Dakota's Materials Characterization Laboratory (UND MCL) which analyzed the samples using a Leica DM2500P microscope, equipped with an ultraviolet/near-infrared spectrometer and CCD (charge-coupled device) detector, and the Geological Survey of Canada (GSC) in Calgary, which used a Zeiss Axioimager II microscope system, equipped with fluorescent light sources and ultrafine pixel-size (0.3 μm) measuring probe. Because of the ultra-fine measuring probe, the GSC system was capable of measuring smaller areas within the samples than that of the UND MCL system, therefore, able to collect more measurements. The measuring area capabilities of the UND MCL system was within the range of 3–5 μm, approximately 10× larger.

Rock Eval Analysis

One of the most widely accepted industry standard methods for determining organic matter content, thermal maturity, and quality in hydrocarbon source rocks is the Rock Eval technique (Carvajal-Ortiz and Gentzis, 2015). This method measures gases evolved from a pulverized rock sample during a programmed heating process ranging from 100° to 850°C. During the initial stages of heating the free hydrocarbons present in the rock sample are measured and recorded as the S1 peak. Upon further heating to approximately 550°C, "cracking" takes place as kerogen in the source rocks is transformed into hydrocarbons and CO_2 release takes place. The transformed and volatized hydrocarbons of this stage are measured and recorded, creating an S2 peak. The measured amount of CO_2 released is measured as S3 and, finally, the remaining residual carbon is measured and recorded as S4. Based upon these data, important characteristics of the source rock can be derived:

- T_{max}, the temperature at which the maximum amount of hydrocarbon generation occurs, is derived from the S2 peak.

- Total organic carbon (TOC) (%), the total percent amount of organic carbon, is derived from the S1, S2, and S4 values.

- The thermal maturity of the source rock can be estimated using the Arrhenius equation in conjunction with T_{max} data and probabilistic distributions of activation energies.

In addition to TOC and thermal maturity information, the direct measurements or subsequent calculations of the measured values, are used to determine hydrocarbon generating capacity and kerogen quality. Definitions of the various types of data that are generated by Rock Eval analysis are provided below. These definitions will be useful in interpreting the values generated in typical Rock Eval analysis reports that are presented later.

S1 Parameter

The S1 peak is the first peak generated from the pyrolysis of the sample and corresponds to free oil and gas that evolve from the rock sample without cracking the kerogen during the initial

stage of heating at 300°C and is reported in milligrams of hydrocarbon per gram of rock (mg HC/g). S1 > 1 mg HC/g rock may be indicative of an oil show.

S2 Parameter

The S2 peak is generated during the second stage of pyrolysis and results from the cracking of kerogen and high molecular weight free hydrocarbons that do not vaporize in the S1 peak and is also reported as mg HC/g of rock. S2 is an indication of the quantity of hydrocarbons that the rock has the potential of producing should burial and maturation continue. This parameter normally decreases with burial depths >1 km.

T_{max} (°C) Parameter

T_{max} = temperature of maximum rate of evolution of the S2 hydrocarbons (top of S2 peak). T_{max} indicates the stage of maturation of the organic matter.

S3 Parameter

The S3 peak corresponds to the CO_2 that is evolved from the thermal cracking of the kerogen during pyrolysis and is reported as milligrams of carbon dioxide per gram of rock. This value is indicative of the amount of oxygen-rich organic matter.

S4 Parameter

The S4 peak is obtained from oxidizing, at 600°C, the remaining organic matter in the sample after pyrolysis and is usually referred to as residual or inert carbon.

TOC Parameter

TOC represents all the pyrolyzed carbon and residual carbon in the rock and is calculated from the S1, S2, and S4 values using the following formula:

$$\text{TOC, wt \%} = [0.083 \times (S1 + S2)] + (S4/10) \qquad \text{[Eq. 2]}$$

Hydrocarbon Index (HI) Parameter

HI = normalized hydrocarbon content of a rock sample and is calculated using the following formula:

$$HI = (S2 \times 100)/TOC \qquad \text{[Eq. 3]}$$

The HI is proportional to the amount of hydrogen contained within the kerogen. High HI indicates a greater potential for oil generation and decreases as the sample matures. Kerogen-type information is derived from the HI value as follows:

- Type I kerogens are hydrogen-rich, containing primarily long-chain *n*-alkanes (>C_{25}) representative of lacustrine algae.

- Type II kerogens are somewhat hydrogen-depleted, containing shorter-chain *n*-alkanes (<C_{25}) representative of planktonic marine algae.

- Type III kerogens are hydrogen-poor, containing aromatic functions from cellulosic precursors and waxy components from plant spores.

- Type IV kerogens are extremely hydrogen depleted, comprised mainly of unreactive "dead" carbon that was recycled or extensively oxidized during deposition.

Oxygen Index (OI) Parameter

OI is the normalized oxygen content of a rock sample and is calculated using the following formula:

$$OI = (S3 \times 100)/TOC \quad \text{[Eq. 4]}$$

OI correlates with the ratio of O to C, which is high for polysaccharide-rich remains of land plants and inert organic material encountered as background in marine sediments. Type III kerogens generally have higher OI than either Type I or II kerogens.

Production Index (PI) Parameter

PI is derived from the relationship between hydrocarbons generated during the first (S1) and second (S2) stages of pyrolysis and is calculated using the following formula:

$$PI = [S1/(S1 + S2)] \quad \text{[Eq. 5]}$$

PI is indicative of the conversion of kerogen into free hydrocarbons and tends to increase with increasing thermal maturation. PI values >0.1 indicate entrance to the oil window.

VRo_{eq} (%)

As previously described, vitrinite reflectance is a measure of thermal maturity of the organics in a sample. When standard vitrinite reflectance measurements are unavailable, a vitrinite reflectance equivalent value, VRo_{eq} (%), can be calculated from the T_{max} value obtained from the Rock Eval analysis using the following equation:

$$VRo_{eq}\ (\%) = (0.018 \times T_{max}) - 7.16 \quad \text{[Eq. 6]}$$

As an initial screening to evaluate the source rock potential of the Bakken samples in this project, samples collected from several intervals within the D, G, and MW wells were submitted to Core Laboratories in Houston, Texas, for analysis using the Rock Eval 6 to determine TOC content, kerogen quality, and thermal maturity. The samples and their descriptions are presented

in Table 2. The samples were cleaned prior to analysis to remove any potential contamination from handling and were ground and sieved through a No. 60 mesh screen (<250 µm). A nominal 60-mg sample was used for the analysis.

Table 2. Study Samples Submitted for Rock Eval

Well Name	Lithofacies	Depth, feet
D	Upper Bakken Shale	10,587.0
	MB-L5	10,589.8
	MB-L4 packstone	10,596.7
	MB-L3 laminated	10,603.2
	MB-L2 burrowed	10,628.3
	MB-L1	10,631.0
	Lower Bakken Shale	10,632.8
G	Upper Bakken Shale	10,652.1
	MB-L5	10,656.1
	MB-L4 packstone	10,668.7
	MB-L3 laminated	10,685.1
	MB-L2 burrowed	10,708.2
	MB-L1	10,711.0
	Lower Bakken Shale	10,712.0
MW	Upper Bakken Shale	10,576.0
	MB-L5	10,586.2
	MB-L4 packstone	10,593.2
	MB-L3 laminated	10,596.2
	MB-L2 burrowed	10,622.4
	MB-L1	10,630.1
	Lower Bakken Shale	10,631.9

Extended Slow Heating Rock Eval

In addition to the standard Rock Eval testing discussed above, the upper and lower shales from the three study wells were further evaluated using a modified Rock Eval procedure called extended slow heating (ESH). This procedure measures the first pyrolysis peak (S1) at a lower temperature than the standard Rock Eval program (150° vs. 300°C) and also uses a slower heating rate (10°C per minute vs. 25°C per minute) (Sanei and others, 2015). These modifications allow for better quantitation of the S1 and S2 peaks in organic-rich shales and other source rocks and also allow for the separation of the S2 peak into the S2a and S2b. Because of the slower heating rate, some of the S1 light hydrocarbons that are typically measured in the standard Rock Eval are released later along with the medium-range hydrocarbons from the S2 peak. This combination makes up the S2a peak. The remaining residual carbon released in the S2b peak is primarily from solid bitumen. As a result, this modified heating program is more suited than the standard Rock Eval for characterizing unconventional tight oil reservoirs where the hydrocarbons are more tightly sorbed to the organic-rich matrix and where there is a higher concentration of solid bitumen.

Source Rock Evaluation Criteria Using Rock Eval and Vitrinite Reflectance Measurements

The organic matter results obtained from Rock Eval analysis and the vitrinite reflectance measurement values can be used to evaluate the production potential and maturity in petroleum systems as well as the type and quality of the kerogen (Peters and Cassa, 1994). Table 3 shows the ranges of values obtained from Rock Eval parameters and how they are used to evaluate petroleum potential. Table 4 gives the ranges of Rock Eval parameters that are used to evaluate the kerogen, and Table 5 shows the parameters used to describe thermal maturation. Note that these are considered general guidelines by the petroleum industry and require experienced geologists, geophysicists, engineers, and petrologists to fully evaluate the production potential of a particular play (Carvajal-Ortiz and Gentzis, 2015).

Table 3. Source Rock Rating Criteria

Petroleum Potential	TOC in shale, wt%	TOC in Carbonate, wt%	S1 mg HC/g Rock	S2 mg HC/g Rock	Bitumen wt%
Poor	< 0.50	0.00–0.12	<0.50	<2.5	< 0.05
Fair	0.5–1.0	0.12–0.25	0.5–1.0	2.5–5.0	0.05–0.10
Good	1.0–2.0	0.25–0.50	1.0–2.0	5.0–10.0	0.10–0.20
Very good	2.0–4.0	0.50–1.00	2.0–4.0	10.0–20.0	0.20–0.40
Excellent	> 4.0	> 1.00	> 4.0	> 20.0	>0.40

Table 4. Kerogen Type and Quality Parameters

Kerogen Type	HI (mg HC/g TOC)	S2/S3	Main Product at Peak Maturity
I	> 600	>10	Oil
II	300–600	5–10	Oil and gas
II/III	200–300	3–5	Gas and oil
III	50–200	1–5	Gas
IV	<50	<1	None

Table 5. Thermal Maturation Parameters

Stage of Maturity of Organic Matter	T_{max}, °C	PI [S1/(S1 + S2)]	VRo, %
Immature	<435	<0.1	<0.60
Early Maturity	435–445	0.1–0.15	0.60–0.65
Peak Maturity	445–450	0.15–0.25	0.65–0.90
Late Maturity	450–470	0.25–0.40	0.90–1.35
Post Mature	>470	>0.40	>1.35

RESULTS AND DISCUSSION

Rock Eval – Standard Analysis

The results for all the samples from the three study wells that were submitted for standard Rock Eval analysis are presented in Table 6. As expected, the results for the S1, S2, and TOC values show that the upper and lower shales are rich in organic matter while the Middle Bakken samples, except for G MB1, are organically lean. As shown in the table, S1 and S2 values vary because of the use of two techniques. The first technique (A) shows the results for samples that were "cleaned" to remove contamination by oil-based drilling mud. The second set (B) were tested in an "as-received" condition. By cleaning the samples, a bulk of the lighter hydrocarbons (represented by the S1 peak) and a portion of the heavier hydrocarbons (included in the S2 peak) were removed and falsely imply that the hydrocarbon potential is poor. The as-received testing gives a more representative value for the potential for hydrocarbon mobilization and long-term resource recovery for the formation.

Figure 33 shows a plot of the HI vs. T_{max} values, which is commonly used by the industry to help define kerogen type and quality. All the points with HI values <50 represent the majority of the middle Bakken samples, which also have very low TOC values (all < 0.5 wt%) and, therefore, not enough kerogen for the HI or T_{max} value to be considered valid. However, the upper and lower shales as well as the MW–MB1 sample all have HI values >100 and TOC values >4 wt% and fall into the kerogen Type II category and oil window.

The thermal maturity and kerogen types from these three study wells are consistent with other published information on the Bakken (Nordeng and LeFever, 2009; Jin and Sonnenberg, 2012).

Extended Slow Heating Rock Eval

The results reported by the GSC using its ESH procedure are presented in Table 7. Note that the upper shale from the MW well was not analyzed because of insufficient sample. These results were reported in a different format than those from the standard Rock Eval, and the raw results were not made available to make direct comparisons to the S2 and S3 values that were reported in the standard Rock Eval report, but the S1 and TOC values can be directly compared. The light oil results determined by the ESH method are what would be considered as the S1 peak in the standard Rock Eval analysis (Table 6, Method B); however, the values from the ESH analysis are significantly higher than those from the standard Rock Eval. in the ESH method, the longer analysis time and the extended temperature ramp (starting at a lower temperature than the standard Rock Eval technique) allows for better resolution of the various hydrocarbon components in organic-rich, tight samples such as the Bakken shales. In the ESH method, some of the components that would show up as light hydrocarbons (the S1 peak in standard Rock Eval) are incorporated in the S2a peak, which comprises medium- to heavy-weight hydrocarbons.

Table 6. Results of Rock Eval

				TOC, wt %			S1, mg HC/g			S2, mg HC/g			Tmax, °C				Calc. % VReq			S4,[3] Bitumen mg C/g		
	STAR	Facies	Depth, ft	A[1]	B[2]	Difference	A	B	Difference	A	B	Difference	A	B	Difference	Maturity	A	B	Maturity level	A	B	Difference
Well D	120799	UBS	10587.0	14.16			0.09			27.19			449.00			Peak	0.92		Late	118.96		
Well D	120800	UBS	10587.0		13.31	−0.85		7.14	7.05		30.87	3.68		446.55	−2.45	Peak		0.88	Peak		101.55	−17.41
Well D	120802	MB5	10589.8	0.23			0.02			0.10			443.00							2.20		
Well D	120802	MB5	10589.75		1.28	1.05		1.51	1.49		1.26	1.16		414.46	−28.54						10.50	8.30
Well D	120807	MB3	10603.2	0.28			0.03			0.12			444.00							2.68		
Well D	121455	MB3	10606.5		0.88	0.60		1.02	0.99		0.60	0.48		409.39	−34.61						7.46	4.78
Well D	120819	LBS	10632.8	12.86			0.06			21.10			450.00			Peak	0.94		Late	111.04		
Well D	120819	LBS	10632.8		12.36	−0.50		5.97	5.91		25.55	4.45		447.65	−2.35	Peak		0.90	Late		97.44	−13.60
Well MW	120849	MB3-1	10593.2	0.16			0.02			0.10			444.00							1.50		
Well MW	120849	MB3-1	10593.2		0.98	0.82		2.30	2.28		1.01	0.91		417.30	−26.70						7.05	5.55
Well MW	129851	MB3-2	10596.2	0.13			0.03			0.08			441.00							1.21		
Well MW	129851	MB3-2	10596.2		0.71	0.58		0.28	0.25		0.21	0.13		437.37	−3.63						6.69	5.48
Well MW	120861	LBS	10631.9	14.47			0.10			49.08			443.00			Early	0.81		Peak	103.88		
Well MW	120861	LBS	10631.9		14.65	0.18		6.27	6.17		54.63	5.55		439.39	−3.61	Early		0.75	Peak		95.95	−7.93
Well G	120820	UBS	10652.1	10.58			0.06			29.15			443.00			Early	0.81		Peak	81.56		
Well G	120820	UBS	10652.1		7.22	−3.36		3.83	3.77		19.43	−9.72		442.00	−1.00	Early		0.79	Peak		52.89	−28.66
Well G	120829	MB3	10685.1	0.28			0.02			0.39			354.00							2.46		
Well G	120829	MB3	10685.1		0.89	0.61		1.09	1.07		0.57	0.18		427.29	73.29						7.52	5.06
Well G	120838	LBS	10712.0	4.13			0.04			9.31			447.00			Peak	0.89		Peak	33.54		
Well G	120838	LBS	10712.0		4.62	0.49		2.30	2.26		10.70	1.39		446.00	−1.00	Peak		0.87	Peak		35.41	1.87

[1] Represents results from samples that were cleaned prior to analysis with a mixture of chloroform and methanol to remove potential oil based drilling mud contaminants.
[2] Represents results of sample splits from the same cores, but were not cleaned prior to analysis.
[3] The S4 carbon, which represents the unpyrolyzed kerogen/solid bitumen, was calculated from the TOC, S1, and S2 values.

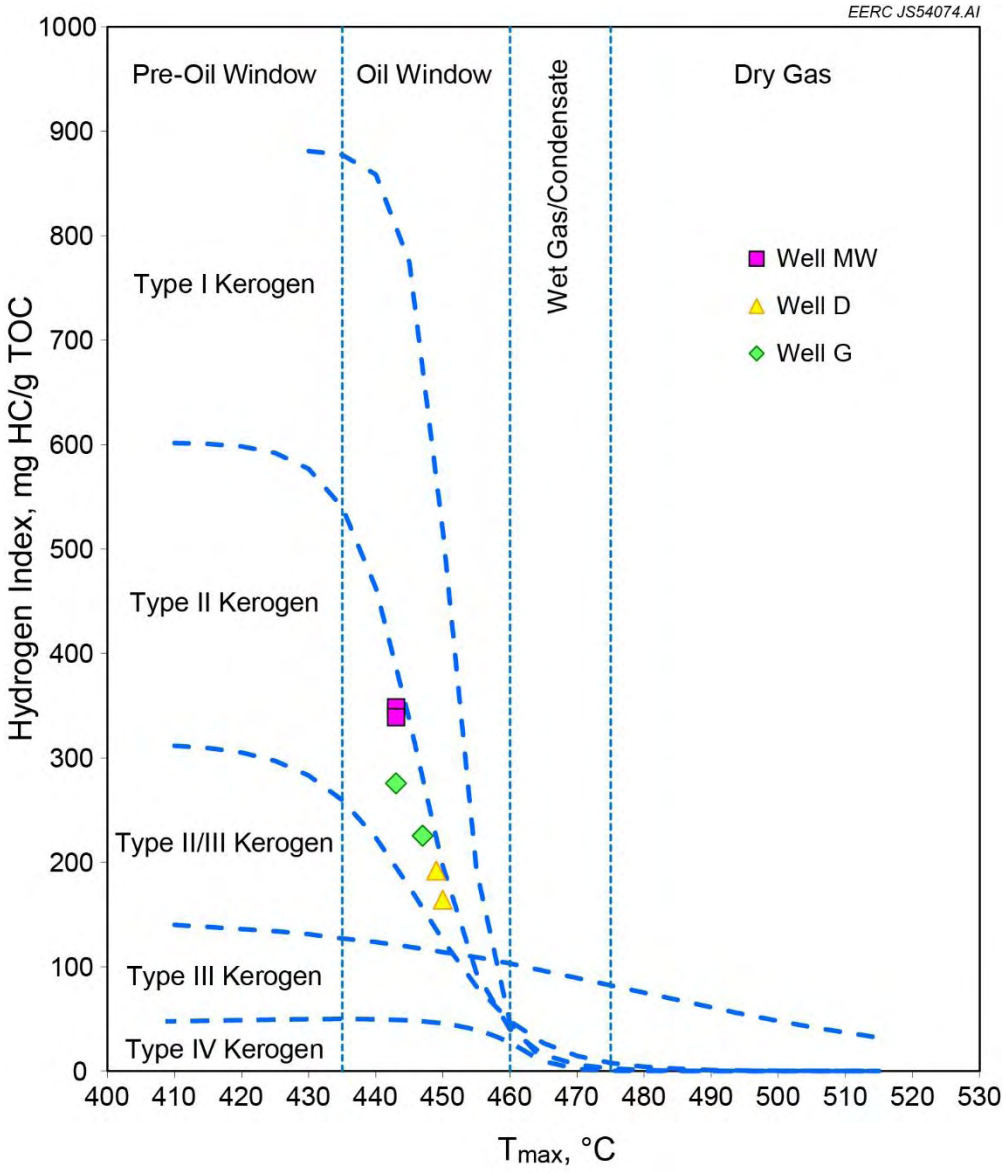

Figure 33. HI vs. T_{max} – showing kerogen type of Bakken shales.

Table 7. ESH Results

Well Name	Lithofacies	Depth, ft	Light Oil, mg HC/g	Heavy Oil	Bitumen, wt%	TOC, wt%	Oil, vol%	FHR,* vol%	Bitumen, vol%
D	UBS	10,587.0	1.44	7.23	13.79	14.56	2.49	2.08	25.61
	LBS	10,632.8	1.04	5.90	12.28	12.90	2.00	1.70	22.81
G	UBS	10,652.1	1.39	4.68	8.02	8.56	1.74	1.34	14.90
	LBS	10,712.0	0.67	2.85	4.50	4.81	1.01	0.82	8.36
MW	LBS	10,631.9	1.84	7.36	14.66	15.47	2.62	2.10	27.23

* Fluidlike hydrocarbon residue.

As stated earlier for the standard Rock Eval analysis, the TOC values are obtained by summing the Sl, S2, and S4 peaks, and this is also the case for the ESH analysis. Although the values for S4 are generally not reported separately, the peak is measured by the analyzer and automatically calculated by the software and used to obtain a TOC value. A comparison of the TOC values from both methods is shown in Figure 34. These results show that the TOC content measured by both techniques agree relatively well, which is consistent with data generated from another study performed by GSC (Sanei and others, 2015).

The S2a and S2b peaks generated from the ESH program are used along with density measurements of the oil and rock to calculate the volume % of fluidlike hydrocarbon residue (FHR) and bitumen, respectively. The FHR is defined by GSC as the medium to heavy range hydrocarbons (oil residue) remaining in the rock after the light S1 hydrocarbons have been released.

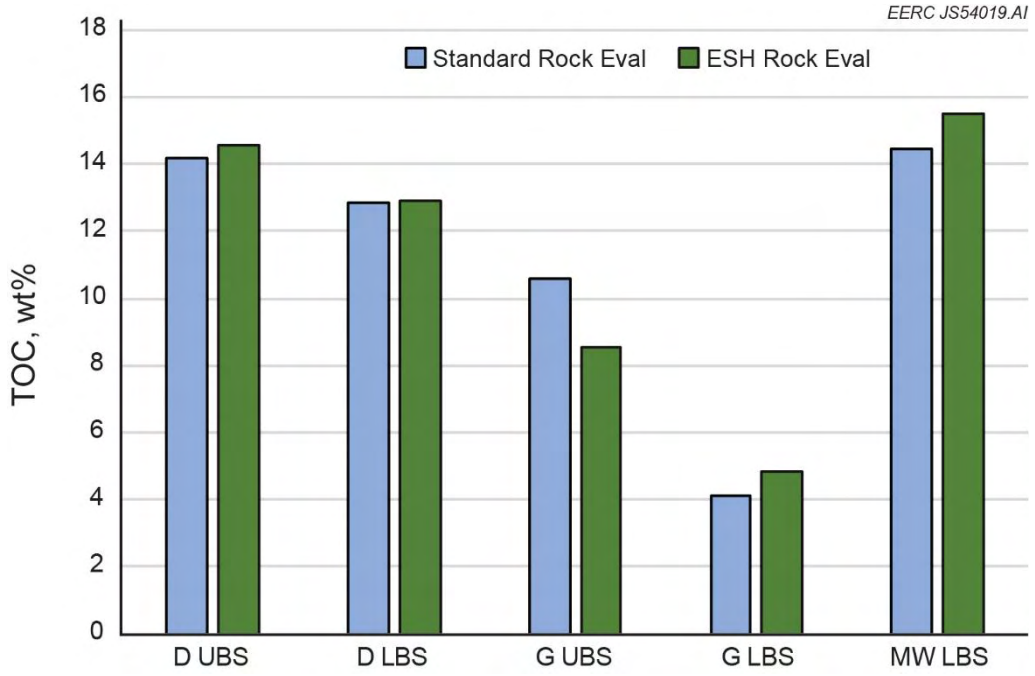

Figure 34. Comparison of TOC values from standard Rock Eval and ESH Rock Eval.

Organic Petrology – Vitrinite Reflectance Results

The results of the reflectance measurements are reported in Table 8, and all measurements from both labs were made on solid bitumen and converted to vitrinite equivalence (VRo_{eq}) using the equation described earlier. Figure 35 is an example of one of the reflectance reports for the MW lower shale, which shows the number of measurements, mean value, minimum, maximum, standard deviation, and frequency distribution in both table format and histogram plot. This is the typical reporting format for laboratories performing vitrinite reflectance measurements. The data generated by Geologic Survey of Canada (GSC) using conventional organic petrography techniques were quite similar to the values determined by standard Rock Eval at UND.

Table 8. Bitumen Reflectance Results Converted to Vitrinite Reflectance Equivalent (%VRo_{eq})

Well Name		Depth, ft	GSC n	GSC %VRo_{eq}	UND – MCL n	UND – MCL %VRo_{eq}	T_{max} %VRo_{eq}
D	UBS	10,587.0	14	0.97	17	1.01	0.92
	LBS	10,632.8	38	1.00	21	1.00	0.94
G	UBS	10,652.1	41	0.82	22	0.84	0.81
	LBS	10,712.0	48	0.75	20	0.72	0.89
MW	UBS	10,576.0	49	0.75		NM*	0.81
	LBS	10,631.9	56	0.83	25	0.87	0.81

* Not measured.

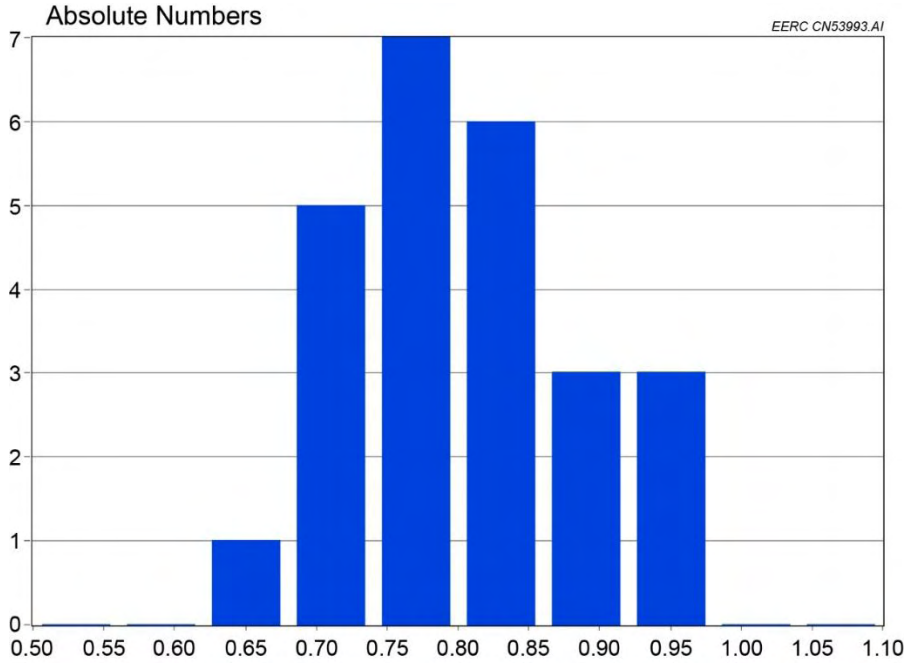

Figure 35. EERC vitrinite reflectance report for the MW well lower shale.

Figure 36 is a photomicrograph of the G upper shale showing examples of solid bitumen with two different reflectance values (0.50% VRo_{eq} and 0.76% VRo_{eq}), which is visually apparent from the different levels of gray. The GSC found a binary distribution of VRo_{eq} values in several of the Bakken shale samples. The lab concluded that the distribution of lower VRo_{eq} values was likely due to suppression of reflectance by free hydrocarbons in the samples and that the distribution of bitumen particles with a higher reflectance was representative of the true VRo_{eq} values. Only the higher VRo_{eq} values are listed in Table 8.

Figure 37 is an image of the D lower shale showing solid bitumen with one reflectance value of 0.93% VRo_{eq}. These images also show the solid bitumen finely dispersed throughout the rock matrix. Because of the measuring area limitations of the UND MCL system and the finely

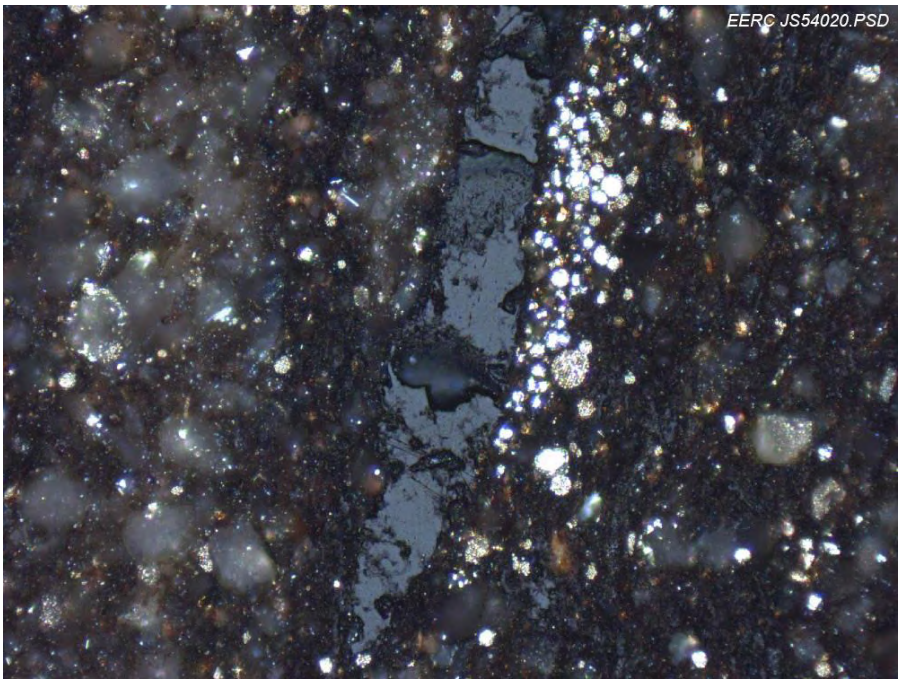

Figure 36. Photomicrograph (oil immersion, incident white light) of the G well upper shale.

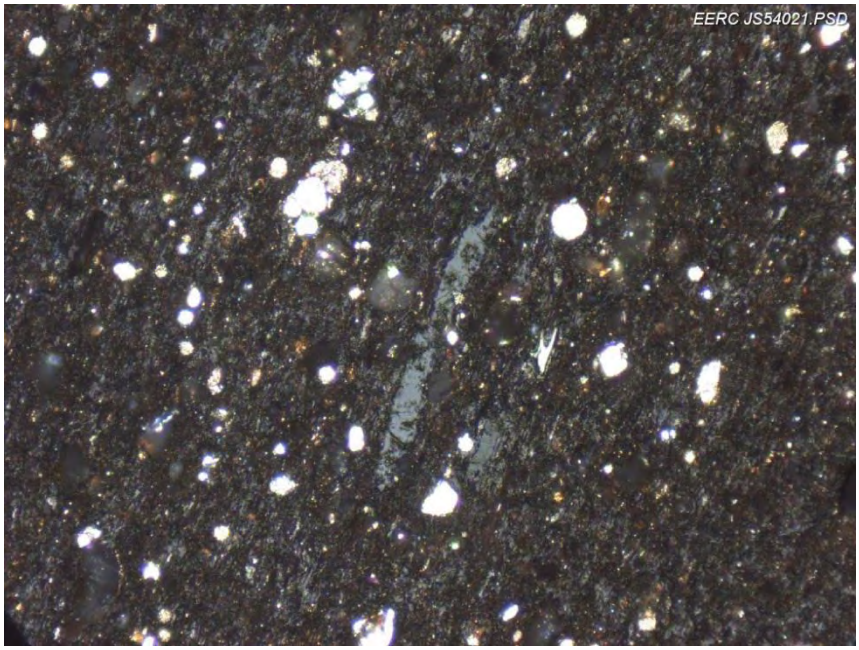

Figure 37. Photomicrograph (oil immersion, incident white light) of the D well lower shale.

dispersed nature of the organic matter, reliable measurements could not be made on the MW upper shale. However, the measurement values from both labs for the other five samples compared relatively well, and the $\%VRo_{eq}$ values from both labs indicate peak maturity for the G and MW wells and late maturity for the D well (Table 5).

Characterizing the type and distribution of organics within the Bakken shales, as well as the thermal maturity of the organics, is important to better understand the potential mechanisms of CO_2 permeation and sorption within these Bakken units. Kerogen and bitumen within organic-rich shale are known to have microporosity, spanning micrometer to nanometer in scale, which influences the generation, storage, and production of hydrocarbons, as well as CO_2 sorption (Loucks and others, 2009; Ross and Bustin, 2009; Curtis and others, 2012; Romero-Sarmiento and others, 2014; Duan and others, 2016). In addition, many studies have noted an increase in the porosity of kerogen with increasing thermal maturity (Hackley and Cardott [2016] and references therein). Large pores and organic-associated fractures that are identifiable via conventional methods such as SEM could dominate the pore volume, but small, undetectable pores may also influence connectivity of the pore network (Ambrose and others, 2010; Kang and others, 2011). This is important because while the larger fractures may be a mechanism by which CO_2 could partially penetrate the Bakken shales, without a mechanism to penetrate the bulk of the organic matrix, it seems unlikely that such a high hydrocarbon recovery could be obtained. Nanoscale pore networks within the kerogen and bitumen could be the mechanism by which CO_2 is able to penetrate the bulk of the organic matrix. It is also important to note that crude oil both adsorbs and absorbs onto kerogen (Pathak and others, 2017); thus accessible porosity within these organics is exactly what would be needed for effective oil removal via CO_2.

CO_2 Permeation and Oil Extraction Experiments Using Bakken Rocks

Experiments to evaluate CO_2 permeation into and oil extraction from the Upper and Lower Bakken Shales and key Middle Bakken lithofacies were conducted on samples from several North Dakota wells, including samples from the same cores that were subjected to the advanced characterization program described above. The goal of that work was to expand on the efforts presented in Hawthorne and others (2013) which looked at the effects of CO_2 on hydrocarbon mobilization in Bakken shales and undifferentiated Middle Bakken samples. The efforts presented here made a point to develop permeation and extraction data for specific major lithofacies types within the Middle Bakken. Another hypothesis driving the work was that the advanced characterization data may help explain the permeation and extraction data generated by these experiments. To provide context for the CO_2 permeation and extraction experimental results, some of the results from Phase I described in detail in preceding sections of this report are described again in the following sections.

Core plug samples provided by the North Dakota Geological Survey and Marathon from the four study wells with Upper, Middle, and Lower Bakken units were submitted for routine core analysis, including porosity, permeability, and oil saturation measurements. A total of 32 plug samples from the shale and nonshale lithofacies of the Bakken Formation were subjected to CO_2 permeation and oil extraction experiments. The petrophysical characterization, CO_2 permeation and hydrocarbon extraction data for each of the plugs are shown in the data sheets provided in Appendix A. To streamline the presentation and discussion of the key results of these experimental

activities, this section will focus on results from a single well, the MT well. The average reservoir properties for each unit of the MT well can be found in Table 9. The rock properties of the Bakken in this well were also very similar to the properties of the rocks taken from the other three wells that provided samples for the advanced characterization; therefore, the insight gained from those activities can be directly applied to the rocks from the MT well. Six plugs representing the Lower Bakken Shale and the Middle Bakken lithofacies MB-L1, MB-L2, and MB-L3 were selected to investigate the ability of CO_2 to permeate these tight rocks and, subsequently, mobilize hydrocarbons.

Table 9. Reservoir Properties of Bakken Units from the MT Well*

Bakken Unit	Number of Plugs Analyzed	ϕ_{avg}, %	K_{avg}, mD	S_{o_avg}, %
UB	4	1.4	0.00075	62.2
MB-L5	3	4.4	0.031	54.3
MB-L4	15	4.4	0.0081	61.0
MB-L3	9	5.0	0.1035	62.0
MB-L2	15	5.3	0.0295	48.3
MB-L1	3	5.4	0.05	60.4
LB	3	3.8	0.00525	52.3

* ϕ_{avg}: average porosity; K_{avg}: average permeability; S_{o_avg}: average oil saturation.

CO_2 Permeation and Hydrocarbon Extraction Test Experimental Design and Setup

Compared to flow in conventional reservoirs, oil and gas move through the tight Bakken matrix via diffusion, which means it requires much more time to observe the oil recovery response than in traditional core flooding experiments (Hawthorne and others, 2013; Tovar and others, 2014; Wang and others, 2015). Therefore, small sample dimensions were used in order to observe the extraction response in a reasonable time. To mimic the oil recovery process in a real reservoir, the experimental pressure and temperature were set to reservoir conditions. Figure 38 shows the schematic of experimental setup for extracting hydrocarbon from Bakken shales. In contrast to conventional core flooding experiments, each core sample (1.1-cm diameter and approximately 4 cm in length, shown as Item 5 in the figure) was put loosely inside the extraction vessel (Item 6 with 1.5-cm diameter and 5.7 cm in length), which was placed into an ISCO Model SFX-210 supercritical extractor thermostatically controlled at 110°C. The pressure throughout the entire system was maintained at 34.5 MPa by an ISCO Model 260D syringe pump operated in the constant pressure mode. Hydrocarbons that were recovered were collected by opening the outlet control valve (see 8 in Figure 38) at certain intervals (hourly for the first 7 hours of exposure and an additional exposure up to 24 hours). The flow rate of CO_2 was controlled at 1.5 mL/min by the flow restrictor (see 9 in Figure 38), and about 2 cell void volumes (ca. 15 mL total) of CO_2 were purged into 15 mL of methylene chloride to collect the hydrocarbons recovered during each exposure time. Following the 24-hour CO_2 exposure, the rock sample was crushed to a fine powder and extracted with the aid of sonication three times in 20 mL of methylene chloride to recover the remaining hydrocarbons.

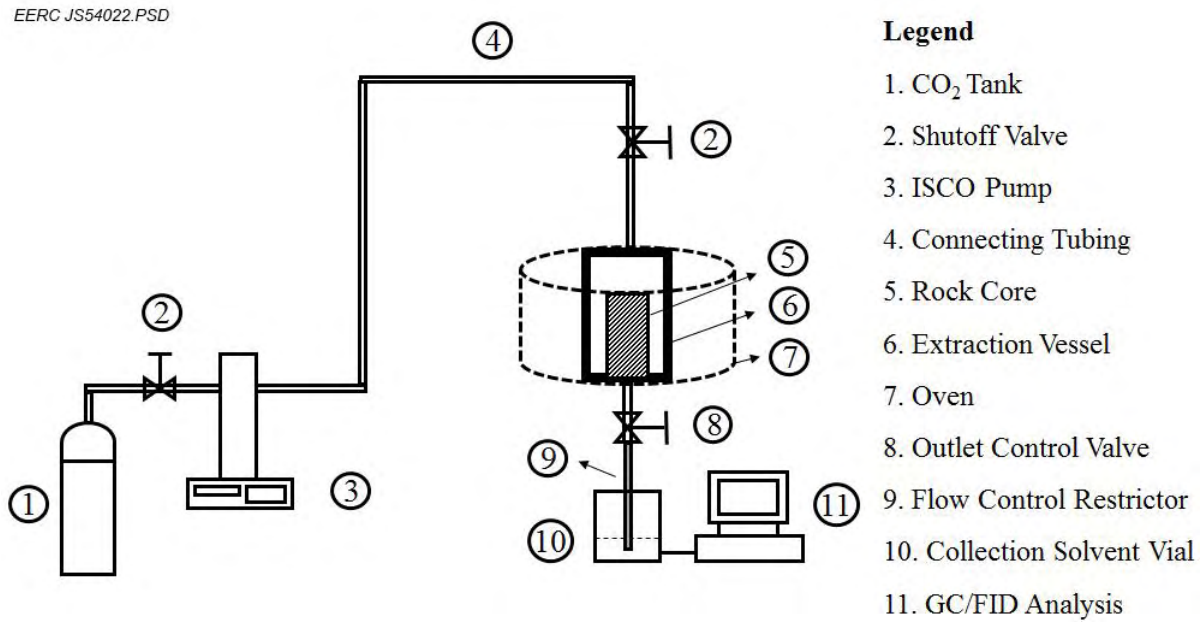

Figure 38. Schematic of experimental setup for extracting hydrocarbon from Bakken shales.

Percent recoveries are defined as the quantity of crude oil hydrocarbons found in the CO_2 extracts in comparison to the total oil hydrocarbons extracted by both CO_2 and by exhaustive solvent extractions. After the 24-hour CO_2 exposures of the 11.2-mm rods were completed, the rods were crushed to a fine powder, mixed with sodium sulfate as a drying/dispersing agent, and exhaustively extracted overnight in a sonicator bath with 1:1 methylene chloride/acetone. Multiple solvent extractions were performed until no detectable crude oil hydrocarbons were recovered to ensure that the sum of the CO_2-extracted hydrocarbons and those solvents extracted from the crushed rock residue are quantitative (i.e., 100% recoveries of the crude oil hydrocarbons from the rock matrix).

The reproducibility of the extraction and gas chromatography/flame ionization detection (GC/FID) analysis methods was tested by performing duplicate CO_2 extractions of rock core samples drilled adjacent to each other (i.e., from the same depth). The method showed excellent reproducibility; i.e., the recovery of oil for the duplicate rock extractions at 24 hours varied by <1% to 2% for each set of duplicate rock extractions from the same core locations. These results clearly demonstrate that 1) the method is reproducible and 2) 11-mm-diameter rock cores collected adjacent to each other are reproducible and are large enough to represent the rock matrix. Additional experimental details and discussion of the mechanism of hydrocarbon recovery have previously been published (Hawthorne and others, 2017).

Hawthorne and others (2013) and Jin and others (2016) showed that the extraction of oil from tight oil formation rocks cannot occur unless CO_2 or another gas first permeate the rock sample. Therefore, the experiments use hydrocarbon recovery over time as a proxy for estimating the ability of CO_2 to permeate the various Bakken lithofacies. Figure 39 shows the 24-hour oil extraction performance of CO_2 for the various Bakken samples. The results clearly demonstrate

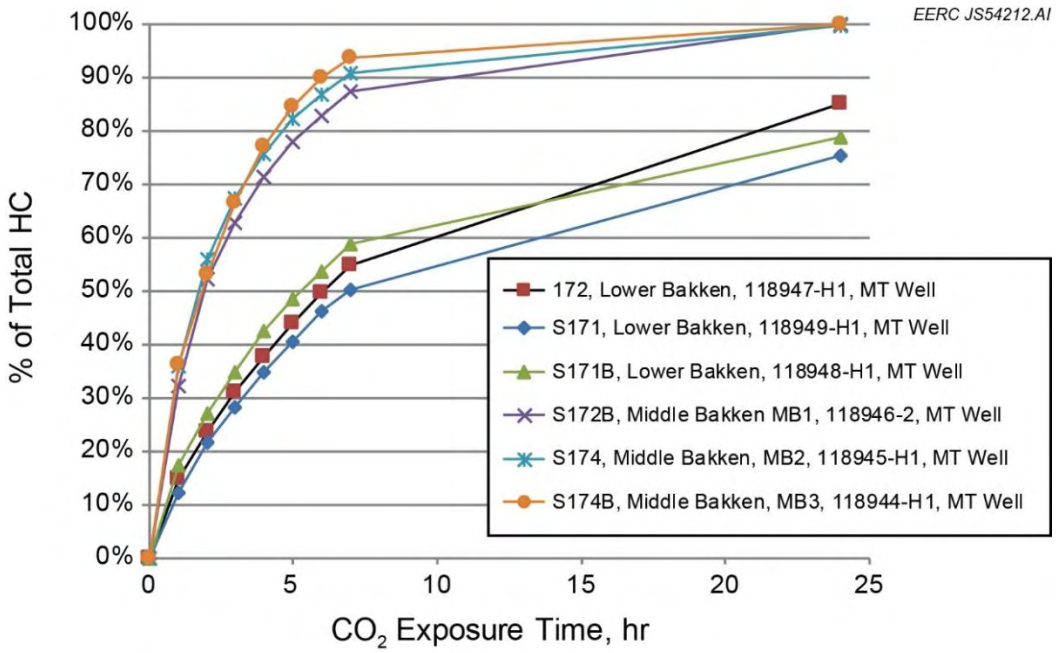

Figure 39. 24-hour oil recovery using different gases for the Middle Bakken cores from the MT well (modified from Hawthorne and others, 2017).

the ability of CO_2 to permeate all of the samples and subsequently mobilize oil. In the Middle Bakken samples, more than 90% of the oil was recovered from the plugs in 24 hours, while over 70% of the hydrocarbons were removed from the Lower Bakken Shale samples. For all of the samples, most of the hydrocarbon mobilization occurred within the first 8 hours of the experiment, with between 85% and 95% removed from the Middle Bakken samples and between 50% and 60% removed from the shales in that initial time period.

Oil recovery results for all of the rock samples from the four study wells and two wells from a previous study are summarized in Table 10, along with summaries of data. Hydrocarbon extraction curves for all of the tests are shown Figure 40. Figure 40 also shows the results from the Forth Berthhold well and the Corrine Olson well, which were used in previous extraction tests (Hawthorne and others, 2013), demonstrating the similarity of results between that study and this study. The same general oil recovery behavior is displayed by the rock samples from all six wells; i.e., all Middle Bakken lithofacies show considerably faster recoveries (averaging 94% to 100% after 24 hours) than both the Upper and Lower Bakken Shales (which average 40% and 43% recoveries after 24 hours, respectively). Some differences in the recovery rates in the Middle Bakken lithofacies may also exist. For example, after five hours of CO_2 exposures, average oil recoveries from two of the typically thicker, vertically adjacent Middle Bakken lithofacies were 84% for the nine samples of MB3 laminated siltstone compared to 74% for the seven samples of the MB2 burrowed lithofacies. This observation is consistent with the experiences and practices of Bakken operators, who typically consider the laminated lithofacies to be better targets for horizontal drilling and stimulation than the burrowed lithofacies. Although the number of rock samples for the MB1, MB4, and MB5 lithofacies is somewhat low to compare the recoveries, the 5-hour recoveries shown in Table 10 do indicate that the rates and extents of hydrocarbon recoveries for the Middle Bakken samples are similar.

Table 10. Summary of Crude Oil Recovery Achieved from 11.2-mm-Diameter Rock Rods Using CO_2 for the Seven Bakken Formation Lithofacies Investigated (note that T_{max} values may be unreliable because of poor S_2 yields during the Rock Eval)

			CO_2 Oil Recovery	
Facie		**Sample Depth, ft**	**5 hr**	**24 hr**
LBS	mean	10,893.04	22%	43%
LBS	min	10,632.00	5%	12%
LBS	max	11,183.70	38%	66%
LBS	n	12	12	12
MB1	mean	11,126.47	67%	97%
MB1	min	11,101.00	55%	94%
MB1	max	11,177.40	73%	99%
MB1	n	3	3	3
MB2	mean	10,775.44	74%	100%
MB2	min	10,612.20	63%	98%
MB2	max	11,168.60	92%	100%
MB2	n	7	7	7
MB3	mean	10,867.10	84%	100%
MB3	min	10,603.00	75%	99%
MB3	max	11,155.50	95%	100%
MB3	n	9	9	9
MB4	mean	11,093.03	76%	97%
MB4	min	11,067.10	61%	96%
MB4	max	11,141.50	88%	99%
MB4	n	3	3	3
MB5	mean	10,592.48	70%	100%
MB5	min	10,589.75	62%	100%
MB5	max	10,595.20	78%	100%
MB5	n	2	2	2
UBS	Mean	10,768.32	19%	40%
UBS	min	10,576.25	9%	18%
UBS	max	11,056.90	35%	67%
UBS	n	8	8	8

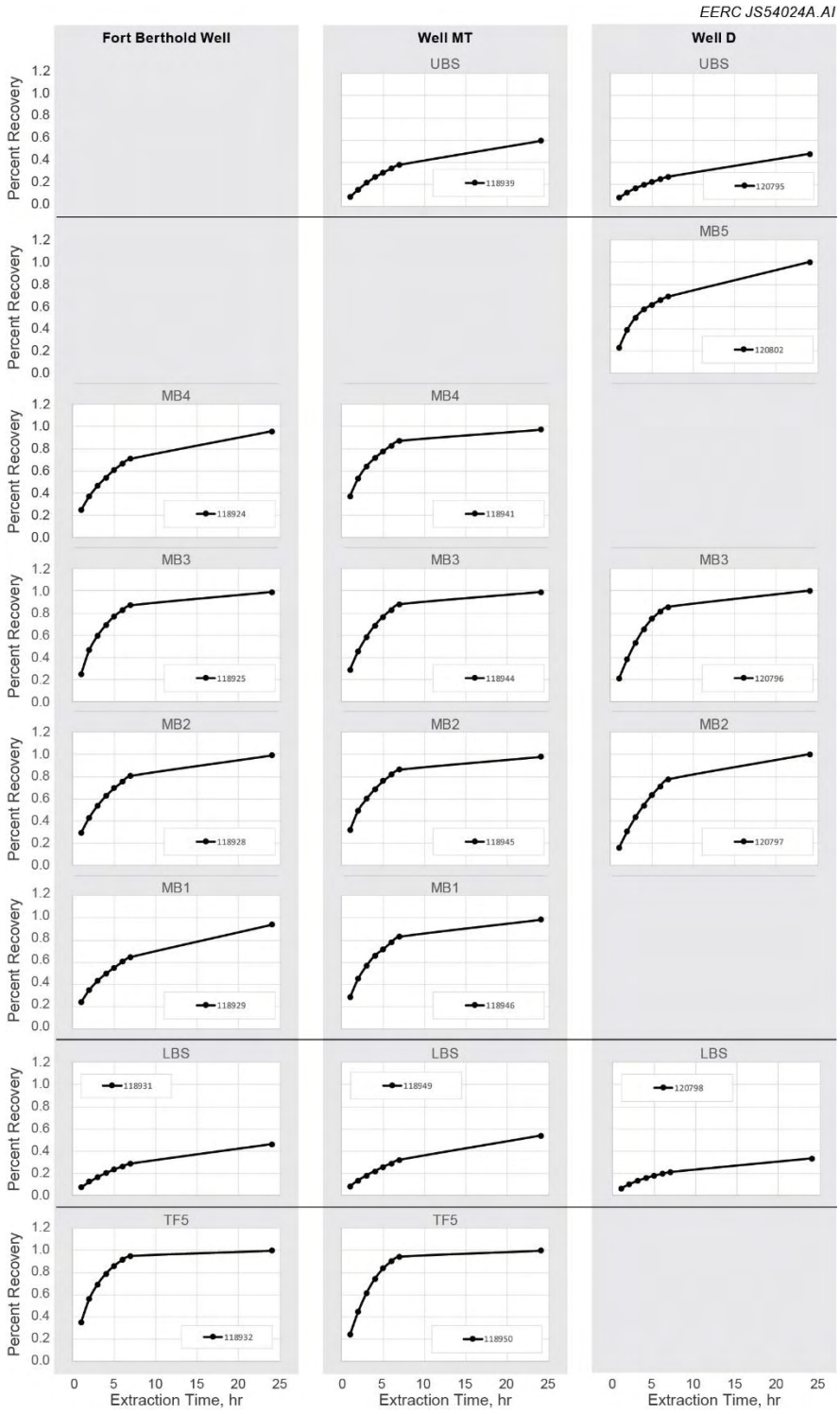

Figure 40. Hydrocarbon recovery curves generated by CO_2 permeation and hydrocarbon extraction tests. Percent recovery refers to the percentage of the hydrocarbon fraction removed by CO_2. Each column represents a well and each row represents a lithofacies (top to bottom: Upper Bakken Shale, MB-L5, MB-L4 packstone, MB-L3 laminated, MB-L2 burrowed, MB-L1, Lower Bakken Shale, and Three Forks 5 [TF5]) (continued).

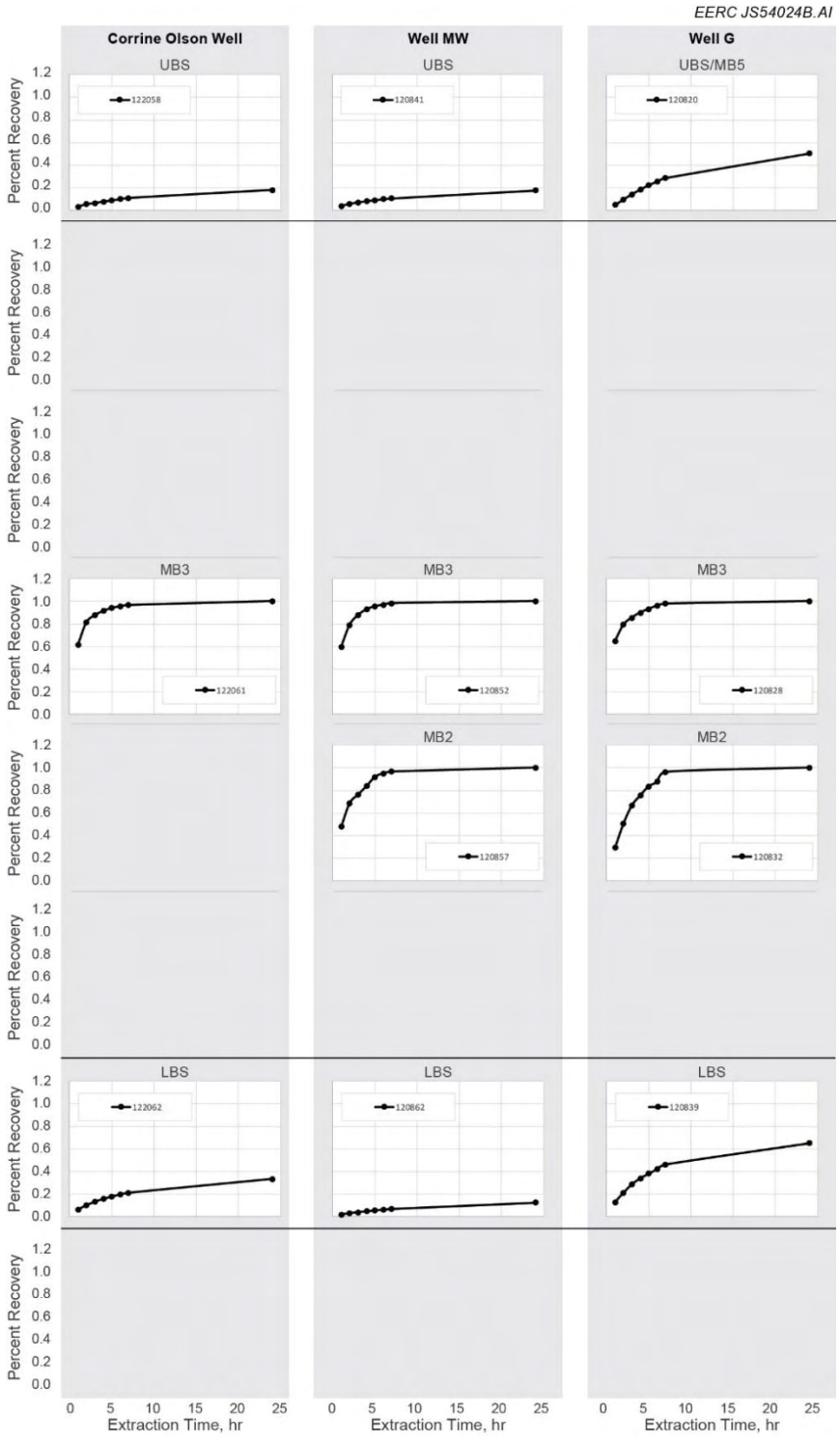

Figure 40. (continued). Hydrocarbon recovery curves generated by CO_2 permeation and hydrocarbon extraction tests. Percent recovery refers to the percentage of the hydrocarbon fraction removed by CO_2. Each column represents a well and each row represents a lithofacies (top to bottom: Upper Bakken Shale, MB-L5, MB-L4 packstone, MB-L3 laminated, MB-L2 burrowed, MB-L1, Lower Bakken Shale, and Three Forks 5 [TF5]).

Petrophysical and mineralogical results to date are also summarized in Table 10. Not surprisingly, there are large differences in TOC between the Upper and Lower shale source rocks and the nonshale Middle Bakken reservoir rocks. For the Middle Bakken samples, the TOC values agree reasonably well with the oil concentrations found in the CO_2 extraction results, with little evidence of organic carbon other than crude oil that had migrated from the source shales. In contrast, the Upper and Lower shales both averaged 12 wt% TOC, of which ca. 1–2 wt% is contributed by crude oil hydrocarbons, with the remaining ca. 10 wt% attributed to kerogen or other nonextractable organic material.

In addition to TOC/kerogen values, there are other obvious differences between the source shales and the Middle Bakken and Three Forks reservoir rocks, as shown in Table 8. For example, as would be expected, the clay content of the shales is substantially higher than the reservoir rocks, which may contribute to somewhat slower oil recoveries since clays may act as weak sorbents for the oil hydrocarbons. More strikingly, the mean pore throat radius for the Upper and Lower shales are 3.2 and 3.3 ***nanometers***, which is approaching the molecular size of the heavier crude oil hydrocarbons. This contrasts with the MB-L2 and MB-L3 which have mean pore throat sizes of 11 and 17 nanometers, respectively.

Based on these results, we speculate that either the differences in pore throat size or the potential for kerogen content in the shales (or both characteristics) could explain the much slower oil recovery rates for the shales as compared to the nonshale Middle Bakken during CO_2 exposure. The very tiny pore throats in the shales could inhibit CO_2 penetration into the pores and hydrocarbon migration out of the pores by simple size exclusion. For perspective, note that since a CO_2 molecule is about 0.34 nm long, ten CO_2 molecules could "hold hands" and reach both sides of typical shale pore throats. Alternatively, the kerogen matrix in the shales (which is absent in the Middle Bakken) could act as a chemisorbent for the crude oil hydrocarbons and thus retard their solubilization and migration by CO_2 while also enhancing the ability of the shales to store CO_2. In either case (or a combination of both), a much better understanding of these processes would aid in exploiting them for EOR and, possibly, CO_2 storage, both in the reservoir rocks and (potentially) in the shales.

While the oil recovery rates from the shales were much smaller than those from the Middle Bakken lithofacies, the fact that so much of the residual oil was extracted from the shales given the extremely small mean pore throat radius was unexpected. FESEM imagery of the Bakken shales collected by Ingrain in collaboration with the EERC suggests the presence of relatively large (when compared to mean pore throat radius) fracture networks that occur within the organic components of the rock (Figure 41). Similar features have been documented in other investigations of organic-rich shales and are thought to be formed as a result of swelling that occurs during the thermal maturation process and subsequent shrinkage following oil expulsion (Er and others, 2016; Loucks and others, 2009, 2012). The fact that the fracture networks occur within the organics, coupled with the fact that the organic material itself may have nanoscale porosity (Loucks and others, 2009, 2012; Bousige and others, 2016) has important implications that may explain the mechanism by which CO_2 is able to access the organics and extract residual hydrocarbons so

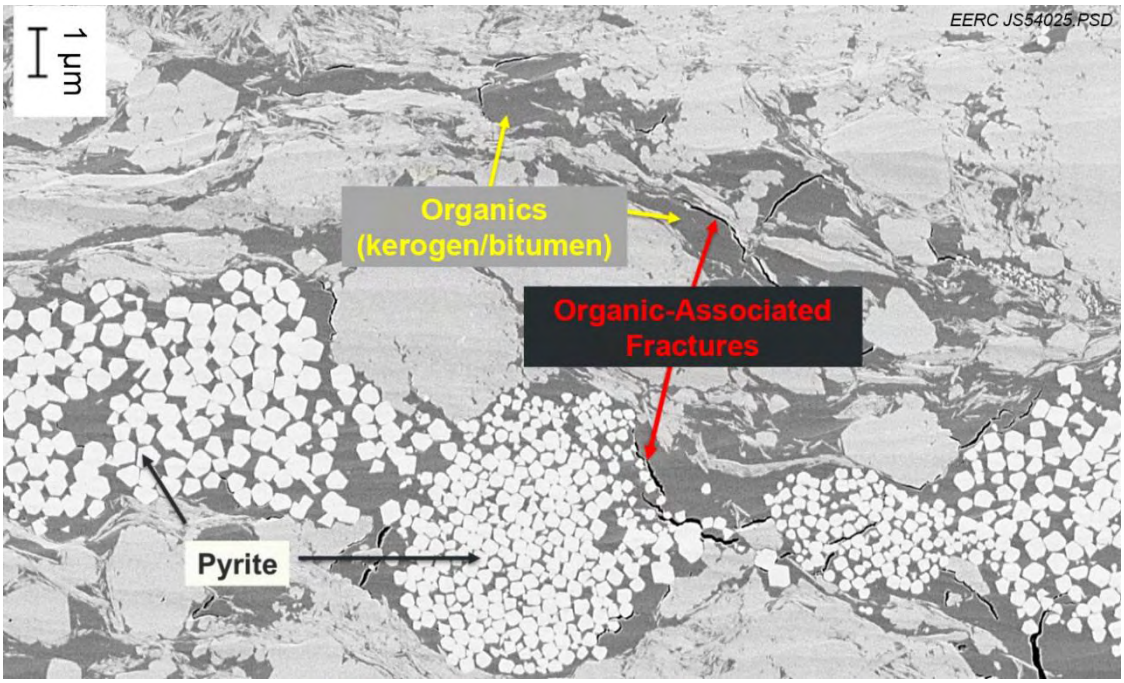

Figure 41. An FESEM image of the Upper Bakken Shale (collected by Ingrain). The black areas of the image are void space, the dark gray is organic matter, the lighter gray represents mineral matter, and the white clusters are pyrite (Hawthorne and others, 2017). Courtesy of Ingrain Inc., modified.

readily. This also has implications for both CO_2 EOR and storage in organic-rich shales and highlights the need to better understand the mechanisms of CO_2 migration through the organic portions of the rock as a function of organic type (i.e., kerogen vs. bitumen) and thermal maturity. It is also important to better understand CO_2 adsorption and/or absorption onto the organics as a function of organic type and thermal maturity.

STATISTICAL ANALYSIS OF EXTRACTION AND CHARACTERIZATION DATA

A statistical analysis of the CO_2 extraction and rock core characterization data was conducted in an effort to identify 1) significant differences in hydrocarbon extraction rates among samples collected from the Middle Bakken lithofacies and 2) potential correlations between the rock core characterization measurements and extraction rates, which may provide insight into mechanisms controlling CO_2 permeation and hydrocarbon mobility. While there are no rock characterization data sets in the literature that are as robust or comprehensive in their scope (i.e., number of wells, geographic distribution of the wells, number of samples and vertical distribution of samples from each well, types of analyses, etc.), the number of samples used in this analysis is still relatively low, which limits the ability to infer significant differences or correlations. In statistical hypothesis testing, this is known as having low statistical power and therefore a greater likelihood of making a Type II Error – failure to detect a significant effect when one is present. This is particularly true when trying to make comparisons between different lithofacies of the Middle Bakken, where small

sample sizes for each lithofacies make it challenging to assess statistical significance. The work conducted under this project should therefore be considered exploratory with respect to determining the factors controlling CO_2 movement and hydrocarbon mobility within tight oil formations. These initial findings provide a screening-level assessment to identify possible trends or correlations that can be examined more closely in the future.

As shown in Figure 40 from the previous section, the percent recovery of hydrocarbons increases as a function of time, resulting in a nonlinear extraction curve over a 24-hr period for each sample. The statistical analysis simplified these curves into three metrics to describe the extraction rate: 2-hr, 5-hr, and 7-hr percent recovery. Samples with faster recovery rates (steeper curves) have greater percent recovery at 2, 5, and 7 hours into the 24-hr extraction. In addition to these three metrics, the statistical analysis fit a nonlinear function to the extraction curve for each sample and then evaluated the slope parameter of that function, θ3, as a proxy for the extraction rate.[1] These four parameters: 2-hr, 5-hr, 7-hr, and θ3, provided the basis for comparing extraction rates among samples. Figure 42 presents results compiled from Kruskal–Wallis tests, which are nonparametric one-way analysis of variance (ANOVA) statistical tests. The Kruskal–Wallis test is used for comparing two or more independent samples of equal or different sample sizes (Corder and Foreman, 2009). For the nonshale Middle Bakken samples, the differences in rates of hydrocarbon recovery were not statistically significant (*p*-values greater than 0.05) between samples collected from MB5 through MB1. However, the data suggest that MB2, MB3, and MB4 as a group (MB4/3/2) have greater hydrocarbon extraction rates than the upper or lower lithofacies, MB1 and MB5 (MB5/1). These results are consistent with the fact that the MB3 and MB4 lithofacies, referred to as the laminated zone and packstone zone, respectively, are the most frequently targeted zones for horizontal drilling. However, the median extraction rates in MB3 and MB4 samples are only 4% to 5% greater than those for samples from other Middle Bakken lithofacies, and the small number of samples combined with the inherent uncertainty of the precision of the extraction method suggests that the statistical difference in extraction rates between the various Middle Bakken samples may not be meaningful. These statistics could be interpreted to suggest that there is validity to the lumping of Middle Bakken lithofacies for simulation purposes. However, the differences in key properties such as mineralogy and fracture characteristics that have been described in earlier sections suggest that keeping those lithofacies separate within a model is also valid. The choice to separate or lump the lithofacies in a modeling exercise will be dependent on the questions that are being addressed by those exercises.

While the statistical analysis suggested there was little significant difference in extraction rates between Middle Bakken lithofacies, some physical properties did correlate with higher rates of hydrocarbon recovery. Figure 43 shows the Spearman rank correlation (Spearman's *rho*) between the different rock core characterization measurements and either θ3 or 5-hr percent recovery. Spearman's *rho* is a nonparametric measure of correlation, similar to Pearson's *r* (Helsel and Hirsch, 2002). A perfect negative correlation between two variables would have a Spearman's *rho* of -1; a perfect positive correlation would have a Spearman's *rho* of +1; and two variables with no correlation would have a Spearman's *rho* of zero. Figure 43 highlights significant positive correlations in green and significant negative correlations in red. Based on these results, the

[1] The nonlinear function used was % Recovery = θ1 + θ2 * [1 − exp(−θ3 * Time)], where θ1, θ2, and θ3 are fitted parameters, and Time is the hour associated with a specific % Recovery (i.e., 1, 2, 3, 4, 5, 6, 7, or 24 hours).

EERC JS54072.AI

Facies	N	Median$_{2\text{-hr}}$	Median$_{5\text{-hr}}$	Median$_{7\text{-hr}}$	Median$_{\theta 3}$
MB5	3	0.436	0.700	0.792	0.268
MB4	7	0.531	0.776	0.871	0.399
MB3	9	0.489	0.783	0.885	0.331
MB2	3	0.320	0.695	0.808	0.269
MB1	2	0.449	0.720	0.833	0.296
p-value		0.363	0.129	0.159	0.282

Facies	N	Median$_{2\text{-hr}}$	Median$_{5\text{-hr}}$	Median$_{7\text{-hr}}$	Median$_{\theta 3}$
MB5/1	5	0.449	0.720	0.833	0.296
MB4/3/2	19	0.489	0.770	0.871	0.331
p-value		0.271	0.070	0.082	0.126

Figure 42. MB differences are not "statistically significant."

EERC JS54073.PSD

= positive correlation, *p* -value <=0.1

= negative correlation, *p* -value <=0.1

MB5-MB1 data set

Measurement	θ_3	%Recovery (5-hours)
TOC	-0.089	-0.132
S1	-0.294	-0.330
S2	0.211	0.207
S3 CO2	0.311	0.302
S3 CO	0.023	0.046
Tmax	0.086	0.056
HI	0.497	0.560
OI	0.250	0.269
PI	-0.273	-0.336
OSI	-0.114	-0.128
HPMI-MIPC R35	0.532	0.630
HPMI-MIPC Mean Throat	0.561	0.624
HPMI-MIPC Max Sb Pc	0.418	0.496
Quartz	0.095	0.227
Alkali-Feldspar	0.576	0.509
Plagioclase	0.331	0.158
Clays	-0.120	-0.210
Carbonates	-0.174	-0.158
Accessory Mineral	-0.336	-0.500

MB4-MB2 data set

Measurement	θ_3	%Recovery (5-hours)
TOC	-0.104	-0.127
S1	-0.265	-0.304
S2	0.238	0.223
S3 CO2	0.319	0.352
S3 CO	0.288	0.311
Tmax	-0.017	-0.153
HI	0.409	0.473
OI	0.212	0.263
PI	-0.112	-0.176
OSI	-0.118	-0.127
HPMI-MIPC R35	0.566	0.621
HPMI-MIPC Mean Throat	0.582	0.609
HPMI-MIPC Max Sb Pc	0.372	0.361
Quartz	-0.091	-0.025
Alkali-Feldspar	0.715	0.713
Plagioclase	0.378	0.240
Clays	-0.510	-0.659
Carbonates	-0.041	-0.047
Accessory Mineral	-0.101	-0.242

Figure 43. Correlations: %recovery and core measurements.

following physical properties showed significant correlations with hydrocarbon extraction rates: hydrogen index (HI) which is an indicator of thermal maturity, mean pore throat size which is an indicator of permeability, maximum volume of mercury (Sb) to capillary pressure (Pc) ratio (Sb Pc) which is an indicator of fluid saturations and recovery efficiency, and the content of noncarbonate minerals (i.e., higher content of feldspar) which is an indicator of depositional environment. The data also suggest that the presence of higher concentrations of accessory minerals and clays may have a negative effect on hydrocarbon recovery. This conclusion is consistent with the results of characterization activities in Phase I, which indicate that naturally occurring microfractures, which in some lithofacies are the dominant flow pathways, can be substantially filled with clays and accessory minerals such as pyrite.

Effect of CO_2 Volume on Crude Oil Recovery from Middle Bakken and Upper and Lower Shales

All of the Bakken rock extractions with CO_2 performed to date support the "soaking" mechanism rather than the "flushing" mechanism that predominates in conventional EOR floods. In addition to hydrocarbon swelling and lowered crude oil viscosity that occurs upon CO_2 contact, the soaking mechanism that controls ultimate hydrocarbon recovery production from tight unconventional rocks is based on concentration gradient-driven diffusion of the hydrocarbons from the saturated CO_2 in the rock to the less saturated CO_2 in the surrounding interstitial spaces. Thus the volume of CO_2 that is used to expose rock samples could affect the rate and efficiency of hydrocarbon recovery. In addition, field operations will necessarily limit the CO_2 available to extract crude oil hydrocarbons, both because of the geometry of the fracture network as well as available CO_2 injectant.

In the standard extraction tests, 11.2-mm-diameter round rods having a total volume of ca. 5 mL were exposed in a 10-mL cell to CO_2 in seven 1-hour increments followed by one additional increment from 7 to 24 hours. This procedure resulted in ca. 5 mL of supercritical CO_2 (5000 psi and 110°C) surrounding the rock samples for each exposure increment for a total of ca. 40 mL of CO_2 for each 24-hour extraction, not including the small volume of CO_2 that permeates the rock samples. Note that the CO_2 volume used to sweep the produced hydrocarbons at each of eight sampling events is not included, since the time the rock is exposed to this sweep is minimal.

Since these volumes of CO_2 to rock ratios are likely higher than those that will exist in a fractured tight reservoir, we manufactured an extraction cell that had an inner diameter of only 11.3 mm, so that the 11.2-mm-diameter round rock rods fit snuggly into the cell. Any remaining volume was filled with an 11.2-mm-diameter Teflon round plug rod so that the entire volume of CO_2 used to expose the rock samples was only ca. 0.08 mL per exposure time, for a total of only ca. 0.6 mL (again, ignoring the volume of CO_2 that permeates the rock).

The results of limiting the CO_2 volume used for each 24-hour exposure on an Upper and Lower Bakken Shale and a Middle Bakken rock core are shown in Figure 44. Note that, for the Middle Bakken rock core, there was no distinguishable difference in the crude oil recovery rates achieved with the high volumes of CO_2 and with the very low (and more realistic from a reservoir standpoint) volume of CO_2 (Figure 44). Even with the Bakken shale cores, there was only a small loss in the recovery rate; i.e., the total oil recovery after 24 hours for the Upper Bakken shale was reduced from 80% to 64% when the volume of CO_2 was reduced, and the recovery from the Lower Bakken shale was only reduced from 74% to 59%. These results clearly demonstrate that hydrocarbon recovery does not require unrealistically high amounts of CO_2, either from the Middle Bakken or the Upper and Lower Bakken Shales.

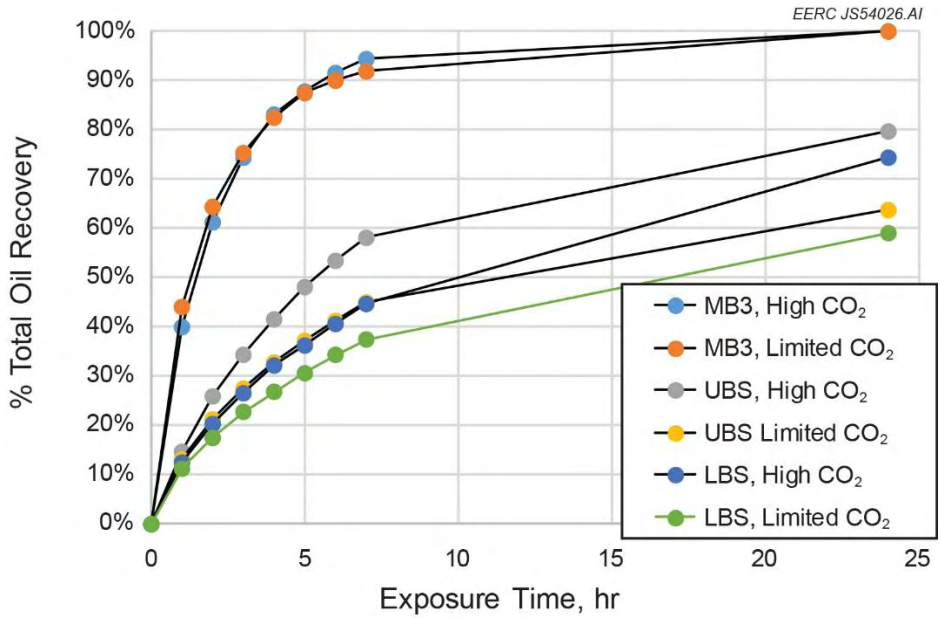

Figure 44. Total crude oil hydrocarbon recovery from 11.2-mm-round rock rods using a high volume of CO_2 (ca. 40 mL over 24 hours) or a low volume of CO_2 (ca. 0.6 mL over 24 hours).

Comparison of Crude Oil Hydrocarbon Recovery with Extended Slow Heating Rock Eval Characterization

Crude oil recoveries reported for the CO_2 extractions of Bakken rock samples are based on crushing the rock sample to a fine powder after the CO_2 exposure and then exhaustively extracting the sample with 1:1 methylene chloride/acetone until no more hydrocarbons can be detected. Each of the CO_2 fractions and the rock residue solvent extractions are analyzed by high-resolution GC/FID for the C7 to C36 range hydrocarbons. Crude oil recoveries are based on the sum of all CO_2 fractions and the rock residue solvent extractions defined as 100%.

Although this procedure yields a valid quantitative definition of the hydrocarbon recoveries achieved with CO_2, we compared the selectivity and efficiency of the CO_2 extractions to recover mature crude oil hydrocarbons (in contrast to kerogen/bitumen components) with a thermal pyrolysis procedure more commonly used in the industry, i.e., Rock Eval. As previously discussed, ESH Rock Eval analysis is much more suitable for tight shales than the conventional Rock Eval procedures. As such, ESH Rock Eval analysis was used to evaluate Bakken rock samples before and after CO_2 exposure (Sanei and others, 2015). In the extended Rock Eval, the hydrocarbons are characterized by S1 or "light oil" fractions, S2a or "heavy oil," and S2b or "bitumen." Since CO_2 is expected to extract only crude oil hydrocarbons and not the kerogen/bitumen matrix, the extended Rock Eval test should show nearly complete loss from the CO_2-exposed rock samples of the S1 light oil content, removal of the majority of the S2a heavy oil content, and little or no removal of the S2b bitumen content.

As shown in Table 11, the CO_2 extractions very efficiently recovered the S1 light oil fraction from all four Bakken lithofacies tested, including the reservoir Middle Bakken rocks and from the Upper and Lower Bakken Shale source rocks. Similarly, the CO_2 extractions removed the majority of the S2a heavy oil fractions, especially from the Middle Bakken reservoir rock samples. Somewhat lower recovery (64% and 77%) of the S2a fraction hydrocarbons from the Upper and Lower Bakken Shales was achieved with the CO_2 extractions, most likely since the pyrolysis temperatures used for the S2a fraction measures some shale organics that are only partially thermally mature and have not become the saturated hydrocarbons that make up the bulk of Bakken crude oil. In any case, these results clearly demonstrate that the CO_2 extractions are both very selective and quantitatively efficient for recovering thermally mature crude oil hydrocarbons from both the reservoir and source rock shales from the Bakken system.

Table 11. Comparison of Extended Rock Eval Hydrocarbon Characterization of Bakken Rock Samples with the Hydrocarbons Extracted Using Supercritical CO_2

	Light Oil (S1), wt%	Heavy Oil (S2a), wt%	Bitumen (S2b), wt%	TOC, wt%	Oil, vol%	FHR, vol%	Bitumen, vol%
Upper Bakken Shale							
Before Extraction	0.14	0.69	9.55	10.38	2.69	2.24	17.74
After Extraction	0.01	0.25	9.5	9.76	0.86	0.81	17.63
% Removed by Extraction	0.90	0.64	0.01	0.06	0.68	0.64	0.01
Middle Bakken Reservoir							
Before Extraction	0.0601	0.19	0.31	0.56	0.8	0.61	0.58
After Extraction	0.0006	0.01	0.33	0.34	0.03	0.03	0.61
% Removed by Extraction	0.99	0.95	-0.06	0.39	0.96	0.95	-0.05
Lower Bakken Shale							
Before Extraction	0.1714	0.94	10.71	11.82	3.6	3.05	19.89
After Extraction	0.0125	0.22	9.37	9.6	0.74	0.7	17.41
% Removed by Extraction	0.93	0.77	0.13	0.19	0.79	0.77	0.12

CO_2 ADSORPTION AND STORAGE POTENTIAL IN THE BAKKEN SHALES

Figure 45 is an illustration of the small pore spaces ($r_{35} \leq 5$ nm) in the shale samples. Before CO_2 extraction, a considerable part of the hydrocarbon molecules exist in an adsorbed state in these nanometer-scale pores, and the volume of oil-filled pores occupied by free fluid is less than 40% based on molecular dynamics simulation using the Bakken's petrophysical properties (Wang and others, 2015).

Figure 45 also shows a schematic of oil and gas distribution in a kerogen pore where the movable oil and gas are recoverable in the extraction process while the adsorbed oil may stay in the pore (Wang and others, 2016; Alvarez and Schechter, 2017). The oil layer adsorbed on the

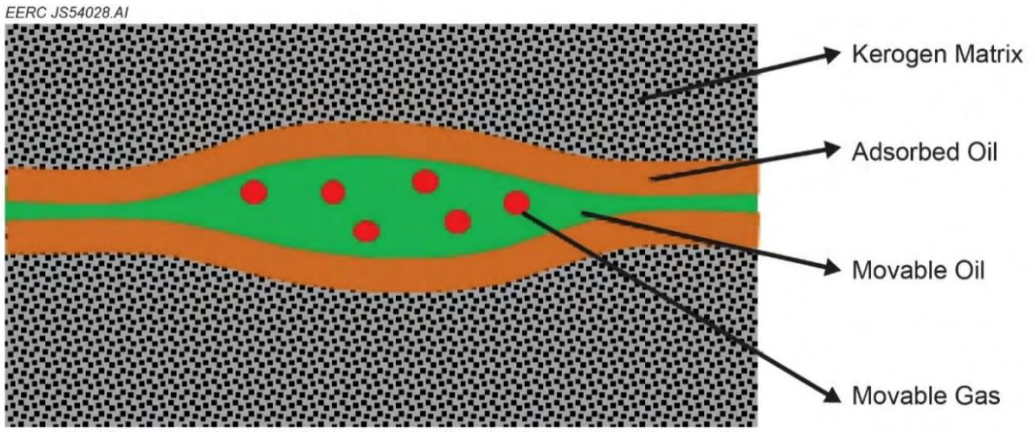

Figure 45. Schematic of oil and gas distribution in kerogen. The radius of the pore throat (orange and green portion in the center of the figure) is 5 nm or less.

pore wall also makes the kerogen more oil-wet, which was demonstrated by various wettability studies of Bakken rocks (Wang and others, 2012, 2016). The percentage of adsorbed oil decreases with increasing pore size.

The pore structures and porosity distribution in shale are usually complicated because of the existence of finely dispersed kerogen (Yin and others, 2016) and/or bitumen (Hackley and Cardott, 2016). Figure 46 shows an image of organic material (either kerogen or bitumen) in a lower Bakken sample captured by FESEM. This image clearly shows the complex pore structures and size distribution in the organic matter. High-pressure mercury injection capillary pressure (MICP) measurements indicate that most of the pore throat radii in kerogen and bitumen are usually very small ($r \leq 4$ nm), as shown in Figure 46. Such small pore throats induce high capillary pressure between phases when oil, gas, and water coexist in the core. The smaller the pore throat size, the more difficult it is to overcome capillary resistance between phases. These mechanisms make it difficult to recover oil from the shales using conventional methods.

Experimental studies on various gas shales have shown that CO_2 is preferably adsorbed by kerogen over other gas components based on comparison of adsorption isotherms (Liu and others, 2013; Heller and Zoback, 2014; Tang and others, 2015, 2016; Guo and others, 2017). However, the CO_2 adsorption behavior has not been studied for the Bakken shales under reservoir conditions. Therefore, a lower Bakken shale sample was selected to measure the CO_2 adsorption isotherm under reservoir temperature (110°C) and covering a wide range of pressures (0–40 MPa). Figure 47 illustrates that the Bakken shale has a considerable ability to adsorb CO_2 under reservoir conditions. The CO_2 adsorption increases with pressure quickly under 13 MPa and then stabilizes around 14 mg/g (CO_2/rock) from 14 to 28 MPa. The maximum adsorption could reach to 17 mg/g when pressure approaches 40 MPa. During the adsorption process, the high surface area of the nanoporous structure in the organic-rich shale appears to act to preferentially adsorb CO_2 and displace oil from the pores in the shale.

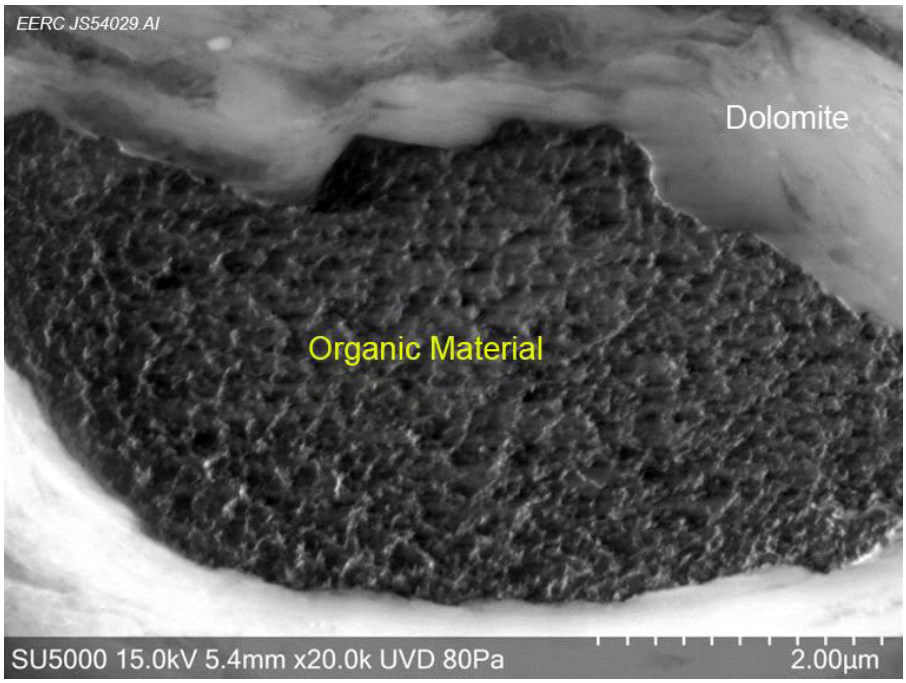

Figure 46. Organic material structure and pore profiles in a lower Bakken sample.

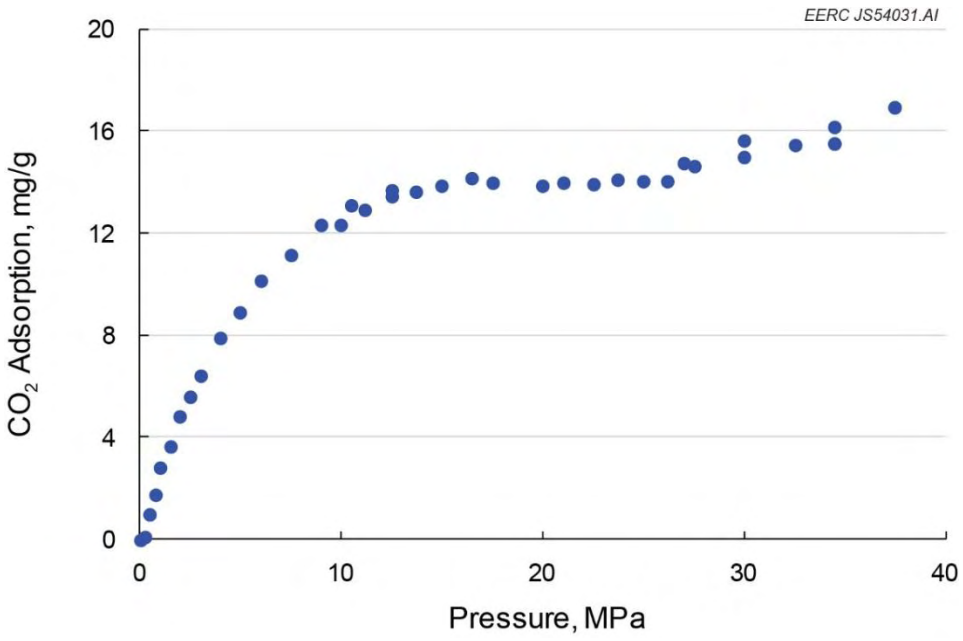

Figure 47. CO_2 adsorption in a Lower Bakken Shale sample at 110°C.

The tremendous gas reserves in the shale gas reservoirs indicate that gas can be trapped permanently in shales because of adsorption in its finely dispersed organic matter (Kang and others, 2011; Li and Elsworth, 2015). This adsorption characteristic will also allow CO_2 to be stored in shale reservoirs for millions of years without the concerns of sealing failure or leakage. As a world-class hydrocarbon-bearing shale formation, the Bakken shales occupy about 520,000 km^2 of the subsurface of the Williston Basin, underlying parts of Montana and North Dakota in the United States and Saskatchewan and Manitoba in Canada. Data from the current producing wells show that the thickness of Upper and Lower Bakken Shales varies around 20 m. Therefore, the potential for application of this principle is very large and may result in many millions of barrels of additional oil recovery and many millions of tons of CO_2 permanently stored.

CO_2 PERMEATION IN THE BAKKEN SHALES AND RESERVOIR ROCKS

The use of CO_2 soluble tracers to evaluate CO_2 permeation rates and flow patterns (e.g. via microfractures and interconnected pores) in both Bakken shales and Middle Bakken reservoir rocks was attempted. Core plug samples were subjected to the same conditions as the extraction experiments described above, but with tracers added to the CO_2. Tracers that were used in the experiments were rhodamine, organometallics (e.g., tetraethyltin), and bromine-containing organics (e.g., 4-bromobiphenyl, 4-bromotoluene) at reservoir conditions of 110°C, and 5000 psi CO_2. 100 to 500 uL of the test tracers were placed in the bottom of a reactor cell with the rock sample suspended above the tracer on a glass vial to ensure that the rock samples were exposed only to CO_2-dissolved tracers. After 24 hours of exposure, the reactor was cooled to room temperature and the CO_2 was vented to ambient conditions. The 11-mm-diameter rock rod samples were cut cross-wise in half, and attempts were made to observe the organic dyes with both visible and UV light. Unfortunately, the rock matrix made it impossible to view any significant response. Similarly, the rock samples exposed to the organometallic and bromo-organic tracers were cut in half, and attempts to observe the presence of bromine (or the metal center of the organometallics) by SEM were not successful, and it was later shown that the tracer species that were sufficiently soluble in CO_2 were too volatile to remain on the exposed rock in the vacuum necessary for the SEM analyses.

Other experimental attempts to determine CO_2 permeation rates in Bakken shales and Middle Bakken reservoir rocks tried to use an approach in which a cylindrical rock sample would be exposed to CO_2 in a high-pressure vessel, and the appearance of CO_2 into a hole drilled through the center of the core would be monitored. The concept for the experiment was that argon or nitrogen back pressure would be applied to the hole in the center of the sample through a fitting sealed to the top of the rock sample, while CO_2 completely surrounds the rock core on the outside. The gas composition exiting the hole in the center of the rock sample would then be monitored for CO_2 appearance, and the appearance profile would then be used to determine CO_2 permeation rate. Unfortunately a combination of sample brittleness, which made drilling the hole without creating fractures in the plug difficult, and difficulties in maintaining the top seal resulted in poor experimental results. A decision was then made to use a more traditional steady-state flow-through experiment to determine CO_2 permeation rates in Bakken shale and Middle Bakken reservoir plug samples.

Bakken Shale Flow-Through CO_2 Injectivity Testing

To better understand the potential injectivity and migration of CO_2 within a Bakken Shale sample for comparison to the static CO_2 extraction tests, a CO_2 permeation study was conducted using a flow-through testing configuration on a plug sample obtained from the Upper Bakken Shale. Because it was demonstrated that CO_2 can be effective at mobilizing hydrocarbons in tight matrix organic-rich shales (Hawthorne and others, 2013), the question remained as to the mechanism for fluid movement and implications for larger-scale CO_2 EOR schemes and associated storage.

The sample tested was obtained from the Upper Bakken Shale interval within a geographic location of the Williston Basin considered to be thermally mature. The plug was 30 mm in diameter and had a length of 30 mm. Rock Eval pyrolysis provides a T_{max} value of 452°C and vitrinite reflectance equivalent (VRo_{eq}) of 0.97%. Based on the work of Dow (1977), these values place the organic matter within the oil generating window. This is supported with the high Rock Eval values of free light hydrocarbon, heavy hydrocarbon, and kerogen (S1 and S2 peaks respectively) and confirms that the shales of the Bakken have excellent source rock potential. Table 12 provides Rock Eval and petrophysical properties for the sample.

Table 12. Rock Eval and Petrophysical Properties

Sample No.	Depth, ft	SRA[1] TOC	S1	S2	S3	T_{max}, °C	% Ro	HI	OI	Porosity, %*	Permeability,[2] nD
118938	11,053	9.62	7.30	13.05	0.41	452	0.97	136	4	9.0	0.06

[1] Source rock analysis.
[2] Based on results of routine core analysis.

The experiment was conducted using a temperature-controlled high-pressure test apparatus. The plug was weighed and loaded into a CO_2-resistant sleeve consisting of an inner layer of Teflon, middle layer of lead, and outer layer of Teflon. The inner sample assembly was inserted into a thick rubber gasket to distribute the confining pressure load evenly across the sample. This was then loaded into a high-pressure (10,000 psi) Hassler-style core holder and placed into a temperature-stable convection oven (Figure 48).

With the core holder in place, the injection and receiver side of the system were plumbed into computer-controlled syringe-style pumps capable of running in constant pressure and flow rate modes. The injection pump contained over 200 mL of supercritical CO_2, while the back end pump had a minimal volume to maintain pressure and to ensure that there was enough volume to receive the injected fluid. Care was taken to minimize all tubing lengths to reduce the system volume in anticipation of the very low flow rates and volumes to be used. After plumbing, the oven was adjusted to 160°F and maintained during a series of long-duration leak checks performed to ensure that no fluid was lost to the oven enclosure. Figure 48 shows the core holder and gasket assemble and Figure 49 shows a schematic diagram of the flow-through system.

At the onset of testing, 5000-psi pressure was applied to the inlet side of the sample while the outlet side was adjusted to 4600 psi, resulting in a 400-psi differential pressure. Throughout

Figure 48. Inner gasket assembly and Hassler-style core holder.

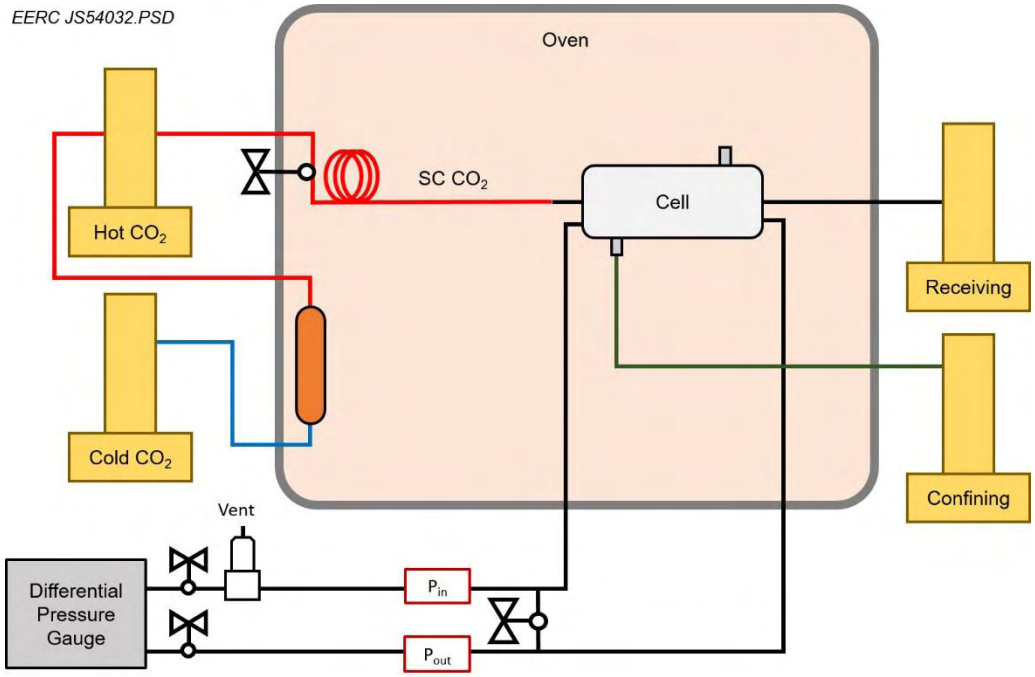

Figure 49. Schematic diagram illustrating the flow-through system as it was configured for low-flow testing.

the test, this differential pressure was not changed. Data collected during testing included injection and receiver pump volume, flow rates, and pressures. Because the pump transducers are prone to drifting, the system pressure was monitored at the core inlet and outlet faces using high accuracy pressure/temperature transducers. Data generated throughout the testing period were collected at a predetermined interval using a data acquisition system communicating with all pumps, regulators, transducers, and temperature probes on the instrument. Overall, the test was conducted over a 375-hour period, with continuous data collection taking place over the same time frame.

Figure 50 shows the results of testing reduced to 1-hour time averages of the data set. As shown, the difference (shown in the green line) between the total CO_2 volume injected (black line) versus the total volume received (red line) is noteworthy. It is believed that the fluid received was a combination of hydrocarbons initially, followed by CO_2. The presence of hydrocarbon was confirmed through GC analysis of the receiver fluids that were slowly purged from the pump by bubbling the combined fluid through a methanol bath. The GC–MS (mass spectroscopy) results demonstrated similar compositional data when compared to previously tested Bakken crude samples. The experimental design did not allow for quantification of the amount of hydrocarbon that was mobilized. The primary goal of this experiment was to determine CO_2 permeation rates in organic-rich shale. The permeation rate was calculated using the equation below:

$$Permeation\ Rate = \left(\frac{Q}{A}\right)/\emptyset \qquad \text{[Eq. 7]}$$

Where:
Q = flow rate in cm^3/hour
A = cross-sectional area
Ø = porosity

As shown in Figure 50, two distinct flow rates were generated during the experiment. During the first half of testing, it is thought that CO_2 is actively permeating the core from inlet to outlet, resulting in an average flow rate (corrected for known system leak rates) of 0.0001 cm^3/min. At approximately 250 hours, CO_2 began to flow through the core plug at a much higher rate of 0.0005 cm^3/min. Using a cross-sectional area of 7.115 cm^2 and porosity of 9%, the resulting penetration rate is calculated to be 0.03 cm/hour (0.70 cm/day) initially, then changes to a sustained rate of 0.13 cm/hr (3.13 cm/d).

While system leaks cannot be ruled out, and were noted to have been taking place at a very low flow rate of (0.00014 mL/min on the injection side and 0.00009 mL/min on the receiver side), the rate of injection and receiving are both outpacing the leak. Figure 51 demonstrates this by showing the volumes injected and received during the leak check, through the testing phase, and in the posttesting phase. Initially, after plumbing, the injection side of the system was found to be leaking; this was fixed and stabilized prior to starting testing. The leak was consistently maintained during the 375-hour time period. At approximately 100 hours, the main test period began. When testing was finished, the system was maintained with 5000 psi on both sides of the core to monitor the final system status (between a 475–550-hour time period). The rate of leakage was determined to have remained the same for the entire duration of the test. While there may have been some level of CO_2 retention in the shale, there is uncertainty regarding the total quantity, and the potential for retention cannot currently be quantitatively determined from this test. Further testing is recommended to replicate the results and move toward a more quantitative assessment.

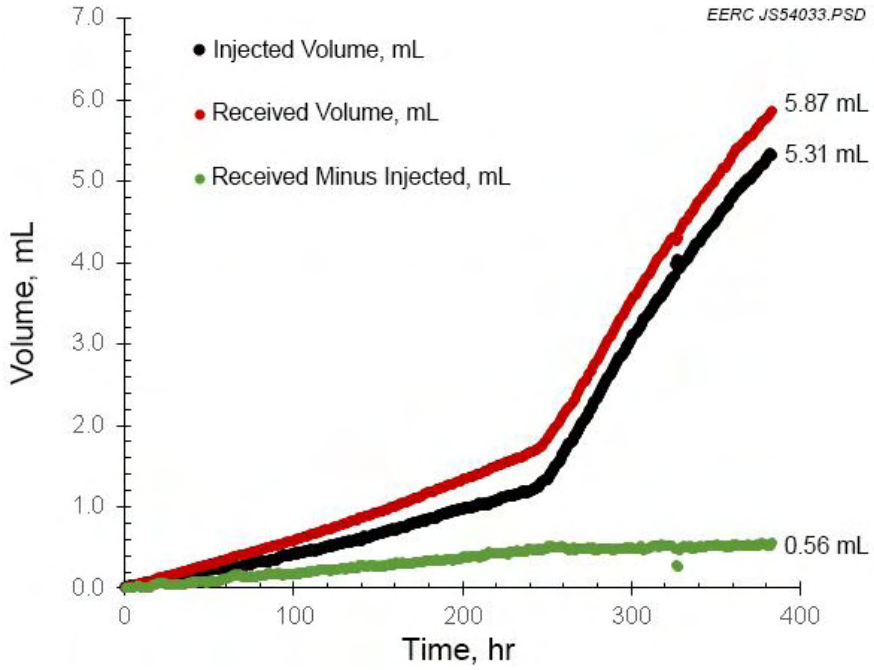

Figure 50. Chart showing results of CO_2 flow-through testing for the Upper Bakken Shale sample.

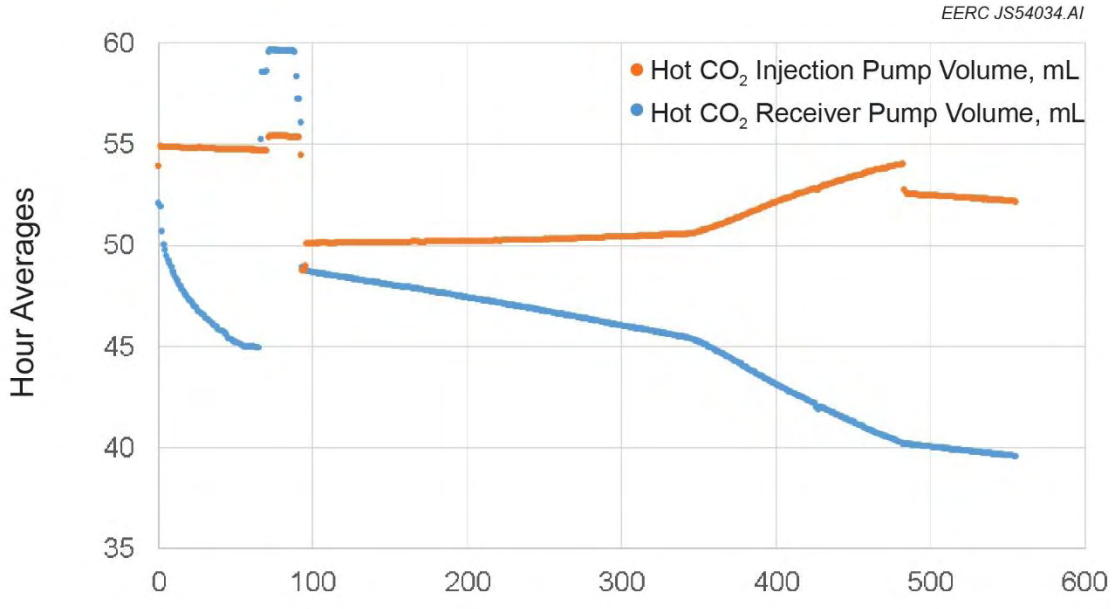

Figure 51. Hour averages of injection and receiver pump performance during testing of the Upper Bakken Shale sample. Between 0 and 100 hours, the system was being evaluated for leaks, the test was conducted between 100 and 475 hours, and this system was leak-checked again at the end of the test.

Middle Bakken Reservoir Rock Flow-Through Testing

A simple steady-state permeability test was conducted for a Middle Bakken Lithofacies 3 (laminated zone) sample from Well D. Using the same approach that was used for the shale plug as described earlier, the sample was inserted into the core holder in an as-received condition (no cleaning was conducted, so there was residual fluid contained in the pore space). Temperature was set at 160°F and pressure was held constant on the injection side of the core at 5000 psi, and the outlet pressure was adjusted throughout the test to determine the pressure where breakthrough occurs and flow is sustained. The test was started with a 200-psi differential pressure and finished at 600-psi differential. Figure 52 shows the data generated throughout the test, with slope corresponding to flow rate over the experiment.

The data shown in Figure 52 were condensed to start at a 400-psi differential, then increased to 500 psi and 600 psi. At 400 psi, no flow was observed and is shown on the red line as no volume change in the receiver pump on the back end of the system. Data indicate that at 500 psi it appears some flow of CO_2 through the sample was initiated. At 600 psi, the data show there is definite flow. The bumps on the data are caused by temperature fluctuations in the laboratory. To mitigate this effect, the transducers were insulated. The data became smoother at about 5000 minutes experimental time as a result. At the end of the experiment, the differential pressure was readjusted to 200 psi, and it is shown that no flow is sustained (no change in pump volume).

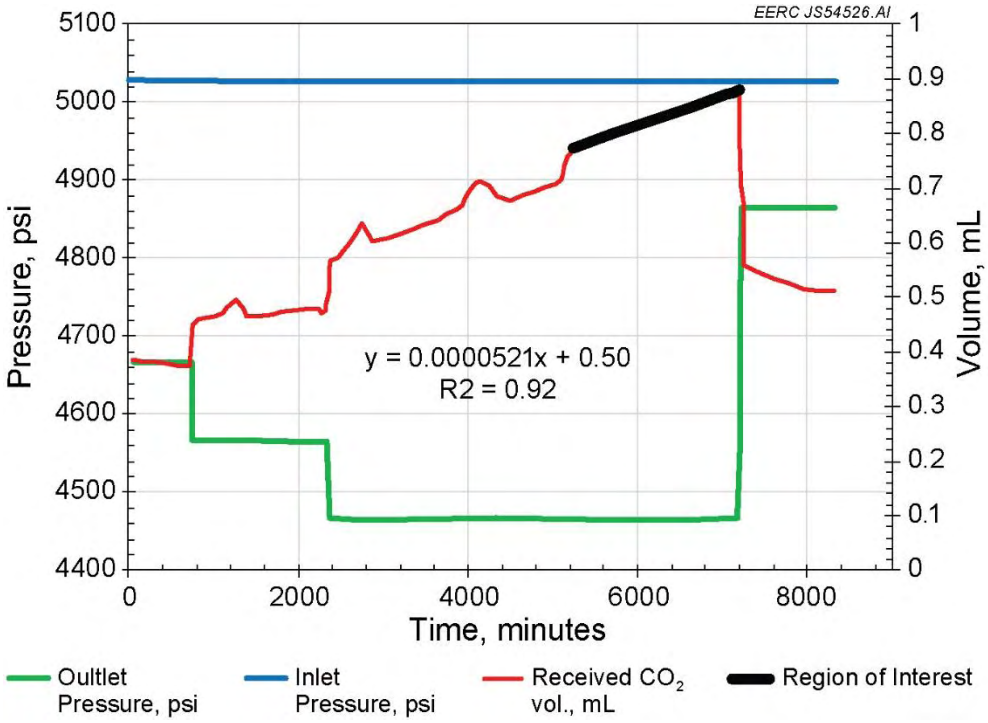

Figure 52. Data from the Middle Bakken flow-through test. The blue line represents the injection pressure, the green line represents the outlet pressure, and the red line represents the flow rate achieved throughout the test. The difference between the blue line and the green line is the differential pressure, which was controlled in a stepwise fashion through the experiment.

The permeability of the sample was calculated using Darcy's law. The following parameters were used in the equation:

Q = calculated flow rate over the experimental time (line slope on charts) (mL/min)
μ = 0.0725 cp based on NIST-reported values of CO_2 viscosity at the average of the experimental pressure range
L = 2.25 inch
D = 1.185 inch
dP = 600 psi

The calculated permeability for the Middle Bakken from the flow-through test was 1.7 nano-Darcy.

During experimentation, the average flow rate was determined to be 0.000054 cm^3/minute or 0.000324 cm^3/hour. With a cross-sectional area of 7.115 cm^2 and porosity of 4.2 percent using Equation 7, the resulting penetration rate is calculated to be 0.0109 cm/hour or 0.26 cm/day.

When considering these results, it is important to keep in mind the high degree of heterogeneity in the petrophysical properties of the Middle Bakken, and the results from this single Middle Bakken test may not be representative of permeation rates in other Middle Bakken lithofacies. The flow-through experiments on these particular samples suggest that, at least in some cases, the permeation rates of CO_2 in Middle Bakken reservoir rock matrix can be considerably slower than permeation rates in Bakken Shale. The results seen in these experiments may be a function of the high capillary entry pressures necessary to achieve sustained flow in the very tight matrix of the Middle Bakken. Figure 53 shows FIBSEM images of each interval tested (left: Upper Bakken Shale, right: Middle Bakken 3) and demonstrates the complexity within the MB3 sample in that grains are tightly packed and pores are poorly connected. This is in contrast to the shale sample that has high connectivity within the organic matrix that is promoting effective CO_2 flow through the sample. The fact that the submicroscale fracture networks identified by FIBSEM occur within the organics (Figure 31), coupled with the fact that the organic matrix may have nanoscale porosity, has important implications that may explain the mechanism by which CO_2 is able to access the organics and extract residual hydrocarbons so readily in the static experiments. It may also explain how CO_2 was able to migrate through a very low permeability shale sample with no visible fracture networks.

This also has implications for both CO_2 EOR and storage in organic-rich shales and highlights the need to better understand the mechanisms of CO_2 migration through the organic portions of the rock as a function of organic type (i.e., kerogen vs. bitumen) and thermal maturity. The submicroscale fracture networks also may correlate to CO_2 adsorption and/or absorption onto the organics as a function of organic type and thermal maturity. With respect to practical application of these results, the data provide insight into how far into the Middle Bakken reservoir matrix CO_2 may permeate during the soak period of a huff 'n' puff cycle and how long that soak period should be in order to mobilize oil from the matrix. However, these interpretations are based on limited data, and additional testing is need to verify and validate these concepts.

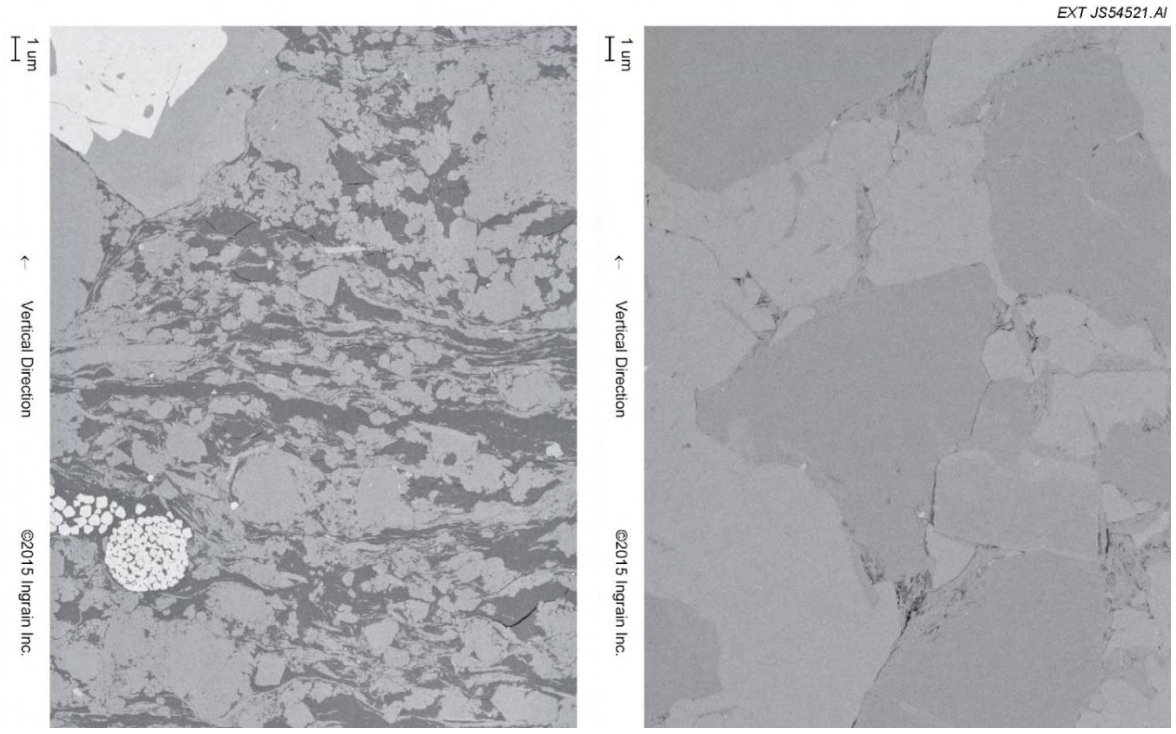

Figure 53. FIBSEM images showing the textural differences between the Upper Bakken Shale and Middle Bakken Zone. On the left, the dark regions are organic matter that shows high connectivity. This is lacking in the figure on the right (MB3) and demonstrates a limited capacity for flow.

GEOCELLULAR MODELING APPROACH

Introduction

The complex nature of the unconventional tight Bakken reservoir requires an understanding of the way CO_2 will fundamentally interact with all of the key elements of the reservoir matrix. Specifically, an accurate model of the minerals, clays, and fluid saturations is critical to predict the interactions that CO_2 will have with the reservoir system. The primary steps for developing the matrix petrophysical model can be categorized as data preparation, selection of key wells, synthetic well log creation, lithofacies correlation, incorporation of core data, MMPA, creation of static geomodels, and simulation modeling. The potential to use fractal analysis data developed under Phase I as a means of applying fracture analysis data acquired at one scale (i.e., core-scale) to larger (i.e., reservoir) or smaller (i.e., microscale) models was examined. However, the software packages that were used to create the static geomodels were not readily compatible with fractal analysis data. Consultations with the software providers (i.e., CMG and Schlumberger) suggested that the modifications of either the data or the software would likely yield results that could not be verified or validated without substantial additional efforts. A determination was made early in the modeling process that developing the static geomodels using more traditional data sets and approaches without the fractal analyses would serve the goals of the project in a more cost-effective manner. A more detailed presentation of the fractal analysis work is provided in Appendix D.

MMPA Efforts under This Project

The proper assignment of matrix petrophysical properties such as porosity, permeability, lithology, and fluid saturations is critical to the creation of models that accurately represent the reservoir system. The use of MMPA is an approach that goes beyond simply assigning properties to a facies. MMPA is typically conducted to determine and adequately account for the complexity of oil and gas reservoirs and the effects of overall mineral content on fluid movement and production estimates. It is a more robust and rigorous means of assigning a multitude of properties to a given lithofacies, particularly with respect to mineral composition and fluid saturations and the relationships between those aspects of a reservoir. Mineral composition ultimately determines the physical parameters of the rocks and can be used as a tool to determine the overall characteristics of the reservoir and the depositional environment. The Quanti.Elan module in Techlog was used to calculate MMPA from the key well log data and determine the overall quantity and volume of different mineral components in each wellbore. This mineral volume calculation aids in determining the stratigraphy and the overall correlation from one wellbore to another, thus describing the geologic structure for property distribution in the 3-D model. MMPA can also help determine the interaction of bulk mineral volume and CO_2. Other key properties calculated by the MMPA process include pore fluid volumes and the calculation of effective and total porosity.

The first step of the MMPA process included the collection and placement of well logs, including the four study wells from which core samples were analyzed, into a Techlog database that allowed for efficient management of the log data and evaluation of data for log analysis and quality control purposes. Techlog is a Schlumberger petrophysics software platform that enables the performance of MMPA. The Techlog application included core data, core photos, thin-section photos (all of which were generated in Phase I), and MMPA precomputational analysis from well files and log headers. Techlog was also used to pick formation tops and lithofacies tops for the vertical portions of wells in the study area. Data preparation also included the use of Petrel for managing and manipulating data on wells and well deviations, well tops, well logs, mud logs, and results generated within Techlog.

Once the Techlog and Petrel databases had been established, detailed well log analysis was performed using logs for the Phase I study wells. The logs were provided by Marathon and the North Dakota Geological Survey. The suite of logs used in the MMPA include gamma ray (GR), bulk density (RHOB), photoelectric effect (PEF), sonic (DT), neutron porosity (NPHI), and resistivity (RT).

After the Middle Bakken member lithofacies had been correlated, core data were integrated into the static geologic model. XRD data from core samples taken from the calibration wells were used to predefine the mineral solver. A RockView geochemical log was used for MMPA calibration and validation. Core lithofacies descriptions were also incorporated, and core data were depth-shifted as part of the quality control (QC) process for finalizing MMPA results. The core data were shifted based on core gamma measurements as compared to the well gamma log. In addition to providing the static geological model with a realistic three-dimensional distribution of petrophysical properties, a static model that has been created using MMPA can yield a wide variety of detailed visual representations of the reservoir, including cross sections, fence diagrams, and

maps. An example of an output from MMPA is provided in Appendix A, which is a correlation cross section created from the four vertical key wells in the study area. Upon completion of MMPA in October 2016, the reservoir properties were imported into Petrel for the creation of the matrix petrophysical model for the Bakken in the project study area.

Creation of Geocellular Models

Geocellular models at different scales were developed using the data sets generated in Phase I and the MMPA results. Small-scale models include plug- and core-scale models. These are used to simulate and history-match laboratory experiments of CO_2 permeation and oil mobilization. Larger-scale models, such as near-wellbore- and reservoir-scale models, are used to simulate and predict CO_2 behavior under conditions that are more representative of what might be expected in the field. Figure 54 provides an example of a plug-scale model, and Figure 55 provides an example of a core-scale model, which were created using core characterization data generated from previous characterization activities. Near-wellbore-scale petrophysical models of the Middle Bakken were also created using rock characterization data, well logs, and MMPA results. An example image from a new-wellbore model is shown in Figure 56. A small reservoir-scale model has been created for the entire Bakken petroleum system in an area in northern Dunn County, North Dakota (Figure 57). The model includes the strata from the Lodgepole Formation to the Three Forks Formation (Figure 58). This model has been developed to capture overpressure in the Bakken petroleum system associated with hydrocarbon generation (Figure 58). This model also included a discrete fracture network within the Middle Bakken Member (Figure 59) in an attempt to better understand fluid flow and pressure response to production/injection within the tight reservoir.

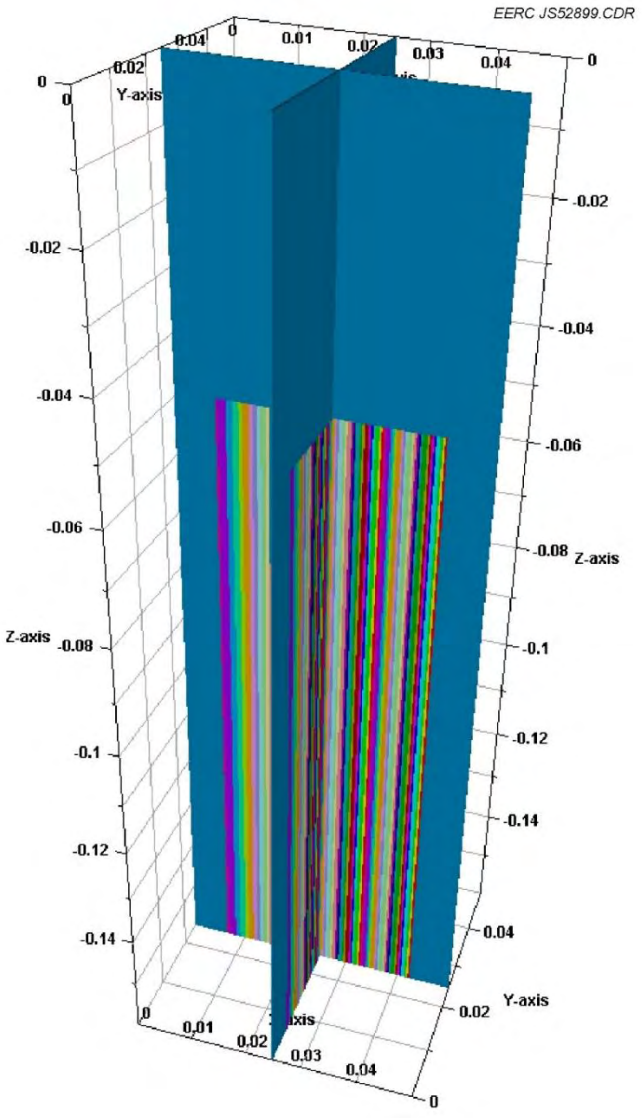

Figure 54. Perpendicular cross sections within a core plug-scale model of a horizontal plug from the Middle Bakken, MB3 (laminated) lithofacies, used in numerical simulations replicating hydrocarbon extraction experiments using CO_2. The dimensions of the model are 15 × 15 × 50 mm. The dark blue surrounding the core plug represents the void volume within the sample vessel. Individual laminae are indicated with different colors. This particular property was used to guide petrophysical property distributions based on the data generated by the microscale characterization data generated by the advanced SEM work in Phase I.

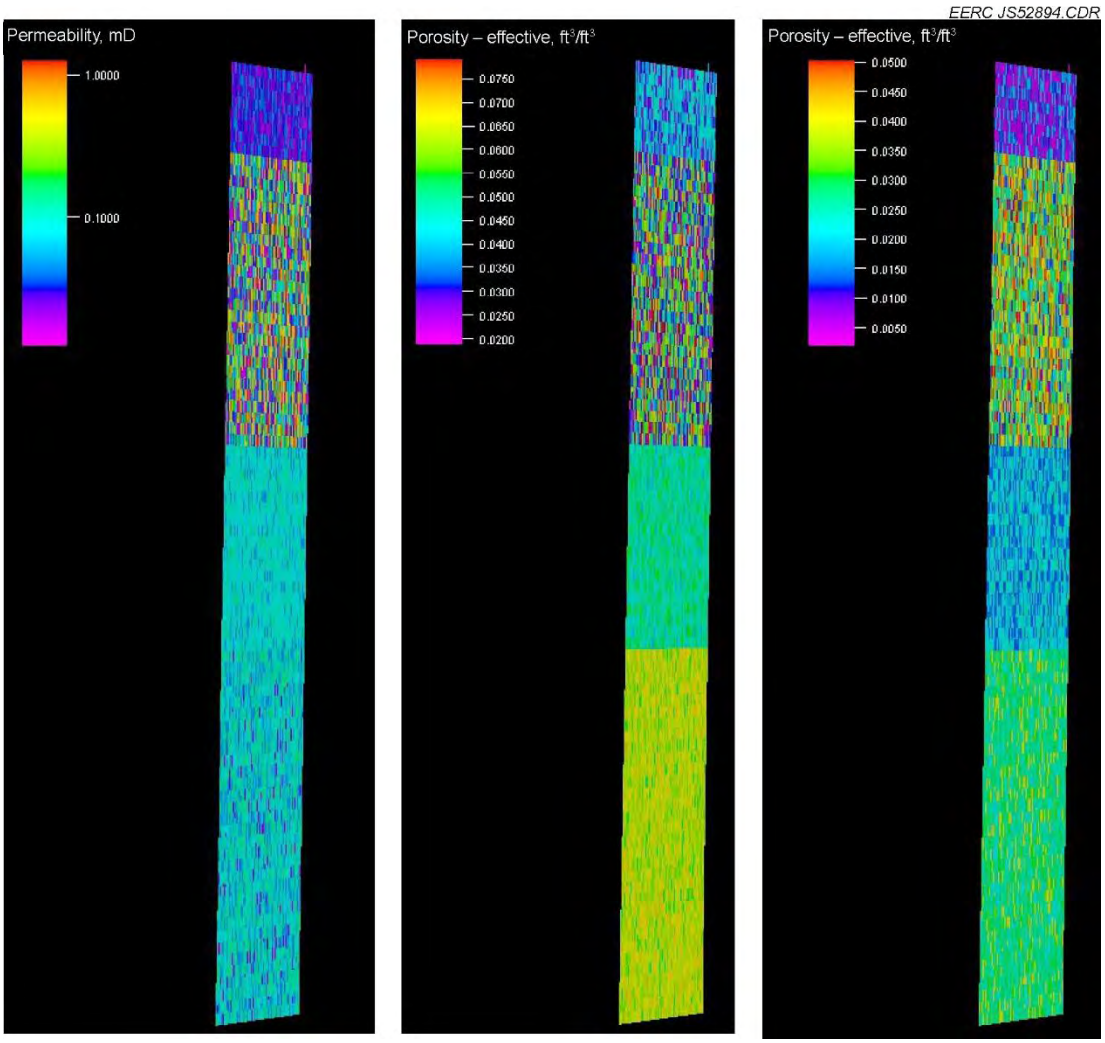

Figure 55. Middle Bakken core-scale model (lithofacies MB2 through MB5; MB1 is not present) showing distribution of permeability (left), porosity (center), and effective porosity (right). The dimensions of the model as shown in this image are not to scale, as the width of the core is 4 inches, while the length is approximately 45 ft.

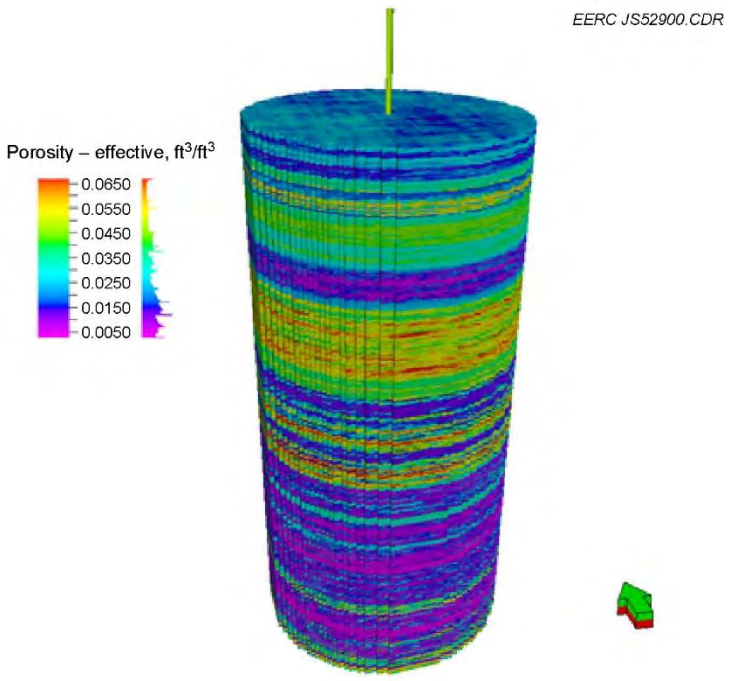

Figure 56. Example image of a near-wellbore geocellular model containing the entire Bakken petroleum system (radius 400 ft; total thickness of 330 ft; vertical exaggeration 2×) showing distribution of porosity in the Middle Bakken.

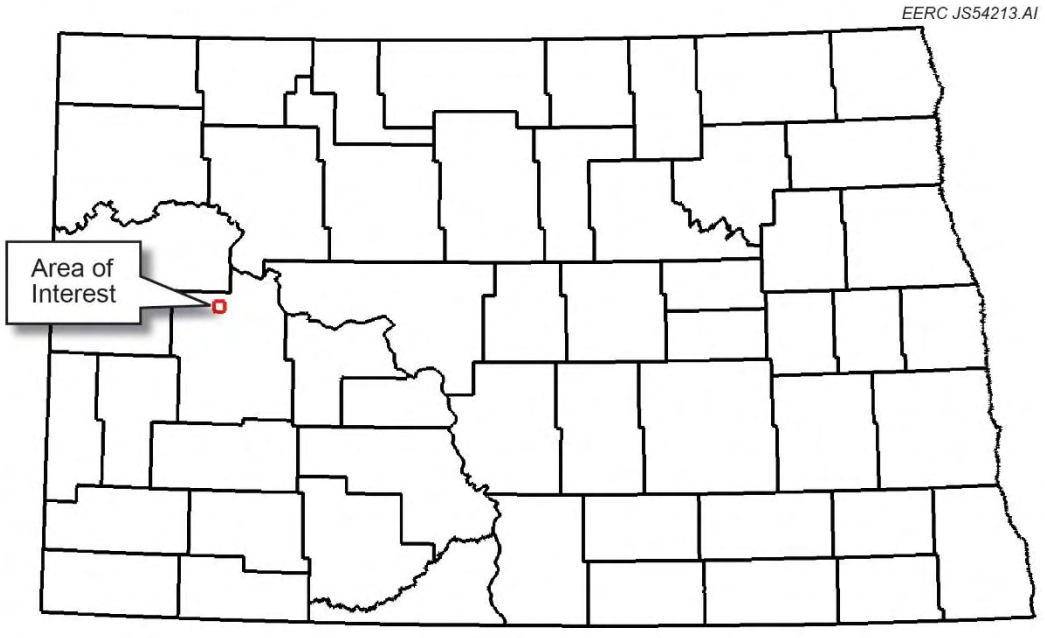

Figure 57. Location of the reservoir-scale geocellular model.

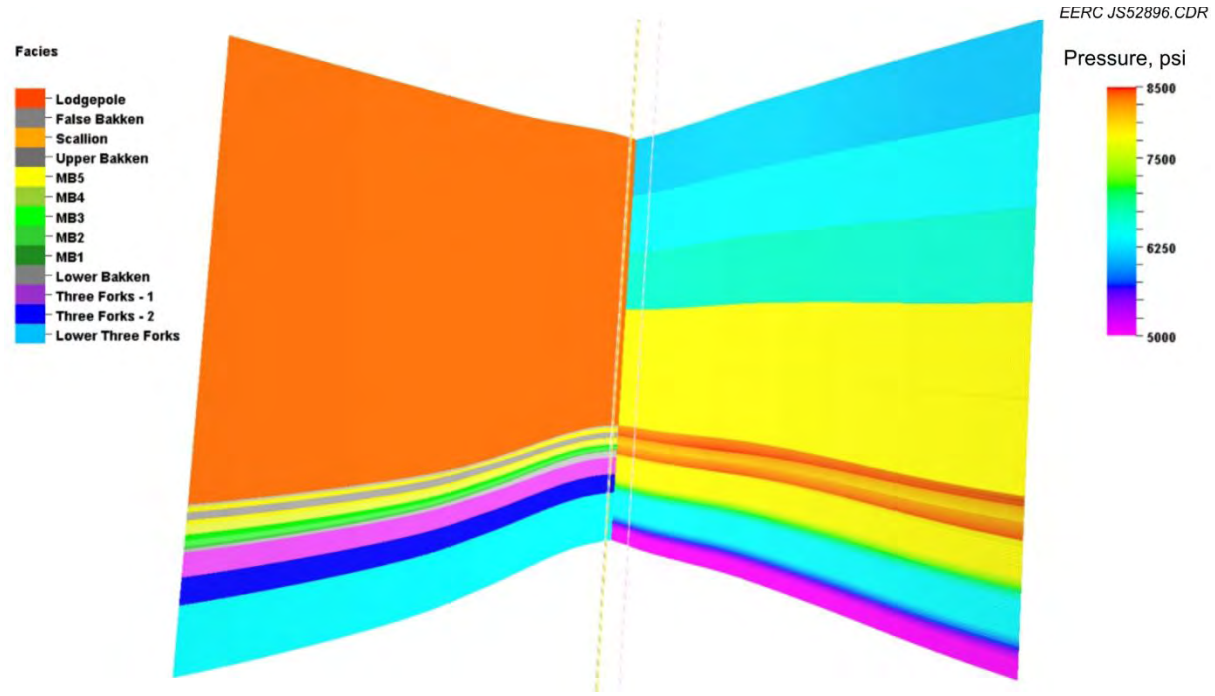

Figure 58. Fence diagram cross section of the reservoir-scale geocellular model showing relative position and thicknesses of the lithofacies included in the model on the left and the distribution of pressure on the right. Note the highly overpressured nature of the Bakken Formation.

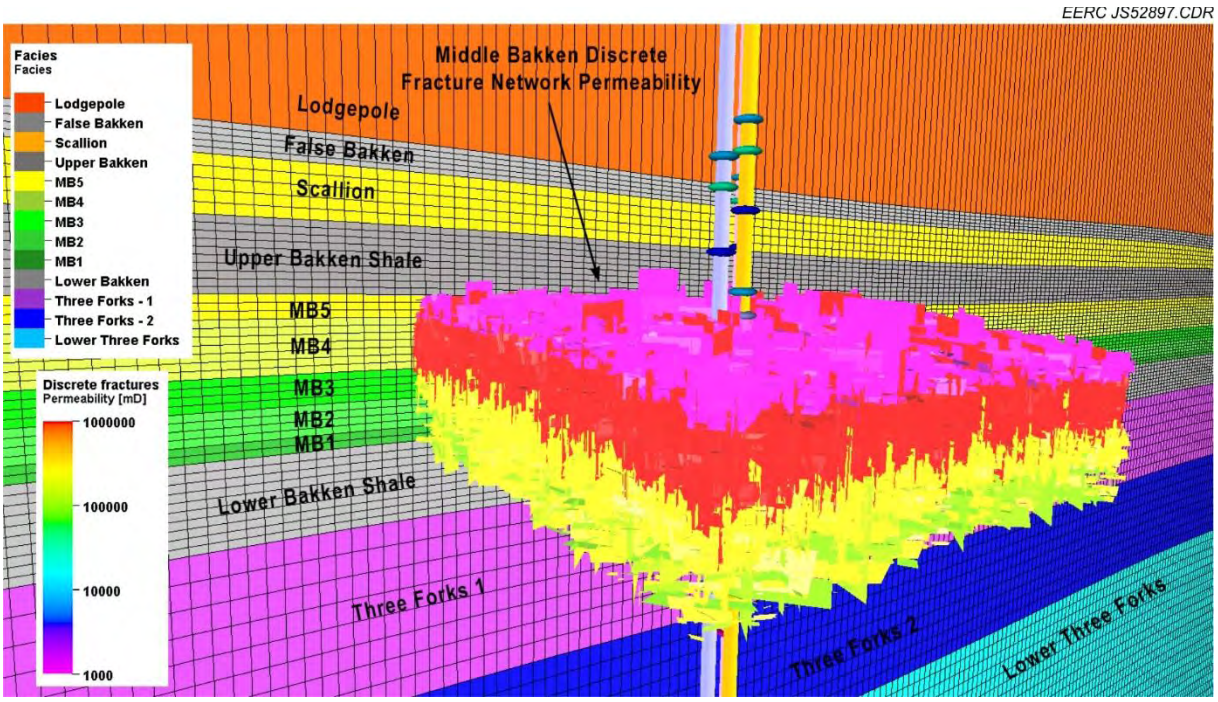

Figure 59. Image of the discrete fracture network component that has been integrated into the reservoir-scale geocellular model of the Middle Member of the Bakken Formation.

TIGHT OIL SIMULATION ACTIVITIES

Multiple scales of modeling and simulation activities were conducted during this project, including submicroscopic-scale (SEM resolution [nanometer-scale] and computed tomography resolution [CT; micrometer-scale]), core plug-scale, and well-scale. The goal of these activities was to increase understanding of fluid flow in tight oil reservoirs and investigate methods of increasing ultimate recovery from these systems, with a focus on CO_2 EOR. Studies have shown that petrophysical properties such as shale content, porosity, permeability, pore-size distribution, capillary pressure, and relative permeability play important roles in unconventional oil-gas multiphase flow (Xiong and others, 2015; Brian and Barrufet, 2017). Thus each of these factors was considered throughout the simulation efforts of this project and is discussed in the following sections.

Analysis of Flow Mechanisms in Unconventional Reservoirs

Although viscous (Darcy) flow is the dominant flow mechanism in conventional reservoirs, the low permeability makes viscous flow difficult to maintain in unconventional reservoirs like the Bakken. Based on pore throat radius, porosity, and permeability, different flow units can be distinguished in conventional and unconventional reservoirs as shown in Figure 60 (Aguilera, 2014; Jin and others, 2016). Conventional reservoirs are usually highly permeable and characterized by relatively large pore throat size (micron-scale). Vertical wells are used to develop conventional reservoirs, where oil flows to the wells via viscous flow. Horizontal wells have been used to increase oil production rate in some conventional reservoirs where permeability is low or oil viscosity is high (e.g., heavy oil). In unconventional tight reservoirs such as the Bakken, permeability ranges in the micro-Darcy or nano-Darcy levels, with pore throat sizes at the nanometer scale. Vertical wells are no longer able to produce oil economically in a reservoir with such low permeability. Hydraulically fractured horizontal wells provide the means to make oil production economically feasible in unconventional tight oil reservoirs. Fracturing divides the reservoir into two parts: induced fractures and matrix, which have different flow regimes: viscous flow in the fractures and diffusion-dominated flow in the matrix. Therefore, molecular diffusion dominates the transportation in the pore space of the tight Bakken matrix. In a highly fractured reservoir, diffusion could also be an important mechanism for the success of CO_2 EOR (Eide and others, 2016). The value of the diffusion coefficient could range from 10^{-7} to 10^{-4} cm^2/s depending on fluid properties and reservoir conditions such as pressure and temperature, etc. (Grogan and others, 1988; Renner, 1988; Upreti and Mehrotra, 2000; Tharanivasan and others, 2004; Jamialahmadi and others, 2006; Leahy-Dios and Firoozabadi, 2007; Guo and others, 2009; Hoteit and Firoozabadi, 2009; Trevisan and others, 2013; Roman and others, 2016).

Plug-Scale Simulation Modeling – Case 1: Replicating the Lab-Based Extraction Studies

Compositional simulations of Bakken shale and nonshale core plugs using radial grid geometry were built to mimic the CO_2 permeation and hydrocarbon extraction process that was conducted experimentally in the lab (Figure 61) using Computer Modelling Group's (CMG's) GEM reservoir simulator to serve as the platform for simulation modeling. In the models, as in the

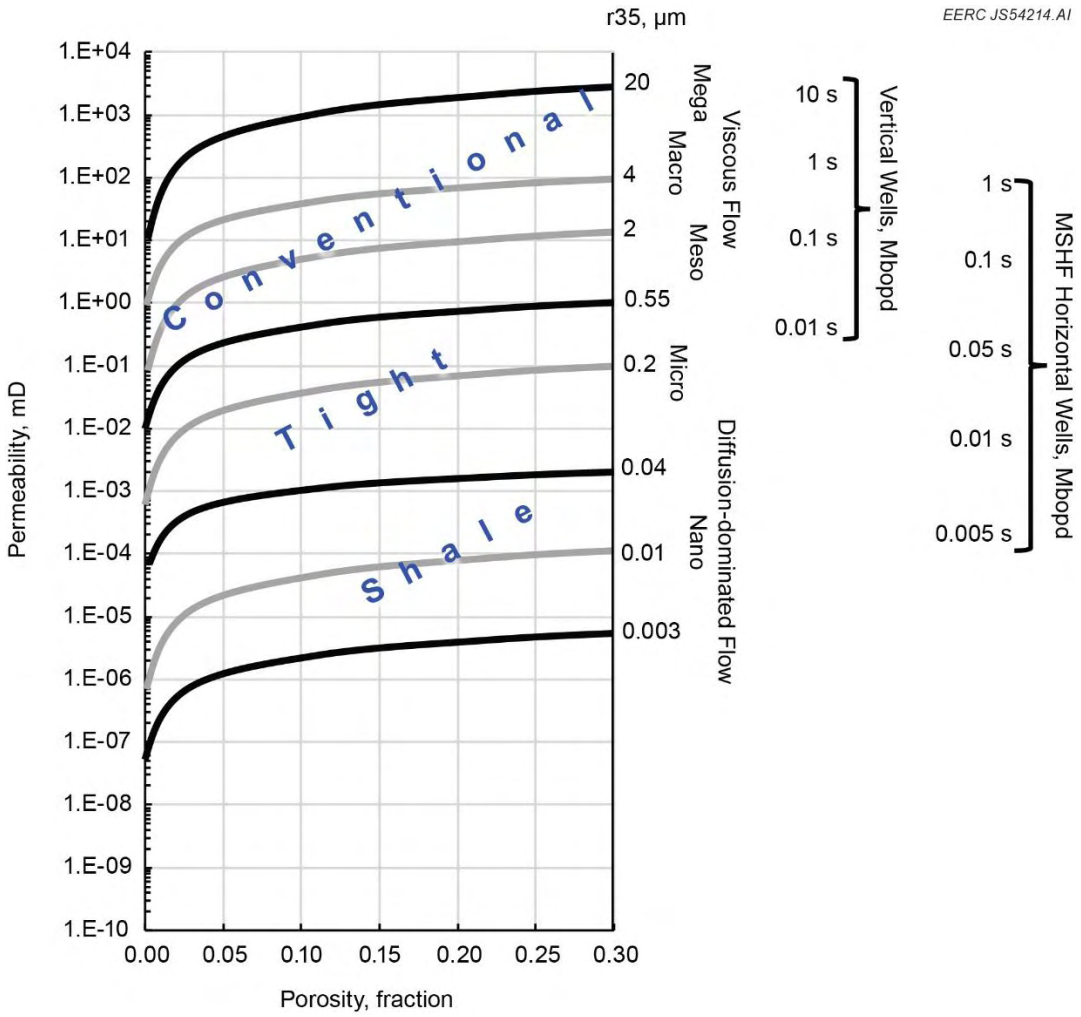

Figure 60. Flow unit division for various oil reservoirs (Jin and others, 2016) (MSHF: multistage hydraulically fractured).

lab experiments, the core was centralized inside the vessel, which is surrounded by an empty space for flowing CO_2. The CO_2 was injected through the empty space of the top layer, and fluids (including CO_2 and hydrocarbons) were produced via the empty space of the bottom layer. The dimensions of the simulation model were set to mimic those of the experimental setup (described in detail in the hydrocarbon extraction section). Properties of Bakken oil were measured and used as input data to the simulation model to ensure the results were representative of fluid behavior in the Bakken reservoir. The basic rock and fluid properties used in the model can be found in Table 13.

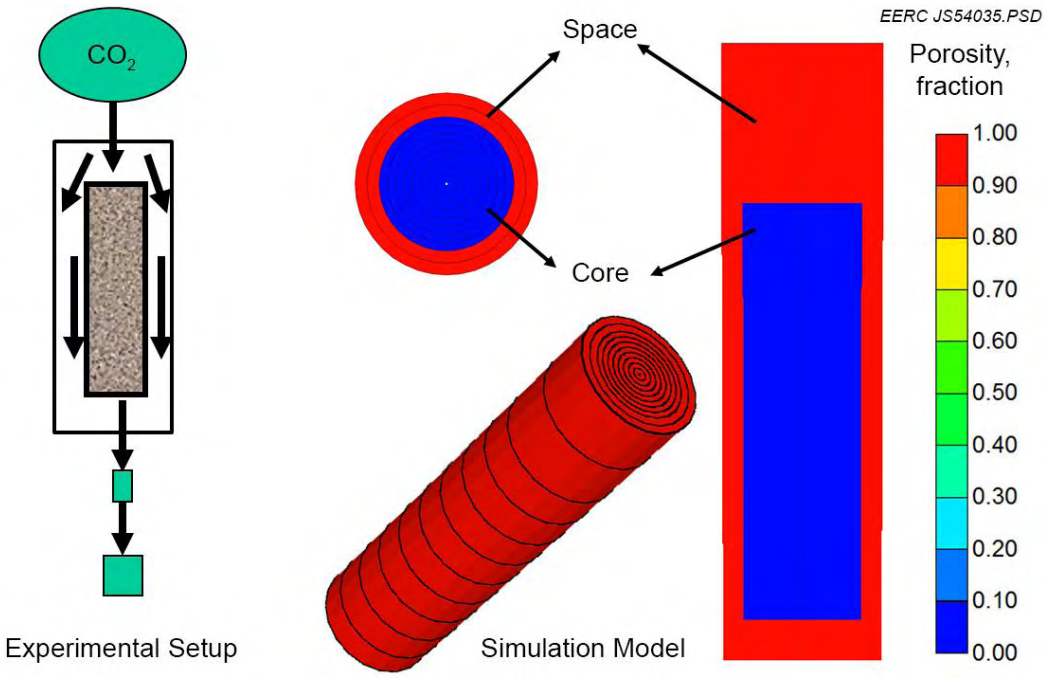

Figure 61. Schematic of plug-scale simulation models (right) in comparison to the experimental setup (left) (Hawthorne and others, 2014).

Table 13. Basic Parameters Used in the Simulation Model

Category	Parameter	Value	Unit
Rock	Porosity	4.8	%
	Permeability	0.008	mD
	Density	2400	kg/m^3
	Compressibility	1×10^{-6}	1/psi
Oil	Density	794.6	kg/m^3
	Viscosity	1.336	cP
Condition	Initial core pressure	150	psi
	Injection pressure	5000	psi
	Temperature	110	°C

The values of the rock parameters in this plug model were based on the measured property values for Lower Bakken Shale core samples from all four study wells (see Figure 3). Iterative modifications of the model, varying input parameters slightly, were simulated until a reasonable match of the extraction results was achieved. As in the laboratory experiments, simulations were run with all sides of the shale sample exposed to CO_2 during the permeation and extraction process. Here diffusion played an important role in mobilizing oil from the sample because pressure drawdown was eliminated during the extraction. Figure 62 shows the comparison of experimental and simulation results for a Lower Bakken Shale core sample. The results indicate the model was able to reproduce the laboratory-measured hydrocarbon extraction results; however, the final

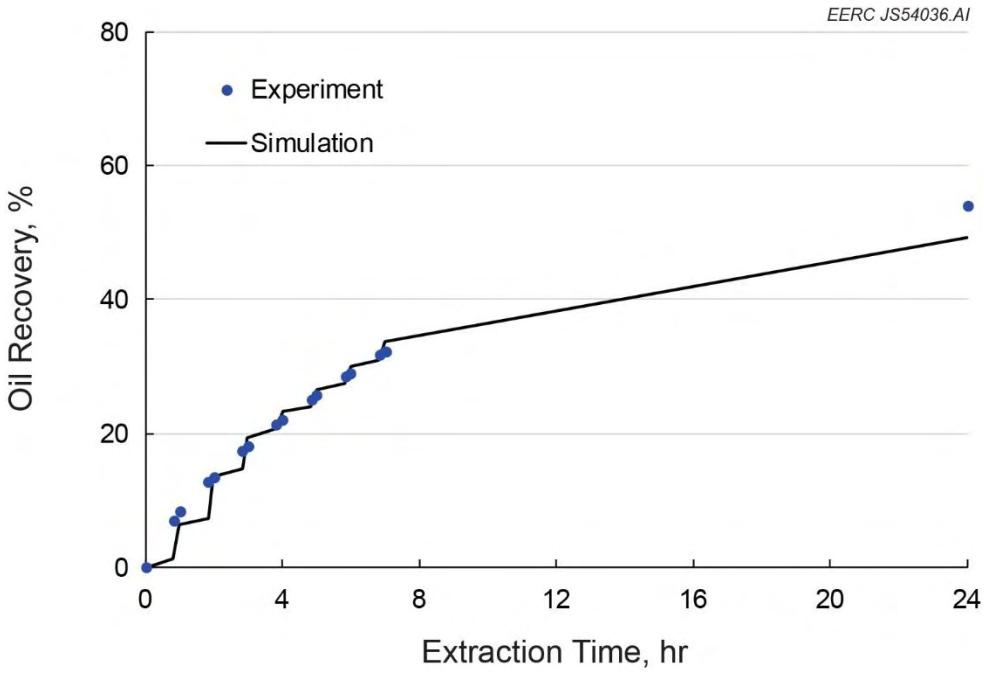

Figure 62. Simulated hydrocarbon extraction reproducing experimental results in a Lower Bakken Shale sample. As described in the methodology section, the operating conditions of the experimental apparatus included interruptions during which gas samples were pulled from the sample chamber, which are reflected in the simulation results by the stepwise shape of the line.

recovery factor was slightly underestimated. The simulation model was also able to imitate the CO_2 penetration process during the extraction (Figure 63). The history-matching exercise resulted in a calibrated shale plug model that could be used in subsequent simulation exercises to evaluate the relative impact of key petrophysical variables on CO_2 behavior and hydrocarbon mobility in shales.

Shale Plug Modeling – Case 2: Sensitivity Testing of Key Properties and Mechanisms

Jin and others (2016) used the same types of experimental data described above and statistical analysis, based on a linear regression of that data, to investigate the significance of parameters likely controlling permeation of CO_2 and oil mobility within organic-rich, oil-wet shales. Results of those simulations have improved the understanding of CO_2 EOR and storage in tight oil formations. Specific parameters evaluated with respect to their sensitivity to oil recovery included porosity, permeability, TOC, pore throat radius, and water saturation. The results of that work showed that the two most important variables correlated with oil recovery in the Bakken shales were TOC and pore throat radius, perhaps because kerogen has a strong affinity for oil and is oil-wet, which challenges the ability of CO_2 to conventionally displace the hydrocarbon molecules. However, CO_2 is known to readily dissolve into oil and has an affinity for (absorbing into) kerogen, suggesting that high TOC may result in relatively higher CO_2 storage potential. Furthermore, the connected pore space observed in the FIBSEM results described above indicate

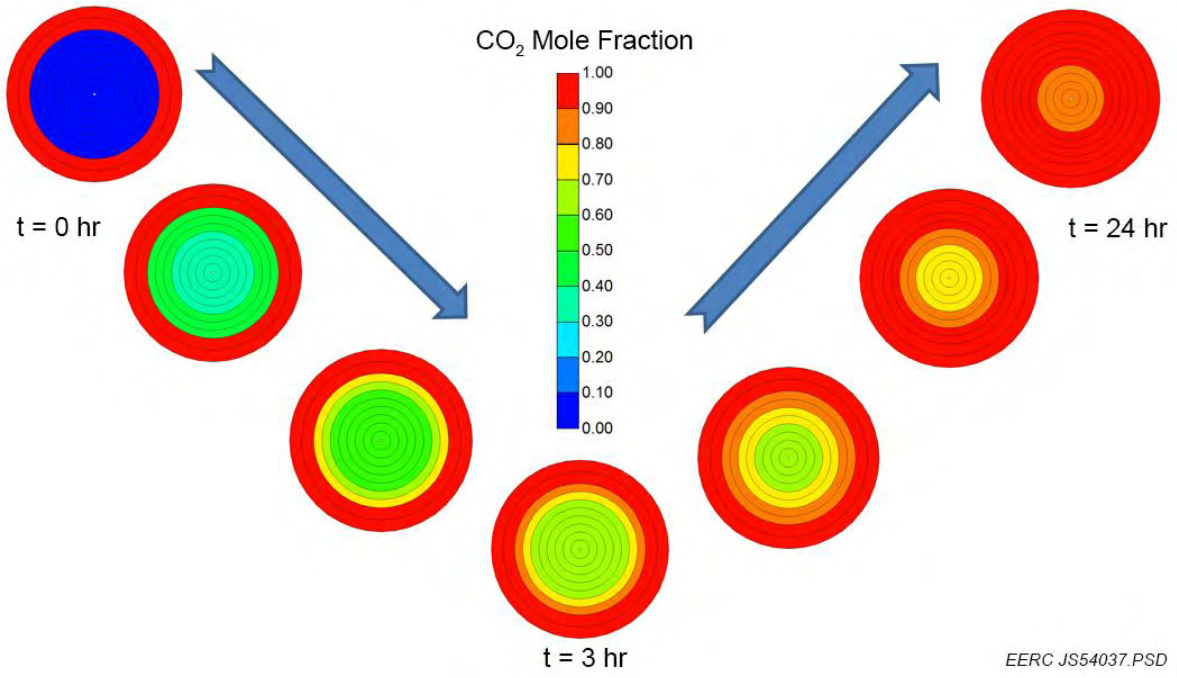

Figure 63. Cross-section illustration of CO_2 penetrating into the modeled core sample because of diffusion during the simulated extraction process (Jin and others, 2017b).

pathways for CO_2 permeation, though small in scale, do exist. In effect, the Bakken shales (and other unconventional/tight reservoirs having high TOC) may have significant CO_2 storage potential while releasing hydrocarbon molecules. This insight, combined with the observation of Hawthorne and others (2013) that diffusion is a primary mechanism for the permeation of CO_2 in Bakken rocks, was the basis for the core plug-scale modeling efforts reported here. Parameters considered in the Case 2 simulations were bottomhole pressure (BHP), porosity (phi), permeability (K), irreducible water saturation (S_{wi}), CO_2 diffusion coefficient, and maximum adsorption. Figure 64 shows the simulation results that most closely matched the experimental results for the Lower Bakken Shale samples, and Table 14 presents the values for each of the parameters used in the simulation.

When the results of the Case 2 plug-scale simulation were compared to the actual CO_2 permeation and hydrocarbon extraction experimental data, it appears that the general shapes of the oil recovery curves are similar, but the simulations again appear to underestimate both the rate of oil extraction and the total amount of oil recovered in 24 hours.

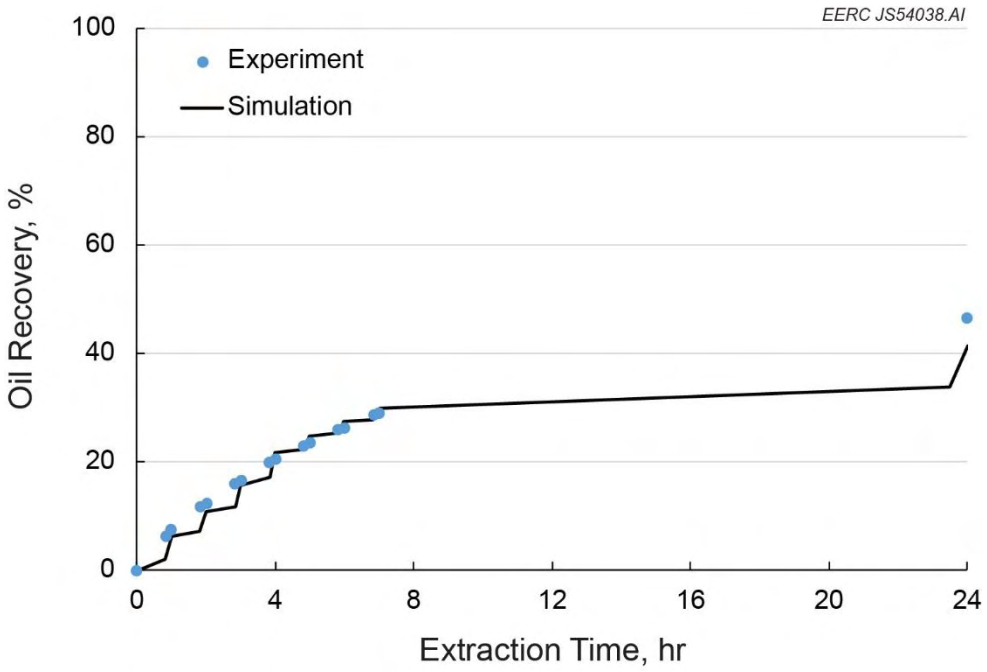

Figure 64. Results of simulated oil recovery from CO_2 exposure in a Lower Bakken Shale plug.

Table 14. Values for Each of the Parameters Used in the Lower Bakken Shale Plug Simulation (results shown in Figure 52 above)

Parameter	LB	Unit
BHP	4995	psi
ϕ	0.0611	fraction
K	0.0113	mD
S_{wi}	0.11	fraction
Diffusion Coefficient	1.67×10^{-5}	cm^2/s
Maximum Adsorption	0.1624	gmole/lb

Shale Core Plug Modeling – Case 3: Further Incorporation of Advanced Characterization

The shale plug models used in Case 1 and 2 simulations were simplified to minimize simulation run time, meaning that little of the high-resolution advanced characterization data (e.g., FIBSEM and CT scans) were incorporated into those models because of the associated high data density. However, the Case 2 simulation results suggested that some of the key insights from the advanced characterization work were not adequately accounted for in the models. A Case 3 effort was outlined, in which a new 3-D geocellular grid that incorporated some of the advanced characterization data would be constructed. FIBSEM and core CT data were investigated to guide

property distributions in the Case 3 model. Iterative exercises were conducted using FIBSEM data to develop training images to create realistic distributions of mineral grains and organic matter within the plug. While this approach yielded highly detailed static geocellular models of shale plugs, the models proved to be too data intensive for the simulation software to effectively manage (the cell size needed to preserve the heterogeneity was very small, resulting in a total cell count too high to be simulated efficiently).

Thus core sample CT data, having a relatively lower data resolution than FIBSEM products, were used to create the Case 3 core plug models. The CT measurements are reported in terms of radiological density, which is expressed in Hounsfield units (HU). For example, the CT value of air is −1000 HU, deionized water has a value of 0 HU, and clastic rocks can range from approximately 1200 to 3300 HU (Geiger and others, 2009). The CT number depends on both the mineral composition of the rock and the gravimetric density. Klobes and others (1997) showed correlations between rock porosity and CT measurements. Initial model cell sizes were set to the same resolution as the CT data such that each cell was represented by a single data point. At this resolution, each cell was 244 µm in the X and Y (I and J) directions and 250 µm in the Z (K) direction, with a total cell count of approximately 2 million cells. As with the previous two cases, the overall dimensions of the Case 3 shale plug model were based upon the dimensions of an actual sample and also included cells outside of the sample to represent the test chamber used in the laboratory.

Petrophysical data, collected from routine core analysis and helium porosimetry, were available for three Bakken core samples for which CT data were also available. Laboratory-measured porosity values were cross-plotted with CT values (Figure 65) and showed a fairly linear

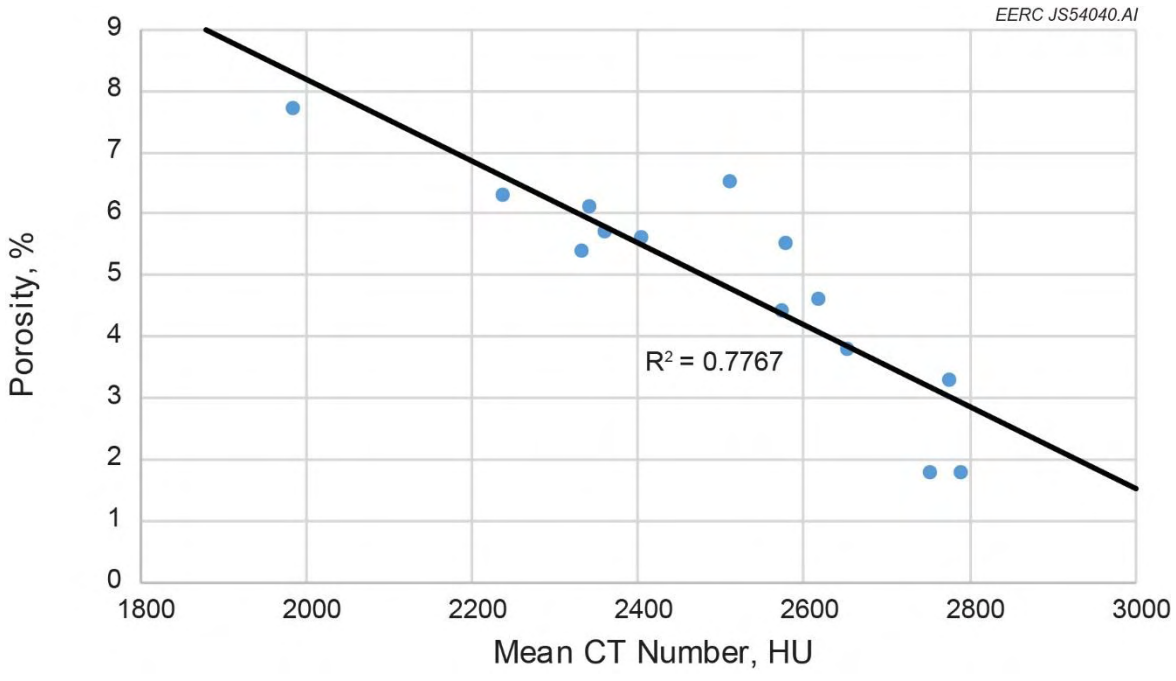

Figure 65. Porosity vs. mean CT number. Regression line represents Eq. 7.

correlation using the method from Skinner and others (2015; Eq. 2). This linear relationship with the CT number was used to distribute porosity throughout each sample (Figure 66). Permeability was distributed bivariately from porosity/permeability crossplots created from routine core analysis.

$$\Phi = -0.0067 \times \mathrm{CTN} + 21.492 \qquad \text{[Eq. 7]}$$

Where Φ is the porosity of the sample and CTN is the CT number (value in HU) of the sample. The equation is derived from the line fit to the core porosity data versus CT values at those depths, based on an approach described by Skinner and others (2015).

Oil saturations were estimated from experimental data by adding the mass of oil extracted during the experimental process and the mass of oil remaining within the rock at the end of the extraction (the rock was crushed and solvated to extract remaining hydrocarbons). This mass, along with an average oil density of 49.6 lb/ft^3 (measured in the laboratory), allowed a volume of oil to be calculated per gram of rock. A grain density transform was used to determine the volume of oil present in each cell. Following, an oil saturation property was created by dividing the volume of oil by the pore volume of each grid cell.

After the model was populated with petrophysical properties, the model was resampled into a secondary grid with the same overall volumetric extent but larger cells oriented in a radial pattern to decrease the final cell count. The total number of cells was reduced from approximately 2 million to 110 in the upscaled radial grid. Figure 67 shows the porosity distribution in the simulation model, based on the upscaled CT data shown in Figure 66.

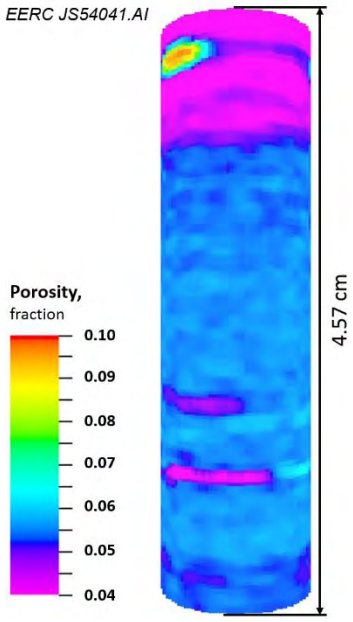

Figure 66. Case 3 model porosity distribution based upon CT data in a Lower Bakken Shale sample.

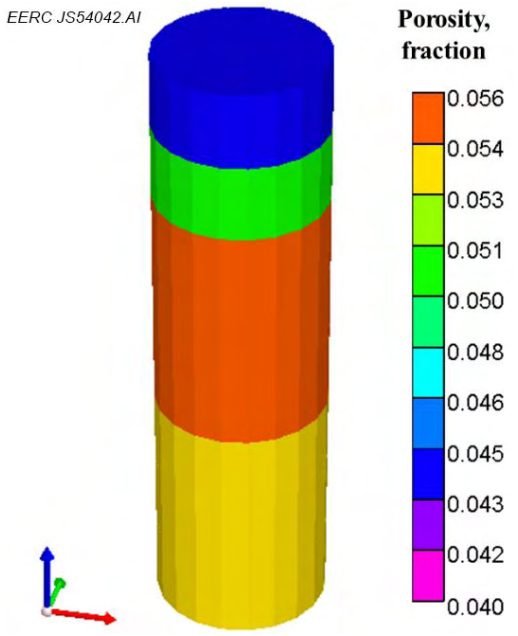

Figure 67. Upscaled porosity distribution in the core sample model.

As described earlier, Rock Eval tests showed there was considerable TOC (10–15 wt%) in both the Upper and Lower Bakken Shales. Previously published experimental studies of various gas shales have shown that kerogen has strong ability to adsorb gas components, including CH_4 and CO_2 (Wang and others, 2012; Liu and others, 2013; Heller and Zoback, 2014; Tang and others, 2015, 2016; Guo and others, 2017). Thus inclusion of adsorption behavior was desired in the Case 3 efforts and was one of the key differences between the Case 3 simulations and other cases. A Lower Bakken Shale sample was tested in the laboratory to measure the CO_2 adsorption isotherm under reservoir temperature (230°F) and a wide range of pressures (0–5800 psi). Based on previous lab studies, the CH_4 adsorption isotherm is usually lower than the CO_2 adsorption isotherm, meaning that CO_2 is preferentially adsorbed by kerogen in comparison to CH_4 (Heller and Zoback, 2014). Adsorption behavior of CH_4 was a necessary consideration in the simulation model as there is a significant amount of CH_4 in the Bakken Formation. Figure 68 shows the measured CO_2 and estimated CH_4 adsorption isotherms for the Lower Bakken Shale sample used in this exercise. The CO_2 isotherm illustrates the Bakken shale has a considerable capacity to adsorb CO_2 under reservoir conditions. Figure 69 shows the simulation results from models with and without CH_4 adsorption settings, suggesting that integration of CH_4 adsorption and core CT data allowed simulations to better reproduce the experimental results. However, as in Cases 1 and 2, this Case 3 simulation was not quite able to reach the final recovery factor measured in the experimental process.

One explanation for this discrepancy may be that the model is not able to account for the connected nature of the porosity that was observed at the submicroscopic scale (observed in FIBSEM analyses). While the porosity of the shale is low, the pore spaces appear to be fairly well connected. Those pathways, however small, may account for the higher CO_2 permeation and oil mobility observed in the experiments.

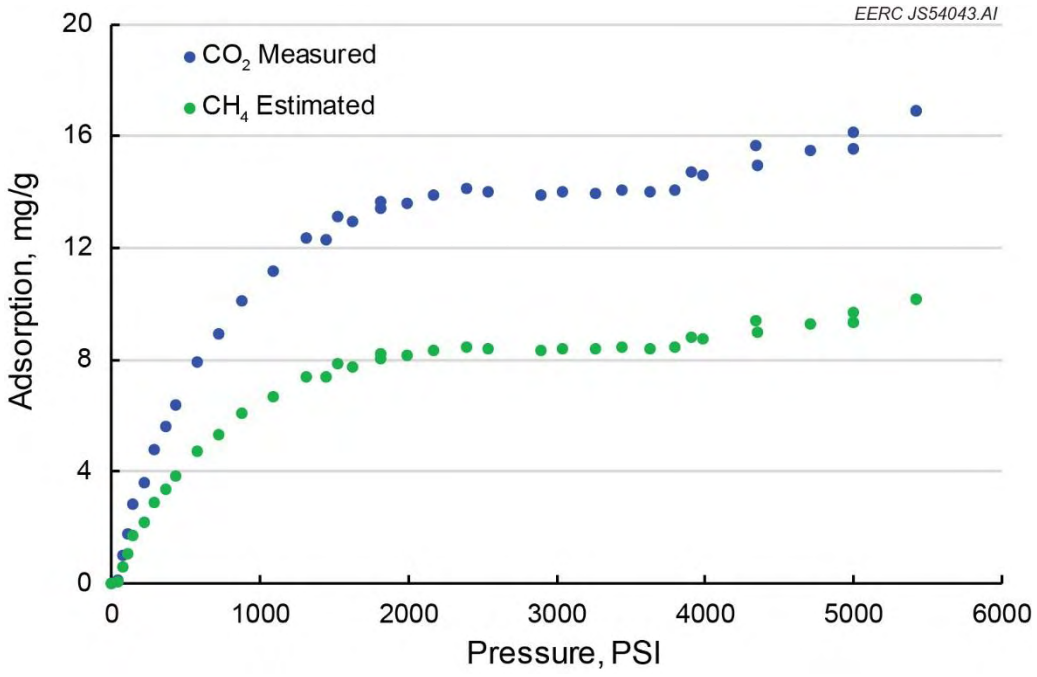

Figure 68. Measured CO_2 and estimated CH_4 adsorption isotherms for a Lower Bakken sample.

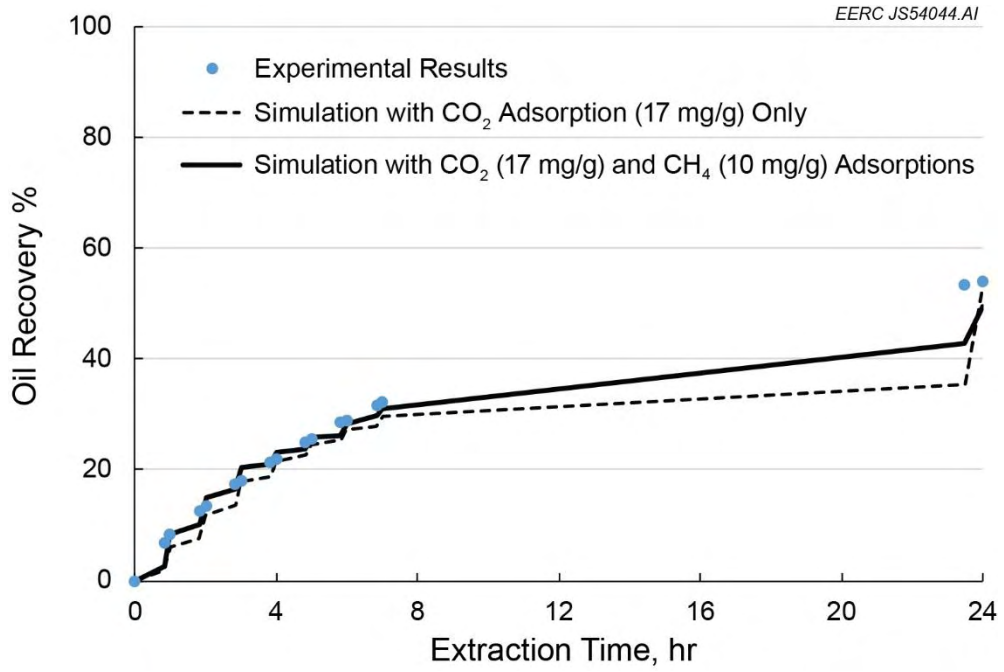

Figure 69. Results of simulations with different adsorption combinations.

Another possible explanation for the simulation's inability to match the experimental recovery factor may be related to capillary forces and relative permeability. The traditional relative permeability theory, as implemented in simulation software, requires knowledge of residual oil saturation in oil-bearing formations, especially when pores are small. Capillary pressure effects are pronounced when pores and pore throats are small, which complicates multiphase fluid flow and results in greater uncertainty of residual oil saturation. Thus determining relative permeability curves for tight/shale formations remains challenging. More studies are needed to understand these effects in unconventional reservoirs and improve simulation technology.

Middle Bakken (nonshale) Plug Modeling – History Matching of CO_2 Permeation and Hydrocarbon Extraction Modeling

Plug-scale models of the Middle Bakken (nonshale) were also used to history-match hydrocarbon extraction experiments. An example of one of the Middle Bakken plug-scale history-matching exercises is presented below. The values of the parameters used in this plug model were based upon measured values for Middle Bakken samples from all four study wells (Table 15).

Experimental hydrocarbon extraction results for Middle Bakken samples were fairly high in comparison to the results from shale hydrocarbon extractions (recovery factors of approximately 98% and 55%, respectively). Jin and others (2016) showed the two most important variables correlated with oil recovery in the Middle Bakken were pore throat radius and water saturation. The average pore throat radius in the Middle Bakken, while still quite small, is substantially larger than that of the shales. Thus capillary forces are relatively lower in the Middle Bakken than in the Upper and Lower Bakken Shales, and concentration-driven diffusion occurs relatively faster, both contributing to greater laboratory-measured extracted hydrocarbon mass. In contrast with the Bakken shales, TOC plays little role in the Middle Bakken. Rock Eval tests showed that there is very little organic matter present. As a result, the Middle Bakken rocks are less capable of adsorbing oil and gas (Figure 70), which may also contribute to increased oil displacement and greater experimental recovery in comparison to the shales.

Table 15. Values of the Rock Petrophysical and Fluid Properties Used in the Middle Bakken Plug Model

Category	Parameter	Value	Unit
Rock	Porosity	3	%
	Permeability	0.023	mD
	Density	165.4	lb/ft^3
	Compressibility	1×10^{-6}	1/psi
Oil	Density	49.6	lb/ft^3
	Viscosity	1.336	cP
Condition	Initial core pressure	15	psi
	Injection pressure	5000	psi
	Temperature	230	°F

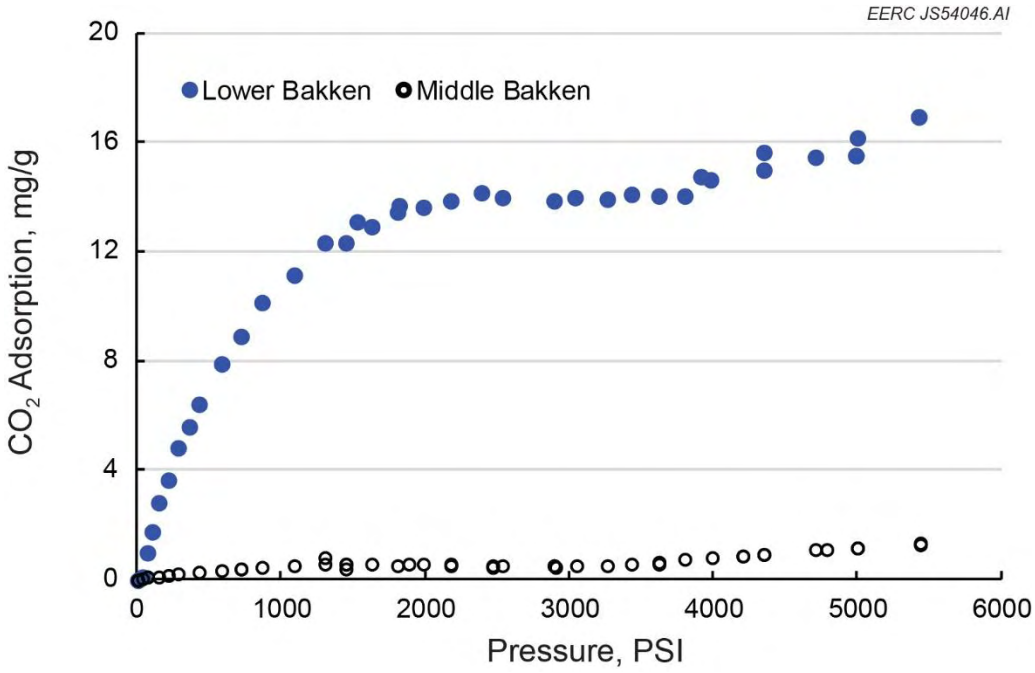

Figure 70. Comparison of CO_2 adsorption capacity for Lower Bakken Shale and Middle Bakken.

A reasonable history match of the extraction results was achieved; however, similar to the shale simulations (Cases 1–3), the Middle Bakken simulation could not reach the 98% oil recovery factor observed at the conclusion of experimental process (Figure 71). The explanation given above in discussing the challenge of matching experimental recovery factors, involving the concepts of connected porosity, capillary forces, and relative permeability, may explain the Middle Bakken simulation results as well.

SIMULATION OF CO_2 INJECTION AND EOR IN A WELL-SCALE BAKKEN MODEL

In addition to plug-scale simulations, a series of well-scale simulation models were prepared to conduct simulations of CO_2 injectivity, CO_2 mobility, and oil production from the Middle Bakken. The goal of these efforts was to better understand the implications of injecting CO_2, CO_2 storage efficiency, CO_2 sweep efficiency, oil mobilization, and the potential for incremental oil recovery through various schemes. Sensitivity studies were performed to quantify the effect of key parameters. Several scenarios were examined in detail, including varied well configurations (vertical or horizontal), well schedules, and targeted injection/production rates.

The models built for the well-scale studies were heterogeneous models, which were used to investigate different injection strategies with two contiguous, hydraulically fractured, horizontal wells. CMG's GEM software was used to perform all simulations, and CMOST, CMG's integrated analysis and optimization tool, was used to perform uncertainty analyses. Reservoir fluid

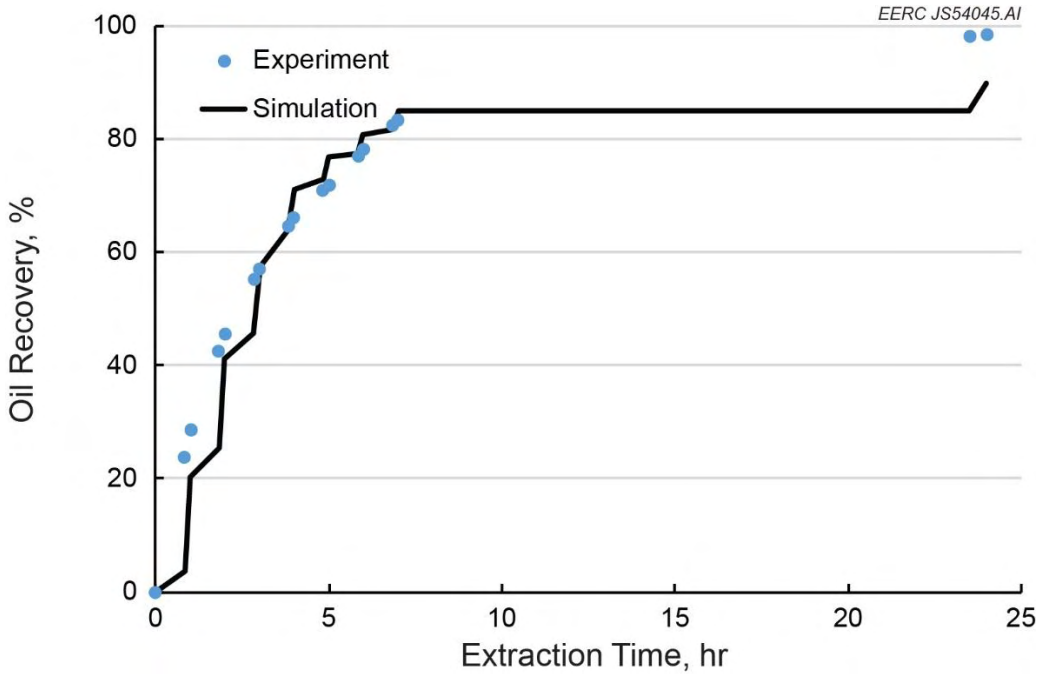

Figure 71. Simulation of CO_2 extraction in a Middle Bakken core sample.

properties and rock–fluid properties were obtained from public literature (Kurtoglu and Kazemi, 2012; Sorensen and others, 2015; Jin and others, 2017b; Hawthorne and others, 2017). Table 16 shows the properties, inputs, and assumptions used to build the model. Element of symmetry were used to reduce the simulation time.

Model Description

The objective of this well-scale modeling exercise was to investigate different CO_2 injection strategies in a sector with two adjacent hydraulically fractured horizontal wells. Dual continuum models were created to estimate the role of natural fractures on CO_2 storage efficiency, CO_2 sweep efficiency, and the potential for incremental oil recovery through various schemes.

The drill spacing unit model had an areal extent of approximately 388 acres (1.57 km^2) with a grid containing 15 layers (layer thickness ranged from 4 to 9 feet), encompassing seven different units including (descending order) the False Bakken, Scallion, Upper Bakken Shale, Middle Bakken, Lower Bakken Shale, and Three Forks (Benches 1 and 2). The model contained two horizontal wells separated by 490 feet. Symmetrical artificial fractures were created, representing a single fracture stage. Fracture half-length and height were fixed at 200 and 94 feet, respectively. The hydraulic fractures propagated from the Upper Bakken Shale through the Lower Bakken Shale units. Figure 72 shows select displays of the geologic model (72a) and the single-stage element of symmetry (Figures 72b to 72f). Preliminary sensitivity analysis showed that results (in terms of the recovery factor) tend to have little sensitivity when varying fracture spacing and number of fracture per element of symmetry.

Table 16. Model Properties, Inputs, and Assumptions

Well Constraints	
• Maximum bottomhole pressure, injector well	3000 psi
• Minimum bottomhole pressure, producer well	1000 psi
Initial Conditions	
• Initial reservoir pressure at 7700 ft	8400 psi
• Vertical average	Water, oil, no free gas
• Water–oil contact	20,000 ft

PVT Properties (after Kurtoglu and others, 2012)

• Oil composition

ID	Pseudo Component	Molar Fraction
1	CO_2	3.22E-02
2	N_2 to CH_4	2.72E-01
3	C_2 to C3	1.85E-01
4	iC4 to nC4	5.37E-02
5	iC5 to C6	7.51E-02
6	C7 to C8	1.18E-01
7	C9 to C13	1.28E-01
8	C14 to C19	6.68E-02
9	C20 to C36	6.96E-02
	Total	1.00E+00

Other Parameters	
Rock Compressibility	1.0e-6 psi^{-1}
Boundary Conditions	Closed boundaries
End Points for Relative Permeability (after Cho and others, 2016)	
• k_{ro} end point at residual water, at S_{wr}	0.4
• Saturation of residual water, S_{wr}	0.5
• k_{rw} end point at irreducible oil, at 1-S_{orw}	0.05
• Saturation of irreducible oil, S_{orw}	0.3
• Exponent for calculating k_{row}, n_{ow}	5
• Exponent for calculating k_{rw}, n_{ow} n_w	1.3
• Trapped oil saturation of irreducible oil, S_{om}	0.05
Elements of Symmetry and Hydraulic Fractures	
• Number of fractures per element of symmetry	2 per 150 ft
• Distance between fractures	50 ft
• Distance between fracture tips and boundary model in X-direction	191 ft
• Distance between fractures and boundary model in Y-direction	41.7 ft
• Distance between fracture tips from another well	76.4 ft
• Hydraulic fracture permeability	1 Darcy

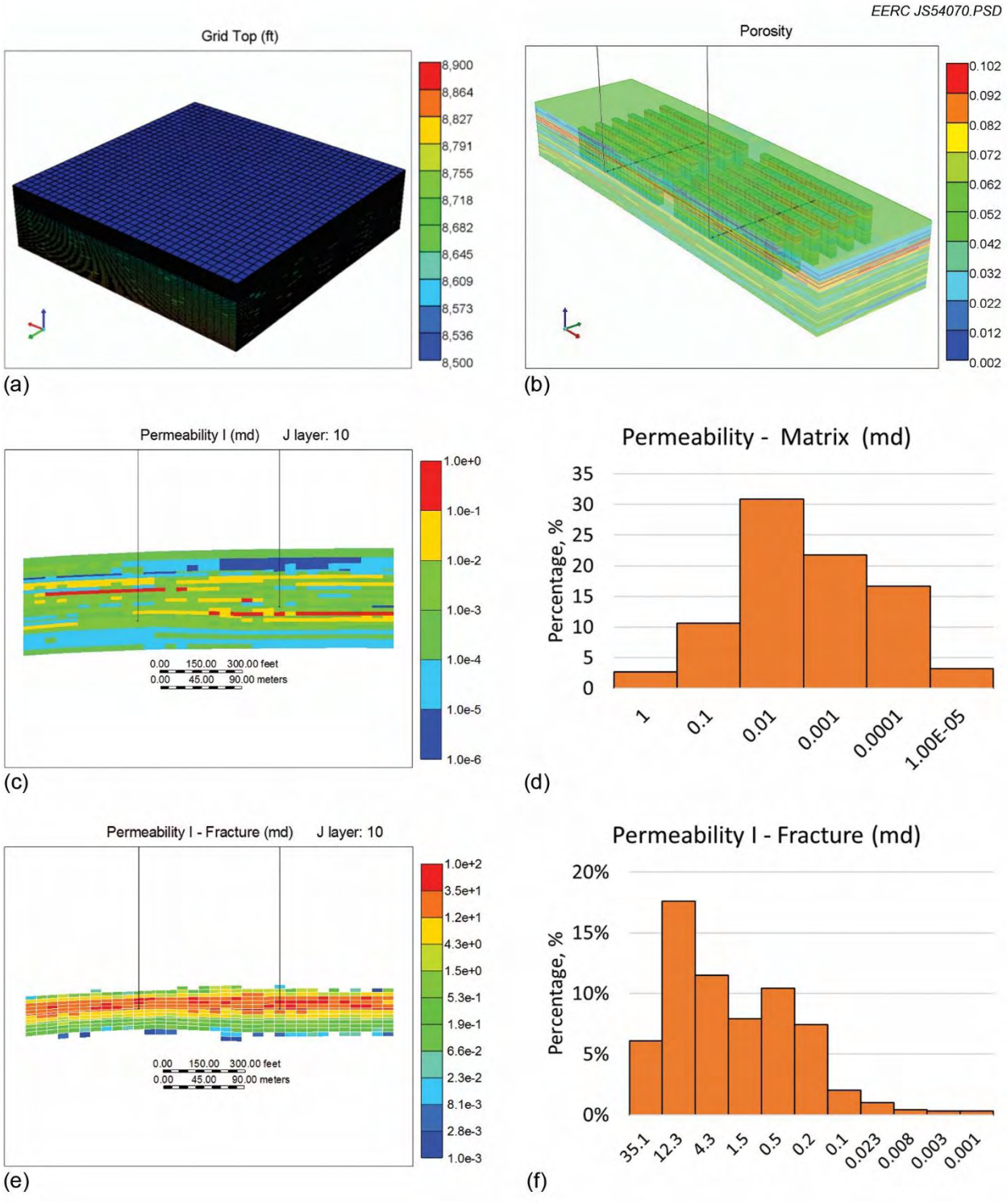

Figure 72. Displays of the geomodel (a) and the single-stage element of symmetry (b–f): 3-D view of the grid top (a), matrix porosity (b), 2-D cross section view of the matrix permeability (c), matrix permeability histogram (d), 2-D cross section view of the fracture permeability (e), and fracture permeability histogram (f). Aspect ratios are 4 (plane XZ) and 1 (plane XY).

Table 16 shows the in situ fluid composition and relative permeability properties, which were obtained from previous works (Kurtoglu and Kazemi, 2012; Sorensen and others, 2015; Cho and others, 2016). The primary production conditions were defined from public reports (Patterson, 2017). Table 17 shows the operational parameters of the six production scenarios, consisting of one reference case undergoing primary production (baseline) and five variants of huff 'n' puff cycles, each cycle containing an injection period of 3 weeks, a soak interval of 1 week, followed by a year of production. This configuration has two potential benefits: 1) CO_2 could help reduce the viscosity of the liquid in the high-permeability channels (either natural or artificial fractures) and adjacent tight pores and 2) CO_2 has been shown to be effective extracting hydrocarbons from tight rocks, as reported in previous EERC lab results (Hawthorne and others, 2017; Jin and others, 2016b, 2017b).

Table 17. List of Operational Scenarios Considered

Case ID	Cycles	Cum. CO_2 Injected, MMscf	Recovery Factor, 30 yr	Gross CO_2 Utilization, Mscf/bbl	Operational Constraints
Reference	0	0	17.9	0	• Minimum BHP (1000 psi) at producers
01	1	3.7	18.5	6.5	• Minimum BHP (1000 psi) at producers • Maximum BHP (3000 psi) at injectors • Cycle length: 3 weeks of injection followed by 1 week of soaking and 1 year of production
02	2	8.1	19.2	6.1	
03	3	12.9	20.0	6.1	
04	6	29.8	21.9	7.2	
05	9	49.5	23.3	8.9	

Simulation Results

For the sake of simplicity, only a subset of the results are presented. Figure 73 shows illustrations of the distribution of the global CO_2 fraction at the end of the first injection cycle. The presence of the natural fractures in the Middle Bakken favors CO_2 transport in the higher permeability region (Figure 73b–c; green- and red-colored blocks ranging from 0.3 to 1 global CO_2 molar fraction). At the same time, the Upper and Lower Bakken Shale layers (Figure 73b–c; blue-colored blocks below 0.1 global CO_2 molar fraction) contain lower CO_2 concentration. However, the adsorption behavior of CO_2 in the Upper and Lower Bakken Shale layers was not considered in these simulations. The natural fracture network acts as an extension of the hydraulic fracture, providing additional contact area, which may lead to more favorable conditions for the recovery process. As expected, the matrix blocks located in the vicinity of hydraulic fractures accumulated higher CO_2 concentration.

A comparison of oil production with and without CO_2 injection is presented in Figure 74. As shown, the incremental production *per injection cycle* remains above the baseline (reference case) for about 4 years before stabilizing at the baseline level. Figure 75 shows the oil recovery factor after 30 years of operation for the different scenarios studied. The reference case exhibited

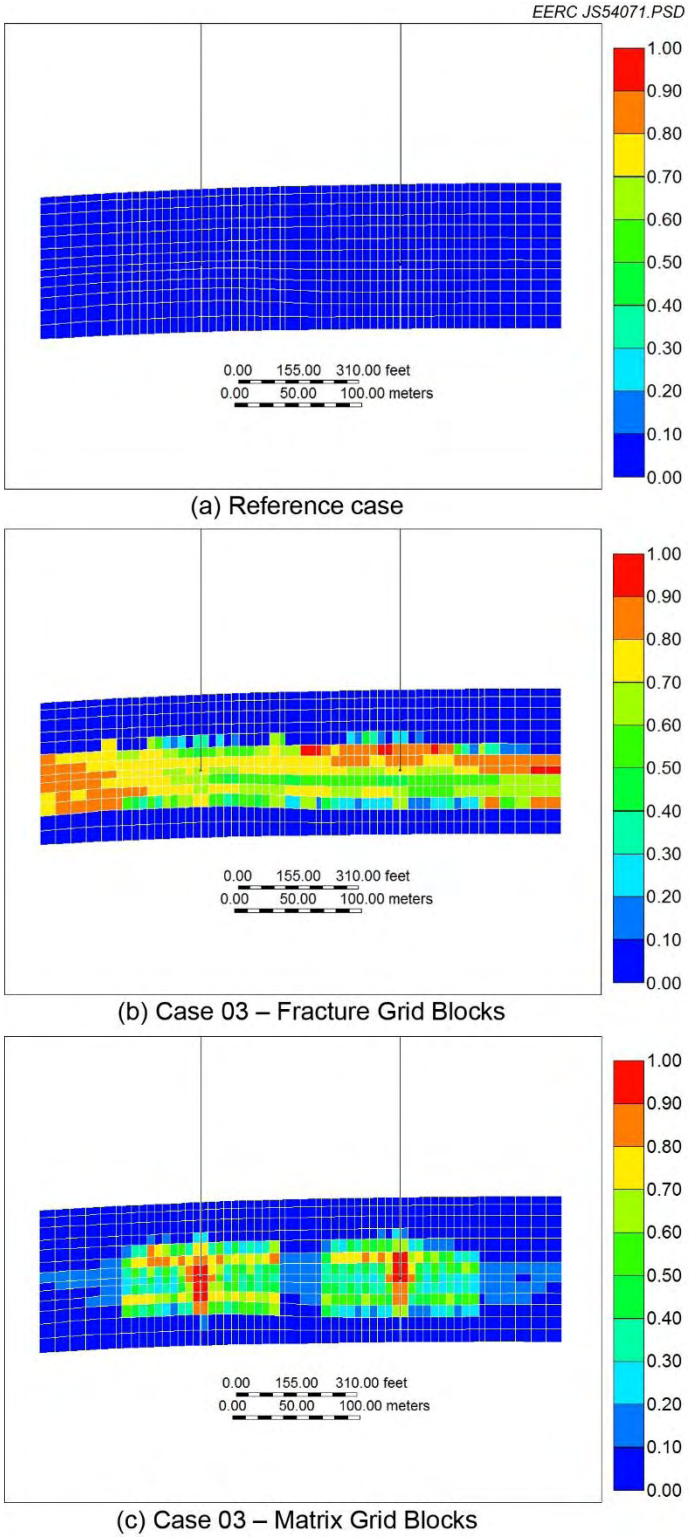

Figure 73. 2-D cross-sectional view at the center of the model showing the spatial distribution of the global CO_2 molar fraction at a time equivalent to the end of the first injection cycle for a) the reference case (primary production without injection), b) fracture blocks – Case 03, and c) matrix blocks – Case 03. Aspect ratio is 4 (Plane XZ).

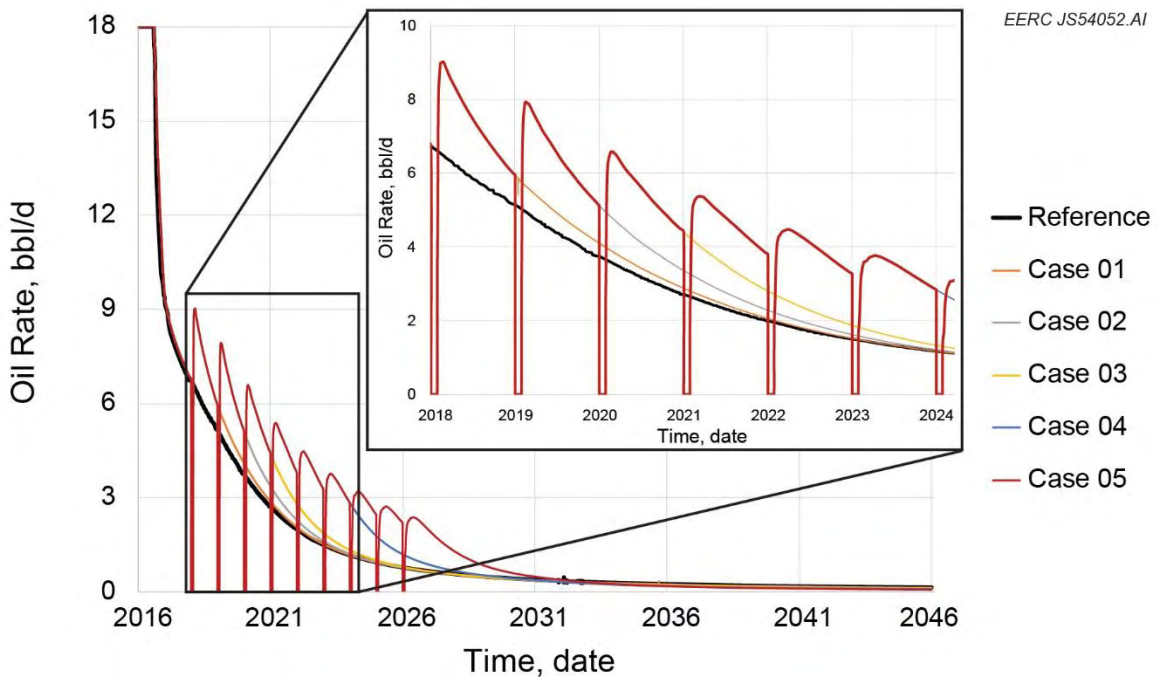

Figure 74. Oil production forecast over 30 years. Inset zooms in on the time frame from 2018 to 2024.

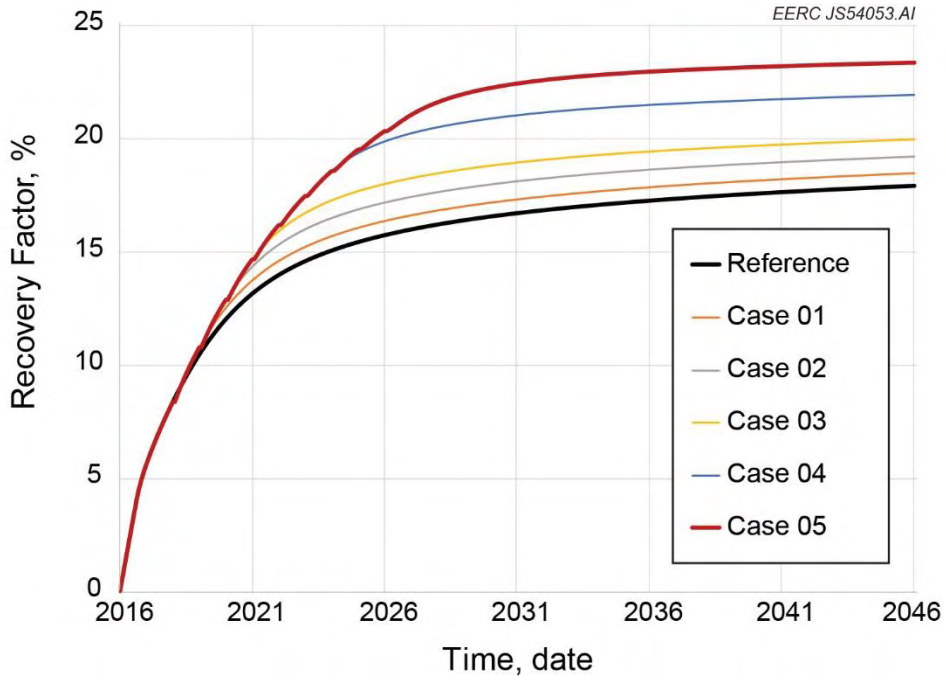

Figure 75. Recovery factor forecast over 30 years.

a recovery factor of nearly 18%. Case 5 (nine huff 'n' puff cycles simulated) resulted in an incremental oil recovery exceeding 5% of the reference case. The gross CO_2 utilization number (amount of CO_2 required per incremental barrel) ranges from 6.1 to 8.9 Msfc/bbl, which indicates an excellent use of the solvent when compared with CO_2 EOR operations for conventional reservoirs (Azzolina and others, 2015).

This work provides a better understanding of the physical mechanisms affecting CO_2 storage efficiency, CO_2 sweep efficiency, and oil mobilization for tight oil reservoirs and shales. Simulation results confirmed the potential benefits of using CO_2 huff 'n' puff injection in drill spacing units having adjacent hydraulically fractured horizontal wells. The effect of fractures on CO_2 storage efficiency, CO_2 sweep efficiency, and the potential for incremental oil recovery through various schemes has been studied with the help of dual porosity–permeability models. Potential benefits from using CO_2 as an injection fluid were quantified in terms of the incremental recovery factor. While this study improved the understanding of the mechanisms of using CO_2 injection as an unconventional EOR process, optimization of both oil production and CO_2 storage remains to be investigated.

Predictions of Incremental Oil Recovery and CO_2 Storage Resource

The key findings and summary discussion of the well-scale scale simulations, including predictions of CO_2-based incremental oil recovery, recovery factor improvement, and potential CO_2 storage resource estimates for the Bakken, are included below:

- The study revealed that the presence of natural fracture networks could result in more favorable CO_2 sweep efficiency and oil mobilization in tight oil reservoirs. The natural fractures may significantly increase the contact area between the formation and the (artificially) stimulated region, leading to more favorable conditions for the recovery process. Consequently, reservoir characterization emerged as a critical element in understanding the effectiveness of CO_2 storage and incremental oil recovery for tight oil formations.

- The reference case of the single fracture stage model resulted in an estimated recovery factor of nearly 18% after 30 years of production. This may be an optimistic estimate; most calculated recovery factors estimated for Bakken wells range in the single digits. However, the simulation time frame assumed 30 years of production, while most Bakken wells have been completed in the past decade. The permeability distribution in the model assumed a discrete (natural) fracture network which translated to an effective permeability up to 1 mD in the Middle Bakken; locations with relatively fewer natural fractures would likely have a significantly lower effective permeability. The simulation also did not take into account geomechanical and stress-dependent permeability effects, which seem to exist in currently operating Bakken wells. Additionally, the results were developed from a single fracture stage; however, not all fracture stages (from heel to toe of a horizontal well) would be expected to behave the same.

- The simulation results showed incremental recovery factors ranging from 0.6% to 5.4%. The highest incremental recovery factor observed from the simulations occurred from

nine huff ‘n’ puff cycles was approximately 5.4%. This number could be increased by conducting more huff ‘n’ puff cycles over the lifespan of an operating well and/or by optimizing the operational parameters. And while 5.4% may still be perceived as a relatively small increase over primary production, the implications for an incremental recovery of 5.4% for production throughout the area of Bakken production is enormous, with Bakken OOIP estimated to be 300 billion barrels (LeFever and Helms, 2008).

- The associated CO_2 storage potential was estimated using the methodology explained by Azzolina and others (2015). The case with nine cycles resulted in a net CO_2 utilization of approximately 1.8 Mscf per barrel of incremental oil produced. Assuming the OOIP mentioned above, an estimated incremental oil recovery range of 0.6% to 5.4% implies additional cumulative production ranging from 1.8 billion to 16 billion barrels. Therefore, simulation results suggest a CO_2 storage volume estimate ranging from 169 Mt to 1.5 Gt for the Bakken in North Dakota. Estimates assumed a conversion factor of 1 metric ton of CO_2 per 19.25 Mscf at standard conditions of 101.4 kPa (14.7 psi) and 21.1°C (70°F) (U.S. Department of Energy, 2010b).

CONCLUSIONS AND KEY FINDINGS

The obvious primary challenge of using the Bakken Formation, or any tight oil formation, as a target for large-scale storage of CO_2 and EOR is the characteristic low porosity and low permeability of the formation. Furthermore, the presence of complex, heterogeneous lithologies (including organic-rich, oil-saturated shales) complicates the ability to understand and predict the effectiveness of various mechanisms (e.g., diffusion, sorption, dissolution, etc.) that will be acting on CO_2 mobility and storage.

In an attempt to experimentally quantify the ability of CO_2 to permeate tight Bakken rocks and mobilize oil from them, a set of laboratory experiments were conducted on small core plugs. While similar experiments on Bakken rocks had been conducted and presented in Hawthorne and others (2013), it was thought that the generation of more CO_2 permeation and oil extraction data from samples obtained from other wells was necessary to confirm those earlier studies. Also, the new experiments were designed to specifically generate permeation and extraction data on the key lithofacies that were the subject of advanced characterization. The results of the CO_2 permeation and oil extraction experimental tests clearly demonstrate, at the core plug scale, the ability of CO_2 to permeate both organic-rich shales and tight nonshale rocks and subsequently mobilize oil from those rocks. In fact, most of the hydrocarbon mobilization occurred within the first 8 hours of the experiment, with between 85% and 95% of the oil being removed from the Middle Bakken samples and between 50% and 60% being removed from the shales in that initial time period.

The characterization efforts confirm that micro- to nanoscale pore throat sizes dominate the fluid flow pathways within both the Bakken shales and the nonshale lithofacies. This underscores the notion that detailed knowledge of nanoscale pore throat networks is necessary to accurately predict fluid-phase behavior. That knowledge, in turn, is needed to determine the mechanisms controlling CO_2 permeation and storage in the Bakken, as well as attendant hydrocarbon mobilization that can lead to EOR. With respect to CO_2, micro- to nanoscale fracture networks will

be the primary means of its movement throughout the unstimulated areas of the reservoir, and the characteristics of those naturally occurring small-scale fracture systems will control the contact time that CO_2 has with the oil in the reservoir. By using advanced characterization techniques, including very high resolution images generated by the FESEM and FIBSEM studies, detailed knowledge of the microscale fractures and nanoscale pore networks was obtained.

The advanced characterization efforts showed that the Bakken shales are dominated by organics, as expected, but also appear to have substantial connected nanoscale porosity in those organics. The presence of nanoscale fracture networks that occur within kerogen following thermal maturation (as described by Loucks and others, 2009; Bousige and others, 2016) was confirmed, providing support to the concept that a nanoscale pore throat network occurs within the kerogens that could serve as a pathway for fluid transport within organic-rich shales. These nanoscale pore throat networks may be the means by which CO_2 can permeate and mobilize hydrocarbons in the Bakken shale, as was observed by the CO_2 permeation and oil extraction experiments.

With respect to the nonshale rocks of the Middle Bakken reservoir, previous work suggests that much of the permeability within unstimulated Middle Bakken lithofacies (i.e., the matrix) is associated with microfractures (Sorensen and others, 2015). However, conventional SEM images of Middle Bakken samples show that microfractures are often filled or partially filled with clays. FESEM analysis of a clay-filled microfracture showed the existence of pore spaces within the clays. The use of FIBSEM analysis on that clay-filled microfracture showed that the nanoscale porosity observed in the clay filling is actually highly connected. This, in turn, suggests that despite the presence of clay the microfracture may indeed serve as a fluid flow pathway for injected CO_2 and subsequently mobilized hydrocarbons. These trends were observed in many of the Middle Bakken samples that were characterized using this method, especially those in the laminated (MB-L3) and packstone (MB-L4) lithofacies. These observations provide compelling evidence that the microfractures and the nanoscale pore network within them may be a substantial portion of the means by which CO_2 can permeate the tight Middle Bakken lithofacies and mobilize hydrocarbons, as observed by the CO_2 permeation and oil extraction experiments.

The data generated by the activities presented yield an improved understanding of the nature and distribution of nano-, micro-, and macroscale pores and fracture networks. Results provide previously unavailable insight on nanoscale pore throat mineralogy and connectivity, rock matrix characteristics, mineralogy, and organic content. These efforts suggest molecular diffusion, total organic content, and pore throat size perhaps exert more influence on CO_2 permeation and storage in tight oil formations than in conventional oil reservoirs. These findings were used to support modeling of EOR schemes, yielding refined estimates of potential incremental oil recovery and the CO_2 storage resource of the Bakken.

Specific key findings of this project include the following:

- High-pressure mercury injection tests indicated that the mean pore throat radius was approximately 3.5 nm in the Bakken shale samples. Such small pore sizes yield high capillary pressure and make fluid flow difficult in the rock matrix.

- Supercritical CO_2 extracted 94% to 100% of the crude oil hydrocarbons from 11-mm-diameter Bakken nonshale reservoir rock rods in 24 hours under typical Bakken reservoir conditions. The recovery of oil in 5 hours from those same rods ranged from 55% to 95%, with the laminated lithofacies MB-3 consistently showing the fastest recovery.

- Supercritical CO_2 extracted 12%–67% of the crude oil hydrocarbons from 11-mm-diameter Bakken shale rods in 24 hours under typical Bakken reservoir conditions (e.g., 34.5 MPa and 110°C).

- CO_2 adsorption isotherm data clearly showed that the Bakken shales have considerable ability to adsorb CO_2 under reservoir conditions and the formation could be a promising target to store a large quantity of CO_2 permanently.

- Carefully tuned numerical models were able to reproduce the experimental oil recovery results and upscale the extraction process from laboratory to field scale.

- All of the Bakken rock extractions with CO_2 testing performed to date support the "soaking" mechanism rather than the "flushing" mechanism that predominates in conventional EOR floods. In addition to the hydrocarbon swelling and lowered crude oil viscosity that occurs upon CO_2 contact, ultimate hydrocarbon recovery from unconventional tight shales and nonshales appears to be based on concentration gradient-driven diffusion.

- The fact that the submicroscale fracture networks identified by the FIBSEM within the organics of the shales, coupled with the fact that the organic matrix may have nanoscale porosity, has important implications that may explain how CO_2 was able to permeate into the shales and oil was able to migrate out.

- History-matching simulations of extraction experiments were not quite able to reach the final recovery factor measured in those experiments. This result was observed in modeling of both shale and nonshale plug experiments. This discrepancy may be caused by the model's inability to account for the connected nature of the porosity that was observed at the submicroscopic scale. Those pathways, however small, may account for the higher CO_2 permeation and oil mobility observed in the experiments.

- Simulation results suggest the use of CO_2 for EOR in the Bakken petroleum system may yield 1.8 billion to 16 billion barrels of incremental oil.

- Simulation results suggest the Bakken petroleum system may have a CO_2 storage resource of 169 Mt to 1.5 Gt.

BEST PRACTICES FOR CHARACTERIZATION AND MODELING OF TIGHT OIL FORMATIONS

Reservoir characterization and modeling are critical components of any efforts to apply CO_2 injection into tight oil formations for the purpose of EOR and/or storage. The results of the laboratory- and modeling-based activities conducted under this project demonstrate that the combination of traditional and advanced rock characterization techniques, innovative permeation and extraction studies, and multiscale reservoir modeling can provide valuable insight on the behavior of CO_2 in tight, organic-rich shales and nonshale reservoirs. The knowledge and experience gained over the course of this project also provide insight to a variety of "best practices" that can be applied to future tight oil formation reservoir characterization and modeling.

Best Practices with Respect to Matrix and Fluid Pathway Characterization

Understanding flow pathways in organic-rich shales and tight nonshale rocks is essential to predicting the behavior of CO_2 in tight oil formations and designing effective injection, production, and storage schemes. A broad suite of traditional and advanced analytical techniques should be applied to any effort to characterize tight oil formations. In broad terms, the prediction of fluid behavior requires detailed, high-resolution data on matrix characteristics, the geometry and distribution of natural fractures and pore throat networks, and the nature of organic matter.

An accurate and robust geologic description of macroscopic features in core such as lithology, fabric, depositional features, fossils, and macroscale fractures is necessary to provide the context within which the data generated by analytical techniques can be interpreted. A wide variety of traditional analytical techniques can be used that yield critical data on the matrix and fluid pathways (i.e., fractures and pore throat networks). Those techniques and their value to tight rock characterization are briefly described below:

- XRD and XRF provide detailed data on the mineralogical composition of the matrix. These data are necessary to predict potential geochemical interactions that might occur with CO_2. It is also invaluable for correlating core samples to well logs, which in turn is an essential component of building geocellular models through the use of MMPA techniques described earlier.

- Porosity and grain density data derived from instruments such as a helium porosimeter are also key parameters that are used for core-to-log correlations and MMPA. Porosity is a critical component of any simulation modeling.

- Optical petrographics yield data on the distribution of mineral phases, grains, macro- and meso-scale fracture characteristics and clues to the depositional environment of the matrix. This information is necessary for the construction of geocellular models at scales ranging from core plugs to reservoirs.

- Traditional SEM techniques (including BSE and EDS imagery) generate data on matrix grain elemental composition which can be used to create mineral distribution maps and quantify mineral composition, providing corroborative data for XRD and XRF results.

SEM also provides insight on pore throat geometry and distribution, particularly with respect to the characterization of microfractures (e.g., determination of natural vs. induced, aperture and length measurements, and orientation).

- Breakthrough pressure tests to provide the entry pressure required for a select fluid, in this case CO_2, to be injected into the matrix can be used as input to simulation modeling.

- Mercury injection capillary entry pressure (MICP) tests yield data on pore throat size and distribution.

- Geomechanical testing generates data on rock mechanical properties, including peak strength, Young's modulus, and Poisson's ratio. These data can aid in the creation of discrete fracture networks in geocellular models. Rock compressibility data can also be derived, which is a basic parameter used in simulation modeling.

There is an expansive set of published literature, often entire textbooks, on each of these analytical techniques, and an exhaustive discussion of them is beyond the scope of this report. However, their application to the shale and nonshale rocks found in tight oil formations warrants some discussion. The low porosity and low permeability of tight rocks, and the dominance of micro- to nanoscale pore throat networks, means that analytical techniques capable of delivering high resolution, high magnification, and high accuracy results are critical to understanding the role the matrix will play in CO_2 behavior in fluid-rich tight rocks. This means that SEM-derived data and MICP testing play a major role in tight rock characterization.

Permeability as it is traditionally defined is one parameter that is considered to be essential in the characterization of conventional reservoir rocks but which is conspicuously absent from the list above. The use of gas permeameters and fluid flow-through testing in whole cores and/or core plugs are common methods for measuring the permeability of a conventional reservoir rock. Permeability distribution is a fundamental aspect of any geocellular modeling, regardless of scale, and is a critical component of any simulation of fluid behavior in a reservoir. However, the low porosity and dominance of nanoscale pore throat networks that are the defining characteristics of tight rocks make the application of traditional permeability analytical techniques difficult in the shale and nonshale rocks of the Bakken. Because of their tight nature, traditional flow-through tests to determine matrix permeability in organic-rich shales and nonshale rocks of the Bakken are typically time-consuming (e.g., hundreds of hours for a single shale sample is not unusual) and, therefore, can be very expensive. Results from different samples of the same lithofacies from the same well can often vary by orders of magnitudes, depending on the abundance and nature of microfractures, or lack thereof. Furthermore, when reservoir-scale injection and production schemes are simulated, the permeability of the naturally occurring and hydraulically induced fracture networks in the reservoir will overwhelmingly control the movement of fluids. When the effort and cost necessary to conduct permeability testing on tight rocks are combined with the limited application of such data in the context of traditional reservoir-scale modeling, it becomes clear that detailed, accurate matrix permeability data for tight oil formations may have limited value. That is not to say that reality-based values for permeability are not necessary for modeling tight shale and nonshale rocks, because they most certainly are. Rather, the research conducted over the course of this project suggests that it may be more cost-effective to use advanced

analytical techniques such as CT, micro-CT, FESEM, and FIBSEM combined with innovative data processing to infer matrix permeability values that can then be applied to plug and core-scale modeling and, ultimately, upscaled to larger-scale applications.

Relative permeability of water, oil, and CO_2 is another parameter that is necessary to conduct model simulations of CO_2-based EOR and storage in conventional reservoirs. However, as with single-phase permeability, the tight nature of the Bakken shale and nonshale rocks makes the generation of relative permeability data very difficult, time consuming, and expensive. It is also further complicated by the complex nature of wettability that has been observed in Bakken rocks. While the Bakken is often reported to be primarily an oil-wet rock in the North Dakota and Montana portions of the Williston Basin, it can also be water-wet and intermediate-wet (Wang and others, 2012). The measurement of wettability in Bakken rocks is challenging, and confidence in Bakken wettability data is limited. Wettability can have a strong effect on relative permeability, and poor understanding of wettability can lead to misinterpretation or misapplication of relative permeability values in a rock.

As mentioned above, wettability is a parameter that is typically determined for conventional reservoirs but which is difficult to measure for organic-rich shale and tight nonshale oil-producing formations. Overall, there are a variety of methods for measuring wettability. The most notable methods described in the literature include imbibition tests, such as the Amott Method, the U.S. Bureau of Mines (USBM) method which is conducted using a centrifuge, microscope examination methods, and the use of nuclear magnetic relaxation analytical techniques. Each of these can be effective when employed within its own sphere of influence. However, these methods all suffer from reproducibility and can provide contrary determinations when compared. In addressing the issue of reproducibility, the quality of the evaluation can be tested by restoring the core to an approximation of its original state and retesting it. If similar results are achieved then the test has been precise, at least with regard to itself (Anderson, 1986). In addressing the issue of contrary results from different methods on the same sample, when comparisons are made between methods, it must be understood that different methods test different characteristics of the core sample in order to make a wettability determination. Some such as USBM average the whole sample, others such as contact-angle focus in on a small mineral crystal, and some such as imbibition can be affected by variables which are not even considered in the others. As a result, it is possible for separate tests to disagree on the wettability of the sample, and this must be considered when results are interpreted. Furthermore, some knowledge of the different characteristics present in the sample must be had in order to determine which method is most appropriate. No method is perfect, and to some extent, each must be considered an approximation of the wettability of the sample, useful only within the set boundaries governing its use.

Focusing in on wettability determinations for the Bakken shale and similar reservoirs, particular consideration must be made to the measurement techniques applied. For the low-permeability tight shales of the Bakken, a review of the literature suggests that the basic methods described above are not capable of yielding consistent, reliable, quantitative results. In overcoming these difficulties, Wang and others (2012) proposed and utilized an altered Amott–Harvey method, testing thin slices of core plugs inside core holders subject to pressurized flow. In organic-rich shales, researchers have also made use of NMR methods to evaluate wettability and to quantify the amount of imbibed fluids (Odusina and others, 2011). From such work, the wettability of the

Bakken shale was determined to range from oil-wet to intermediate-wet (Wang and others, 2012, 2016b). Some have taken this further and propose that the Bakken is of more intermediate wetting with mixed wetting resulting from oil-wet organic pores and water-wet inorganic pores (Alvarez and Schechter, 2016). As with relative permeability testing, all of these more recently developed approaches to wettability testing in the Bakken are complicated, time-consuming, expensive, and open to interpretation.

Best Practices in the Acquisition and Use of the Rock Eval Technique

Data obtained through the Rock Eval pyrolysis technique are commonly applied to assessments determining the in-place hydrocarbon resource within a specific reservoir. The Bakken Formation has been investigated using the technique with the intent of gaining insight regarding the petrographic and petrophysical characterization of the formation, specifically, the contribution of organic content to the ultimate productivity of the formation. Studies by Nordeng and LeFever (2009), Hackley and Cardott (2016), Aderoju and Bend (2013), and others have focused on the Bakken Formation using the Rock Eval technique as the basis for geochemical interpretations of source rock potential, thermal maturity, and resource quantification. The results of previous efforts show that the organic matter in the Bakken is of marine origin (Type II) and the thermal alteration is well within the oil generating window (Hackley and Cardott, 2016). Thermal maturity for the Bakken within the Williston Basin is variable and ranges from immature through mature.

As part of the efforts to further the understanding of the nature of the organic matter in the Bakken, this project included Rock Eval testing of samples from the four study wells. In the context of discussing best practices with respect to the use of Rock Eval data, a summary of key learnings about the technique and interpretations of the data generated by this project and others is discussed below, as well as the challenges encountered in assessments of tight unconventional oil reservoirs. Specific limitations with the technique and cautions regarding interpretation are identified and summarized.

While the Rock Eval technique and use of the data produced has been well documented in the literature (Carvajal-Ortiz and Gentzis, 2015; Dembicki, 2009; Jarvie, 1991), a brief summary of the sample preparation process and data generated is provided. In short, Rock Eval is a pyrolysis process whereby the gases evolved from the rock sample are analyzed by a flame ionization detector (FID) capable of detecting hydrocarbons, inorganic carbon, and oxygen liberated as the temperature of the instrument is gradually increased from 150° through 850°C. This is performed on a crushed rock sample (60–100 mg) sieved to approximately 100 µm to ensure a uniform combustion and release of gases. Samples are placed into a crucible, loaded onto an automated carriage, and (with the instrument programmed for either reservoir or source rock analysis) allowed to cycle through the specified temperature range. The difference between the two analytical techniques pertains to an extended temperature ramp profile currently referred to as extended slow heating or ESH. This is preferred for known source rocks and has been demonstrated to separate the S2 peak into heavy hydrocarbon plus solid bitumen and kerogen with no oil generative potential (Sanei and others, 2015). Figure 76 shows a typical pyrogram generated using the Rock Eval technique, and Figure 77 shows the ESH pyrogram.

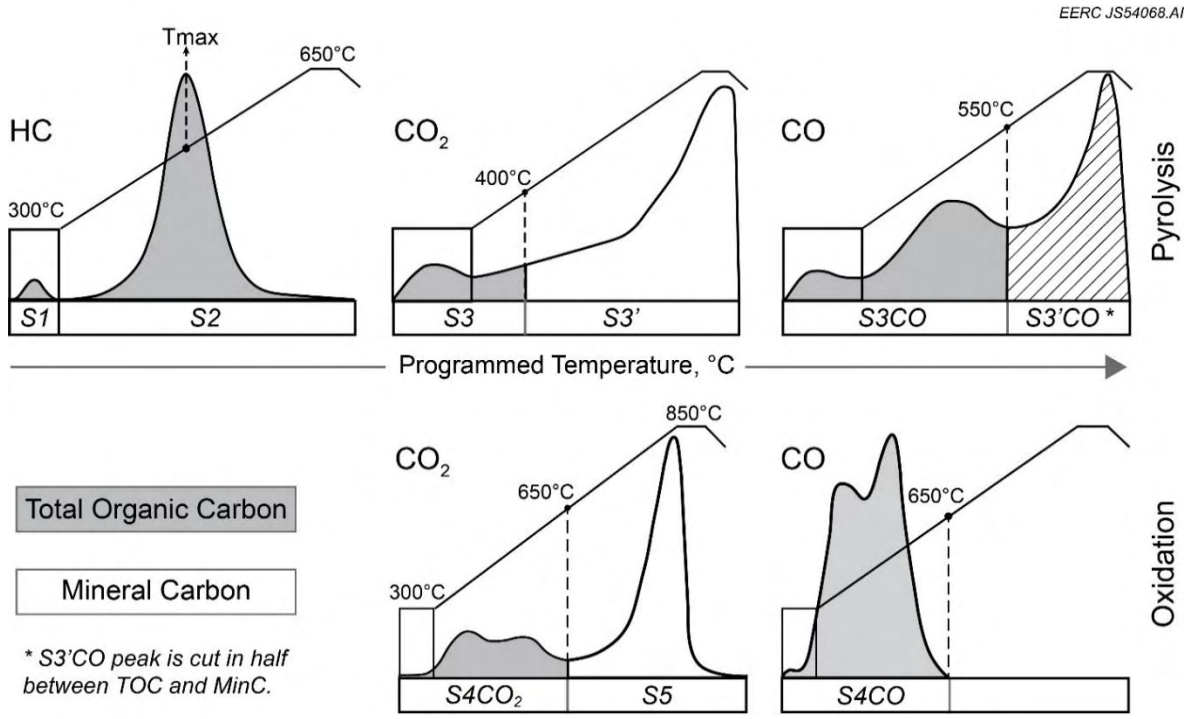

Figure 76. Diagram illustrating the temperature ramp used to develop the S1 to S4 peaks using Rock Eval pyrolysis (Behar and others, 2001).

Additional data obtained for both techniques include the mobile light hydrocarbon, or S1 peak, and the S3 peak interpreted as the CO_2 content of the sample. Calculated parameters include the hydrogen index (HI), oxygen index (OI), and vitrinite reflectance equivalent (Vro). Each of these calculated values provides information regarding the depositional source of the in-place organic matter as well as the thermal maturity of the resource.

Several advantages of the Rock Eval technique have been identified, including the small sample size needed for analysis (60–100 mg of crushed rock), quick turnaround time, and the ability to run a large number of samples using a single analytical instrument setup. However, if the individual using the data is unfamiliar with the technique and changes in the shape of the resulting pyrograms due to different sample preparation and heating profiles, misinterpretations can easily be made with regard to estimating paleoenvironmental setting, degree of thermal maturity, in place hydrocarbons, or in the direct correlation of the TOC to reservoir quality.

Despite the wide variety of source rock characteristics that can be analyzed through Rock Eval pyrolysis, shortcomings do exist. Routine analytical methods used in reservoir characterization of conventional reservoirs are not wholly applicable in unconventional reservoirs and this holds true for source rock analysis by pyrolysis. According to Carvajal-Ortiz and Gentzis (2015), classical guidelines used for well-understood and familiar rock sources are not applicable in every lithology, leading to both errors in measurement and interpretation.

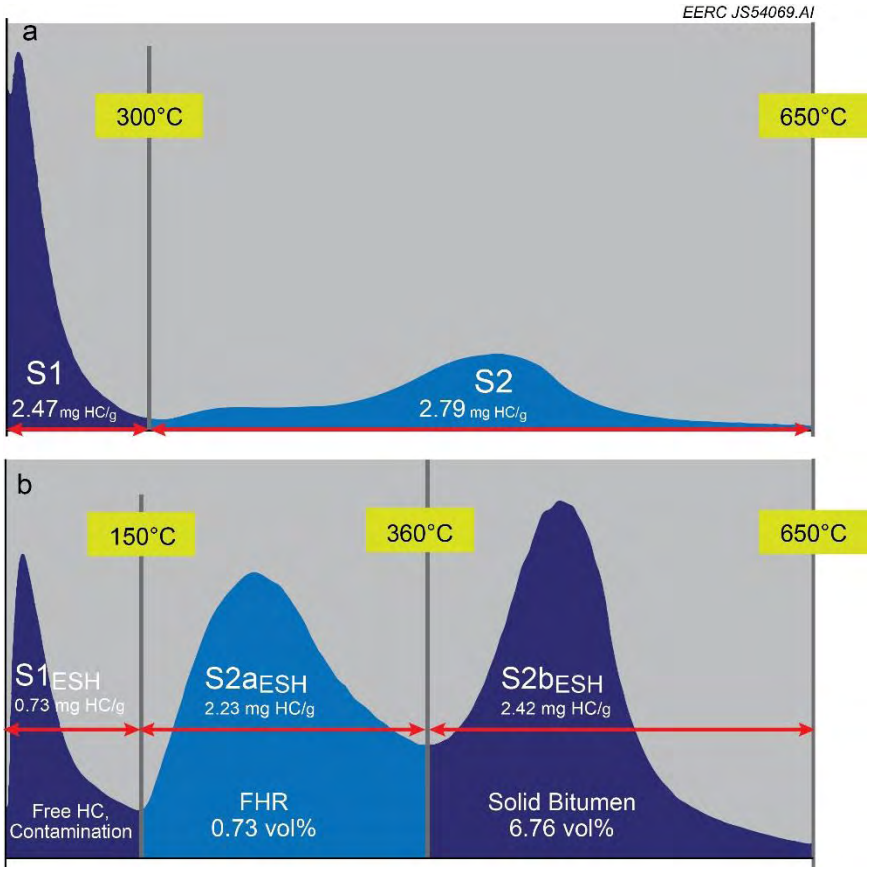

Figure 77. Example of pyrogram generated using the ESH method. As shown, the technique splits the S2 peak into two distinct portions and enables the interpreter an opportunity to better evaluate the total free (S1) and heavy hydrocarbon resource.

Regarding errors in measurement, several authors have discussed the failings of Rock Eval when confronted with samples of high or very low organic content (Carvajal-Ortiz and Gentzis, 2015; Hart and Steen, 2015; Jarvie, 1991). This is related to the detection limits of the flame ionization detectors (FID) which are responsible for measuring the amounts of hydrocarbons emitted and thus determine the S1/S2 peaks. On the current Rock Eval systems, these are only accurate in providing S2 readings between 0.3 mg HC/g Rock and 33 mg HC/g Rock (Carvajal-Ortiz and Gentzis, 2015). In the excess case, there is so much organic matter and associated hydrocarbons in the sample that the device cannot measure it all. This error results in the underestimation of the S2 value which leads to underestimations of both TOC and the HI. This is detected on pyrograms where the S2 temperature peak plotted against the FID voltage response exceeds 125 mV. Samples rich in free hydrocarbons which spill over from S1 into S2 provide a similar response. A correction can be made if high organic content is suspected. A smaller sample weight with a longer evaluation time (ESH) reduces the amounts of hydrocarbons present at any one stage and allows for improved readings (Jarvie, 1991). An important consideration is the characteristics of the samples being tested when Rock Eval pyrolysis is performed, as data reviewed and corroborated with other sources can be used for economic determinations of

viability. The Bakken Shale, for example, is one source rock with high enough organic content to cause measurement errors if a large sample size is used.

Further errors in measurement can result from oil-based mud contamination which upon cleaning of the sample, renders the S1 values and thus TOC data useless (Carvajal-Ortiz and Gentzis, 2015), bitumen carryover between heating phases causing high HI values (Carvajal-Ortiz and Gentzis, 2015; Hart and Steen, 2015), S2 reductions associated with mineral matrices (Dahl and others, 2004; Hart and Steen, 2015; Katz, 1983), and the inherent error of non-Gaussian pyrograms from whose peaks T_{max} is derived (Carvajal-Ortiz and Gentzis, 2015).

The most egregious errors associated with Rock Eval pyrolysis are not those of the analytical technique but rather those associated with misinterpretation and misuse of generated data. For Rock Eval pyrolysis to provide the most meaningful paleoenvironmental data, thermally immature samples are preferred because mature samples have lower TOC and hydrogen content because of postdepositional impacts to organic matter and generation of hydrocarbons. This requirement creates sampling constraints and can restrict analysis to the fringe of a formation, limiting in some cases the usefulness (Chen and others, 2017) of the data. Furthermore, analysis must be done with reverence given to the geologic setting being studied. Source rock mineralogy and associated properties are heterogeneous and vary throughout any defined region, requiring the use of probabilistic models when trying to generalize results. Rock Eval alone cannot indicate thermal maturity, as TOC and HI vary with maturation and free hydrocarbon presence is not indicative of production (Dembicki, 2009). However, with the combination of the Arrhenius equation, activation energies with Gaussian distributions, and kinetic curves, estimations can be made on the maturity of the rock sample. A common misuse of Rock Eval data is the interpretation made with modified Van Krevelen-type diagrams to determine the types of organic content/kerogen in the sample. This method relies upon the use of HI and OI to substitute in for H/C and O/C ratios which leads to inaccuracy (Katz, 1983). HI and OI are not valid in determining the mixture of kerogen-types present in a sample as different combinations can have the same HI and OI (Dembicki, 2009). A more appropriate method is provided through vitrinite reflectance and pyrolysis-gas chromatography which can accurately provide kerogen type and compositions.

Overall, Rock Eval pyrolysis is an efficient and useful technique for source rock analysis, although sources of error must be understood so they can be minimized. The following summarizes several key concepts to consider when Rock Eval pyrolysis is used in tight unconventional resource reevaluation:

1. With proper utilization, Rock Eval pyrolysis is an important tool for source rock evaluation. Prior to making interpretations, a working/institutional knowledge of depositional setting, burial history, and thermal maturity should be considered.

2. Rock Eval is subject to only being accurate for certain ranges of TOC and overall hydrocarbon presence. Paleoenvironmental and resource interpretations should be supported through the use of additional geochemical techniques, including vitrinite reflectance.

3. Sample selection and preparation play a critical role in determining the hydrocarbon resource available. Cleaning samples for oil-based mud contamination destroys the S1 peak and limits the S2 peak, leading to errors associated with T_{max} and generatable hydrocarbons.

4. Interpreters of data should be wary of FID detector saturation values above 125 mV. This provides a misleading interpretation of thermal maturity and generation potential for source rocks. If this is observed, the sample can be reanalyzed using a reduced mass.

5. In the interpretation, the following must be considered: geological setting from which a sample is taken, heterogeneous nature of that setting when making generalizations, careful application and simulation of activation energy heterogeneity when determining thermal maturity, and not to utilize Rock Eval for unsuitable tasks, i.e., gas chromatography.

6. Depending on the sample (reservoir vs. source rock), an extended heating profile may be advantageous (Sanei and others, 2015). Using this technique on known source rocks, the S2 peak is broken into two peaks and is interpreted as one peak being potentially mobile heavy hydrocarbons (S2a) and the second being solid bitumen/pyrobitumen (S2b) with no oil-generative potential. This information can help refine hydrocarbon-in-place estimates and assess the overall reservoir quality of tight reservoirs.

Best Practices with Respect to Modeling of Tight Oil Formations

The modeling activities conducted during the project and described above used industry standard software packages offered by Schlumberger and CMG. Those software packages and the methods and work flows described in the modeling section of this report were found to be effective at addressing the questions that were posed over the course of this project. However, in terms of best practices, it is difficult and perhaps even not appropriate to recommend that any of the approaches and workflows applied to this project be considered to be "best practices." At less than 20 years old, the exploitation of unconventional tight oil resources is still in a relatively early phase of development, and it has become clear that the modeling approaches that are standard practice for conventional reservoirs do not adequately take into account the unique properties of unconventional tight reservoirs (Rassenfoss, 2016). The concept of injecting CO_2 into unconventional tight oil formations for storage and/or EOR has only been seriously examined over the past decade, and there are still significant knowledge gaps with respect to how recent advances in understanding the mechanisms controlling CO_2 behavior in tight, organic-rich formations can be coupled with predictive modeling. Despite the technical advances that have been made by this project and by other researchers at other institutions in recent years (e.g., the Bakken Research Consortium at the Colorado School of Mines, the Tight Oil Consortium at the University of Calgary, and the Unconventional Shale Consortium at the University of Oklahoma), there are still no clear, globally accepted protocols for modeling unconventional tight oil formations. One of the primary shortcomings in identifying best practices for modeling CO_2 storage and EOR in unconventional tight oil formations is that there are very few data sets from pilot-scale field tests that allow for validation and verification of modeling efforts. Until more data from real-world, pilot-scale CO_2 injection tests in tight oil formations, and the lessons learned from those tests, can

be integrated into modeling exercises, it is difficult to suggest that any particular approach to modeling these unconventional reservoirs is any better than another. In short, more research activities that integrate laboratory- and field-based data sets are necessary to identify best practices for modeling CO_2 storage and EOR in unconventional tight oil formations.

RECOMMENDATIONS FOR FUTURE RESEARCH ON CO_2 STORAGE AND EOR IN UNCONVENTIONAL TIGHT OIL FORMATIONS

To better evaluate the efficacy of CO_2-based EOR and storage in unconventional systems, future work should focus on better understanding the factors that affect long-term injectivity, migration, and storage of CO_2 in different unconventional rock types. The present effort performed advanced characterization and modeling on different rock types contained within the Bakken, including carbonate-rich clastics and organic-rich shale source rocks. These investigations enabled the identification of future work needs specific to different unconventional rock types.

Substantial progress was made toward achieving the goals and objectives of the present project, including the development of new insight on the use of advanced characterization techniques, fluid mobility and CO_2 storage potential in organic-rich shales and tight nonshales, and the integration of that data into multiscale modeling. However, many challenges remain with respect to achieving the ultimate goal of commercial deployment of CO_2 storage and EOR in unconventional tight oil formations. Specific topics in which more research is needed are described briefly below.

- Within the Bakken nonshale reservoir rocks, a key question is "At what rate would CO_2 traveling within induced fractures (in the field) permeate into naturally occurring microfractures and into the unfractured rock matrix, thereby accessing hydrocarbons for EOR?" The key factors that control the rate of CO_2 permeation into the reservoir matrix should also be identified and further evaluated. For example, the acidification of formation fluid as a result of CO_2 injection could induce geochemical reactions with particular minerals within the rock matrix. Flow pathways within the Bakken reservoir rocks appears to occur within clay-filled pore networks and naturally occurring fractures. Therefore, understanding potential interactions between CO_2 and various clay types that might occur within the reservoir over time is important to understanding long-term CO_2 transport and storage.

- For the Bakken shales, the results of this study suggest that the nano- to microscale porosity within the organic material could play a major role in CO_2 transport and storage. Additional work is needed to understand the role of organics including: 1) how the types of organic material (i.e., kerogen, bitumen, solid bitumen, etc…) within the organic-rich shale matrices affect CO_2 transport and adsorption/absorption and 2) how the thermal maturity of organic-rich shales affects the occurrence and distribution of porosity within the organic matrix. Understanding these processes is also necessary to better assess the efficacy of hydrocarbon recovery by CO_2 in organic-rich shales, both with respect to volume of hydrocarbons recovered and the time periods required for extraction.

- A new paradigm is needed for assessing relative permeability and fluid behavior in unconventional tight oil formations. In particular, the role of Darcy flow versus non-Darcy flow is a topic of intense debate both in academia and industry. Both laboratory and modeling-based studies are needed to address questions of fluid/flow behavior in the context of relative permeability. Such data are essential to achieve accurate modeling of CO_2 behavior and fate in tight oil formations.

- Production of oil from, and subsequent injection of CO_2 into, tight oil formations requires hydraulic fracturing. A detailed understanding of the geomechanical properties of both shale and nonshale lithofacies in tight oil formations is another aspect of these reservoirs that is necessary to develop accurate predictive models. While the application of geomechanical modeling to design hydraulic fracturing programs is widely practiced in industry, there are currently no globally accepted methods for coupling geomechanical models with reservoir matrix and fluid property models. Such coupled models are necessary to address the complexity inherent in understanding and predicting fluid behavior in flow regimes that range from macroscale hydraulically induced fracture networks down to nanoscale pore throats in organic material such as kerogen and bitumen. In addition, while rock mechanical constitutive equations for the solid matrix is an active area of research, experimental data to validate model assumptions for unconventional tight oil reservoirs are scarce.

- Laboratory and modeling work should be reconciled for improving the understanding on the dynamics of relevant physicochemical mechanisms occurring in production from tight oil reservoirs. Fluid characterization techniques needs to be adapted to the CO_2 EOR recovery process for guaranteeing an accurate modeling of the physicochemical mechanisms occurring at the microscopic scale in nanoporous rocks (molecular diffusion, sorption, matrix-fracture mass transfer, capillary pressure-controlled viscous flow, etc.). Compositional data from the lab experiments at the core scale are necessary to provide fundamental information for bridging multiple scales using commercial modeling tools. For example, multicomponent adsorption and matrix-fracture mass transfer could influence the hydrocarbon extraction with CO_2 from the ultralow permeability organic matrix. Novel multiscale simulation methods could help to clarify how the water–CO_2, CO_2–hydrocarbon interfaces, and solid–fluid interactions at the micro- and mesopores affect the macroscopic conditions.

- The dynamic nature of production (e.g., reservoir pressure can go from several thousands of psi to hundreds of psi during depletion and back up again when a neighboring well is hydraulically fractured) and how those dynamics may affect porosity, permeability, and fluid behavior with respect to CO_2 and hydrocarbon mobility need to be understood. Interplay between operational conditions and rock mechanical effects, such as stress-dependent permeability, may significantly influence fluid flow in the reservoir and production performance.

- Relative permeability tests need to be modified to account for the unique properties of unconventional tight oil formations. In particular, the temporally dynamic nature and role of Darcy flow and the role of organics need to be more fully understood and considered

to develop models that accurately predict fluid behavior. The role of changing gas-to-oil ratios (GOR), interfacial tension of in situ fluids, pore pressure, geomechanical stress fields, and the effects those parameters can have on relative permeability also needs to be better understood.

- More representative CO_2 EOR and storage laboratory experiments should be designed to mimic the CO_2–oil–water interactions in actual reservoir conditions for both shale and nonshale rocks.

- Natural fracture systems and more representative hydraulic fracture profiles should be integrated into the simulation models to better mimic fluid flow behavior in the fracture-matrix system. Molecular diffusion, gravity segregation, and oil swelling are mechanisms that may play a principal role in naturally fractured reservoirs and need to be accounted for in the modeling and simulation studies. Physically accurate models at reservoir conditions are required to represent nonideal, multicomponent mixtures in the oil and gas phases.

- The significance and impacts of pore size distribution, capillary pressure, and relative permeability curves should be studied as a part of future modeling efforts. The role of the capillary pressure threshold needs to be investigated with and without the presence of water-filled pores.

- More effective simulation methods and grid settings should be developed to improve simulation efficiency in order to enable the models to predict CO_2 EOR and storage performance in multiwell scenarios. Representative models need to include transport mechanisms from ultralow permeability matrix and complex fracture networks. Geomechanical effects during production must be included to account for stress-dependent properties and dynamic fracture conductivity effects. Well interference and fracture spacing require a special consideration to evaluate the long-term CO_2 EOR performance.

- More data from real-world, pilot-scale CO_2 injection tests in tight oil formations, and the lessons learned from those tests, are needed to verify and validate modeling approaches that have been developed by this and (other) projects.

BIBLIOGRAPHY OF PAPERS AND PRESENTATIONS

The references cited below are papers published and presentations delivered at technical conferences and meetings that were based on the results of the activities conducted under this project.

Published Papers and Journal Articles

Hawthorne, S.B., Jin, L., Kurz, B.A., Miller, D.J., Grabanski, C.B., Sorensen, J.A., Pekot, L.J., Bosshart, N.W., Smith, S.A., Burton-Kelly, M.E., Heebink, L.V., Gorecki, C.D., Steadman,

E.N., and Harju, J.A., 2017, Integrating petrographic and petrophysical analyses with CO_2 permeation and oil extraction and recovery in the Bakken tight oil formation: Paper SPE-185081-MS presented at SPE Canada Unconventional Resources Conference, Calgary, Alberta, Canada, 15–16 February.

Jacobs, T., 2015, Unconventional resources will require unconventional EOR: Journal of Petroleum Technology, v. 67, no. 9, p. 68–69, Society of Petroleum Engineers, September.

Jin, L., Hawthorne, S., Sorensen, J., Pekot, L., Kurz, B., Smith, S., and Harju, J., 2017, Extraction of oil from the Bakken shales with supercritical CO_2: Paper presented at the SPE-AAPG-SEG Unconventional Resources Technology Conference, Austin, Texas, 24–26 July 2017, p. 1934–1950, URTeC 2671596.

Jin, L., Hawthorne, S.B., Sorensen, J.A., Pekot, L.J., Kurz, B.A., Smith, S.A., Heebink, L.V., Herdegen, V., Bosshart, N.W., Torres Rivero, J.A., Dalkhaa, C., Peterson, K., Gorecki, C.D., Steadman, E.N., and Harju, J.A., 2017, Advancing CO_2 enhanced oil recovery and storage in unconventional oil play—experimental studies on Bakken shales: Applied Energy, ISSN 0306-2619, in press.

Jin, L., Sorensen, J. A., Hawthorne, S. B., Smith, S. A., Bosshart, N. W., Burton-Kelly, M. E., and Harju, J. A., 2016, Improving oil transportability using CO_2 in the Bakken system—a laboratory investigation: Society of Petroleum Engineers, February 24, doi:10.2118/178948-MS.

Rassenfoss, S., 2016, Pores to predictions—nanoscale clues to larger mysteries: Journal of Petroleum Technology, v. 68, no. 12, p. 27–33, Society of Petroleum Engineers, December.

Sorensen, J.A., Kurz, B.A., Smith, S.A., Walls, J., Foster, M., and Aylsworth, B., 2016, The use of advanced analytical techniques to characterize micro- and nanoscale pores and fractures in the Bakken: Paper presented at the SPE-AAPG-SEG Unconventional Resources Technology Conference, San Antonio, Texas, USA, 1–3 August 2016, URTeC 2433692.

Sorensen, J.A., Kurz, B.A., Hawthorne, S.B., Jin, L., Smith, S.A., and Azenkeng, A., 2017, Laboratory characterization and modeling to examine CO_2 storage and enhanced oil recovery in an unconventional tight oil formation: Paper presented at 13th International Conference on Greenhouse Gas Control Technologies, GHGT-13, 14–18 November 2016, Lausanne, Switzerland, published in Energy Procedia, v. 114, p. 5460–5478, Elsevier, July 2017.

Presentations at Technical Conferences

Hawthorne, S.B., Jin, L., Kurz, B.A., Miller, D.J., Grabanski, C.B., Sorensen, J.A., Pekot, L.J., Bosshart, N.W., Smith, S.A., Burton-Kelly, M.E., Heebink, L.V., Gorecki, C.D., Steadman, E.N., and Harju, J.A., 2017, Integrating petrographic and petrophysical analyses with CO_2 permeation and oil extraction and recovery in the Bakken tight oil formation: Presentation delivered at SPE Canada Unconventional Resources Conference, Calgary, Alberta, Canada, 15–16 February.

Jin, L., Hawthorne, S., Sorensen, J., Pekot, L., Kurz, B., Smith, S., and Harju, J., 2017, Extraction of oil from the Bakken shales with supercritical CO_2: Presentation delivered at the SPE-AAPG-

SEG Unconventional Resources Technology Conference, Austin, Texas, 24–26 July 2017, p. 1934–1950, URTeC 2671596.

Sorensen, J.A., and Hamling, J., 2016, Improved characterization and modeling of tight oil formations for CO_2 enhanced oil recovery potential and storage capacity estimation: Presentation delivered to 2016 Carbon Capture, Utilization, and Storage Conference, Tysons, Virginia, June 15.

Sorensen, J., Hawthorne, S., Kurz, B., Smith, S., Jin, L., Bosshart, N., Steadman, E., and Harju, J., 2015, Improved characterization and modeling of tight oil formations for CO_2 enhanced oil recovery potential and storage capacity estimation: Presentation delivered to 2015 DOE NETL Carbon Storage R&D Project Review Meeting, Pittsburgh, Pennsylvania, August 18.

Sorensen, J., 2016, Improved characterization and modeling of tight oil formations for CO_2 enhanced oil recovery potential and storage capacity estimation: Presentation delivered to 2016 DOE NETL Mastering the Subsurface Through Technology Innovation & Collaboration: Carbon Storage & Oil & Natural Gas Technologies Review Meeting, Pittsburgh, Pennsylvania, August 17.

Sorensen, J., 2017, Enhanced oil recovery in unconventionals: Presentation delivered to 2017 Williston Basin Petroleum Conference, Regina, Saskatchewan, Canada, May 4.

Sorensen, J, 2017. Improved characterization and modeling of tight oil formations for CO_2 enhanced oil recovery potential and storage capacity estimation: Presentation delivered to 2017 DOE NETL Mastering the Subsurface Through Technology Innovation & Collaboration: Carbon Storage & Oil & Natural Gas Technologies Review Meeting, Pittsburgh, Pennsylvania, August 2.

Sorensen, J.A., Kurz, B.A., Smith, S.A., Walls, J., Foster, M., and Aylsworth, B., 2016, The use of advanced analytical techniques to characterize micro- and nanoscale pores and fractures in the Bakken: Presentation delivered at the SPE-AAPG-SEG Unconventional Resources Technology Conference, San Antonio, Texas, 1–3 August 2016, URTeC 2433692.

Sorensen, J.A., Kurz, B.A., Hawthorne, S.B., Jin, L., Smith, S.A., and Azenkeng, A., 2016, Laboratory characterization and modeling to examine CO_2 storage and enhanced oil recovery in an unconventional tight oil formation: Presentation delivered at 13th International Conference on Greenhouse Gas Control Technologies, GHGT-13, Lausanne, Switzerland, 14–18 November 2016.

Sorensen, J., 2017, Improving unconventional production through advanced characterization techniques—a Bakken story: Presentation delivered to the Society of Petroleum Engineers Chapter Monthly Luncheon, Oklahoma City, Oklahoma, May 24.

REFERENCES

Aderoju, T.E., and Bend, S.L., 2013, A rock-evaluation of the Bakken formation in southern Saskatchewan: summary of investigations 2013, v. 1, Saskatchewan Geological Survey, Saskatchewan Ministry of the Economy, Misc. Rep 2013-4-1, Paper A-2, p. 14.

Aguilera, R., 2014. Flow units—from conventional to tight-gas to shale-gas to tight-oil to shale-oil reservoirs: SPE Reservoir Evaluation & Engineering, v. 17, p. 190–208.

Alharthy, N.S., Nguyen, T.N., Teklul, T.W., Kazemil, H., and Graves, R.M., 2013, Multiphase compositional modeling in small-scale pores of unconventional shale reservoirs: Paper presented at SPE Annual Technical Conference and Exhibition, New Orleans, Louisiana, September 30 – October 2, SPE 166306.

Alvarez, J.O., and Schechter, D.S., 2017, Wettability alteration and spontaneous imbibition in unconventional liquid reservoirs by surfactant additives: SPE Reservoir Evaluation & Engineering, v. 20, p. 107–17.

Alvarez, J.O., and Schechter, D.S., 2016, Altering wettability in Bakken shale by surfactant additives and potential of improving oil recovery during injection of completion fluids: Society of Petroleum Engineers, April 11, doi:10.2118/179688-MS.

Anderson, W., 1986, Wettability literature survey – Part 2—wettability measurement: Society of Petroleum Engineers, November 1, doi:10.2118/13933-PA.

ASTM International, 2014, ASTM Method D7708-14 standard test method for the microscopical determination of refectance of vitrinite dispersed in sedimentary rocks: ASTM International, West Conshohocken, Pennsylvania.

Azzolina, N.A., Nakles, D.V., Gorecki, C.D., Peck, W.D., Ayash, S.C., Melzer, L.S., and Chatterjee, S., 2015, CO_2 storage associated with CO_2 enhanced oil recovery—a statistical analysis of historical operations: International Journal of Greenhouse Gas Control, v. 37, p. 384–397.

Behar, F., Beaumont, V., and Penteado, H.L.D.B., 2001, Rock–Eval technology—performances and developments: Oil & Gas Science and Technology, v. 56, n. 2, p. 111–134.

Bertrand, R., 1990, Correlations among the reflectances of vitrinite, chitinozoans, graptolites and scolecodonts: Organic Geochemistry, v. 15, p. 565–574.

Bish, D.L., and Howard, S.A., 1988, Quantitative phase analysis using the Rietveld method: Journal of Applied Crystallography, v. 21, no. 2.

Bousige, C., Ghimbeu, C.M., Vix-Guterl, C., Pomerantz, A.E., Suleimenova, A., Vaughan, G., Garbarino, G., Feygenson, M., Wildgruber, C., Ulm, F.J., Pellenq, R.J.M., and Coasne, B., 2016, Realistic molecular model of kerogen's nanostructure: Nature Material, v. 15, p. 576–583.

Brian, S., and Barrufet, M., 2017, Constructing oil/gas capillary pressure and relative permeability curves from a distribution of pores in shale reservoirs, *in* Proceedings of Unconventional Resources Technology Conference: Austin, Texas, July 24–26, 2017, p. 1035–1054, URTeC-2670123.

Carvajal-Ortiz, H., and Gentzis, T., 2015, Critical considerations when assessing hydrocarbon plays using Rock Eval pyrolysis and organic petrology data—data quality revisited: International Journal Coal Geology, v. 115, p. 113–122.

Casas, L., 2005, Large-scale hydraulic fracturing test on a rock with discontinuities: M.S. thesis, Colorado School of Mines, Golden, Colorado.

Chen, Z., Liu, X., Guo, Q., Jiang, C., and Mort, A., 2017, Inversion of source rock hydrocarbon generation kinetics from Rock-Eval data: Fuel, v. 194, p. 91–101.

Cho, Y., Uzun, I., Eker, E., Yin, X., and Kazemi, H., 2016, Water and oil relative permeability of Middle Bakken Formation—experiments and numerical modeling: Unconventional Resources Technology Conference, San Antonio, Texas, August 1.

Continental Resources, Inc., 2012, Bakken and Three Forks: www.contres.com/operations/bakken-and-three-forks (accessed May 30, 2013).

Corder, G.W., and Foreman, D.I., 2009, Nonparametric statistics for nonstatisticians: Hoboken, New Jersey: John Wiley & Sons, p. 99–105, ISBN 9780470454619.

Dahl, B., Bojesen-Koefoed, J., Holm, A., Justwan, H., Rasmussen, E., and Thomsen, E., 2004, A new approach to interpreting Rock-Eval S2 and TOC data for kerogen quality assessment: Organic Geochemistry, v. 35, p. 1461–1477.

Dembicki, H., Jr., 2009, Three common source rock evaluation errors made by geologists during prospect or play appraisals: AAPG Bulletin, v. 93, p. 341–356.

de Pater, C.J., Cleary, M.P., Quinn, T.S., Barr, D.T., Johnson, D.E., and Weijers, L., 1994, Experimental verification of dimensional analysis for hydraulic fracturing: SPE Production and Facilities, November, p. 230–238.

Eide, Ø., Fernø, M.A., Alcorn, Z., and Graue, A., 2016, Visualization of carbon dioxide enhanced oil recovery by diffusion in fractured chalk: SPE Journal, v. 21, p. 112–120.

Energy Information Administration, 2013, Technically recoverable shale oil and shale gas resources—an assessment of 137 shale formations in 41 countries outside the United States: U.S. Department of Energy Washington, D.C., www.eia.gov/analysis/studies/worldshalegas/pdf/fullreport.pdf (accessed 2013).

Er, C., Yangyang, L., Jingzhou, Z., Wang, R., Bai, Z., and Han, Q., 2016, Pore formation and occurrence in the organic-rich shales of the Triassic Chang-7 Member, Yanchang Formation, Ordos Basin, China, Journal of Natural Gas Geoscience, http://dx.doi.org/10.1016/j.jnggs.2016.11.013.

Erdman, N., and Drenzek, N., 2013, Integrated preparation and imaging techniques or the microstructural and geochemical characterization of shale by scanning electron microscopy, *in* Camp, W., Diaz, E., and Wawak, B., Eds., Electron microscopy of shale hydrocarbon reservoirs: AAPG Memoir 102, p. 7–14.

Geiger, J., Hunyadfalvi, Z., and Bogner, P., 2009, Analysis of small-scale heterogeneity in clastic rocks by using computerized x-ray tomography (CT): Engineering Geology, v. 103, nos. 3–4, p. 112–118.

Grogan, A.T., Pinczewski, V.W., Ruskauff, G.J., and Orr Jr, F.M., 1988, Diffusion of CO_2 at reservoir conditions—models and measurements: SPE Reservoir Engineering, v. 3, p. 93–102.

Guo, W., Hu, Z., Zhang, X., Yu, R., and Wang, L., 2017, Shale gas adsorption and desorption characteristics and its effects on shale permeability: Energy Exploration & Exploitation, v. 35, p. 463–481.

Guo, P., Wang, Z., Shen, P., and Du, J., 2009, Molecular diffusion coefficients of the multicomponent gas−crude oil systems under high temperature and pressure: Industrial & Engineering Chemistry Research, v. 48, p. 9023–9027.

Habibi, A., Binazadeh, M., Dehghanpour, H., Bryan, D., and Uswak, G., 2015, Advances in understanding wettability of tight oil formations: Society of Petroleum Engineers, September 28, doi:10.2118/175157-MS.

Hackley, P.C., and Cardott, B.J., 2016, Application of organic petrography in North American shale petroleum systems—a review: International Journal of Coal Geology, v. 163, p. 8–51, ISSN 0166-5162.

Hart, B.S., and Steen, A.S., 2015, Programmed pyrolysis (Rock Eval) data and shale paleoenvironmental analyses—a review: Interpretation, v. 3, no. 1, p. SH41-SH58.

Hawthorne, S.B., Miller, D.J., Grabanski, C.B., Sorensen, J.A., Pekot, L.J., Kurz, B.A., and Melzer, S., 2017, Measured crude oil MMPs with pure and mixed CO_2, methane, and ethane, and their relevance to enhanced oil recovery from Middle Bakken and Bakken shales: Society of Petroleum Engineers, February 15, doi:10.2118/185072-MS.

Hawthorne, S.B., Gorecki, C.D., Sorensen, J.A., Miller, D.J., Harju, J.A., and Melzer, S., 2014, Hydrocarbon mobilization mechanisms using CO_2 in an unconventional oil play: Energy Procedia, v. 63, p. 7717–7723.

Hawthorne, S.B., Gorecki, C.D., Sorensen, J.A., Steadman, E.N., Harju, J.A., and Melzer, S., 2013, Hydrocarbon mobilization mechanisms from Upper, Middle, and Lower Bakken reservoir rocks exposed to CO_2: Paper presented at the SPE Unconventional Resources Conference – Canada, Society of Petroleum Engineers, SPE 167200-MS.

Heller, R., and Zoback, M.. 2014, Adsorption of methane and carbon dioxide on gas shale and pure mineral samples: Journal of Unconventional Oil and Gas Resources, v. 8, p. 14–24.

Helsel, D.R., and Hirsch, R.M., 2002. Statistical methods in water resources techniques of water resources investigations: Book 4, chapter A3, U.S. Geological Survey, 522 p.

Hoffman, B.T., and Evans, J.G., 2016, Improved oil recovery IOR pilot projects in the Bakken formation: Society of Petroleum Engineers, doi:10.2118/180270-MS, May 5.

Hoteit, H., and Firoozabadi, A., 2009, Numerical modeling of diffusion in fractured media for gas-injection and-recycling schemes: SPE Journal, v. 14, p. 323–337.

Hubbert, M.K., and Willis, D.G., 1957, Mechanics of hydraulic fracturing: AIME Petroleum Transactions, v. 210, p. 153–168.

IEA Greenhouse Gas R&D Programme, 2009, Development of storage coefficients for CO_2 storage in deep saline formations: 2009/12, October 2009.

Jamialahmadi, M., Emadi, M., and Müller-Steinhagen, H., 2006, Diffusion coefficients of methane in liquid hydrocarbons at high pressure and temperature: Journal of Petroleum Science and Engineering, v. 53, p. 47–60.

Jarrell, P.M., Fox, C.E., Stein, M.H., and Webb, S.L., 2002, Practical aspects of CO_2 flooding: SPE Monograph v. 22, Henry L. Doherty Series, Richardson, Texas, 220 p.

Jarvie, D.M., 1991, Total organic carbon (TOC) analysis, *in* R.K. Merrill, Ed., Handbook of petroleum geology, source and migration processes and evaluation techniques: AAPG, Treatise of Petroleum Geology, p. 113–118.

JEOL-USA, Inc., 2013, JSM-7800f extreme-resolution analytical field emission SEM: www.jeolusa.com/PRODUCTS/ElectronOptics/ScanningElectronMicroscopesSEM/FESEM/JSM7800F/tabid/869/Default.aspx#227380-specifications (accessed June 28, 2013).

Jin, H., and Sonnenberg, S.A., 2012, Source rock potential of the Bakken shales in the Williston Basin, North Dakota and Montana: American Association of Petroleum Geologists Search and Discovery Article No. 20156.

Jin, L., Hawthorne, S., Sorensen, J., Pekot, L., Kurz, B., Smith, S., and Harju, J., 2017a, Extraction of oil from the Bakken shales with supercritical CO_2: Unconventional Resources Technology Conference, July 24.

Jin, L., Hawthorne, S.B., Sorensen, J.A., Pekot, L.J., Kurz, B.A., Smith, S.A., Heebink, L.V., Herdegen, V., Bosshart, N.W., Torres Rivero, J.A., Dalkhaa, C., Peterson, K., Gorecki, C.D., Steadman, E.N., and Harju, J.A., 2017b, Advancing CO_2 enhanced oil recovery and storage in unconventional oil play—experimental studies on Bakken shales: Applied Energy, ISSN 0306-2619, in press.

Jin, L., Sorensen, J. A., Hawthorne, S. B., Smith, S. A., Bosshart, N. W., Burton-Kelly, M. E., and Harju, J. A., 2016, Improving oil transportability using CO_2 in the Bakken system—a laboratory investigation: Society of Petroleum Engineers, February 24, doi:10.2118/178948-MS.

Josh, M., Esteban, L., Delle Piane, C., Sarout, J., Dewhurst, D.N., and Clennell, M.B., 2012, Laboratory characterisation of shale properties: Journal of Petroleum Science and Engineering, v. 88–89, p. 107–124.

Kang, S.M., Fathi, E., Ambrose, R.J., Akkutlu, I.Y., and Sigal R.F., 2011, Carbon dioxide storage capacity of organic-rich shales: SPE Journal, v. 16, no. 4, p. 842–55.

Katz, B.J., 1983, Limitations of "Rock-Eval" pyrolysis for typing organic matter: Organic Geochemistry, v. 4, p. 195–199.

Klobes, P., Riesemeier, H., Meyer, K., Goebbels, J., and Hellmuth, K.H., 1997, Rock porosity determination by combination of x-ray computerized tomography with mercury porosimetry: Journal of Analytic Chemistry, v. 357, p. 543–547.

Kurtoglu, B., and Kazemi, H., 2012, Evaluation of Bakken performance using coreflooding, well testing, and reservoir simulation: Society of Petroleum Engineers, doi:10.2118/155655-MS, January 1.

Kurtoglu, B., Sorensen, J., Braunberger, J., Smith, S., and Kazemi, H., 2013, Geologic characterization of a Bakken reservoir for potential CO_2 EOR: Unconventional Resources Technology Conference, Denver, Colorado, August 12–14, 2013, URTeC 1619698.

Leahy-Dios, A., and Firoozabadi, A., 2007, Unified model for nonideal multicomponent molecular diffusion coefficients: AIChE journal, v. 53, p. 2932–2939.

LeFever, J., and Helms, L., 2008, Bakken Formation reserve estimates: North Dakota Geological Survey white paper, Bismarck, North Dakota, March, p. 6.

Li, X., and Elsworth, D., 2015, Geomechanics of CO_2 enhanced shale gas recovery: Journal of Natural Gas Science and Engineering, v. 26, p. 1607–19.

Liu, F., Ellett, K., Xiao, Y., and Rupp, JA., 2013, Assessing the feasibility of CO_2 storage in the New Albany Shale (Devonian-Mississippian) with potential enhanced gas recovery using reservoir simulation: International Journal of Greenhouse Gas Control, v. 17, p. 111–26.

Löhr, S.C., Baruch, E.T., Hall, P.A., and Kennedy, M.J., 2015, Is organic pore development in gas shales influenced by the primary porosity and structure of thermally immature organic matter?: Organic Geochemistry, v. 87, p. 119–132.

Loucks, R.G., Reed, R.M., Ruppel, S.C., and Jarvie, D.M., 2009, Morphology, genesis, and distribution of nanometer-scale pores in siliceous mudstones of the Mississippian Barnet shale: Journal of Sedimentary Research, v. 79, p. 848–861.

Loucks, R.G., Reed, R.M., Ruppel, S.C., and Hammes, U., 2012, Spectrum of pore types and networks in mudrocks and a descriptive classification for matrix-related mudrock pores: AAPG Bulletin, v. 96, no. 6, p. 1071–1098.

Mittemeijer, E.J., and Welzel, U., 2013, Modern diffraction methods: Wiley Online Library, January.

Mukhopadhyay, P.K., and Dow, W.G., 1994, Vitrinite reflectance as a maturity parameter—applications and limitations: ACS Symposium Series, v. 570, p. 294.

Nordeng, S.H., and LeFever, J.A., 2009, Organic geochemical patterns in the Bakken source system: North Dakota Geological Survey Geologic Investigations No. 79.

Odusina, E.O., Sondergeld, C.H., and Rai, C.S., 2011, NMR study of shale wettability: Society of Petroleum Engineers. doi:10.2118/147371-MS, January 1.

Patterson, R., 2017, Bakken decline rates worrying for drillers: http://oilprice.com/Energy/Crude-Oil/Bakken-Decline-Rates-Worrying-For-Drillers.html (accessed October 10, 2017).

Peters, K.E., and Cassa, M.R., 1994, *in* Applied source-rock geochemistry, Magoon, L.B., and Dow, W.G., Eds., The petroleum system—from source to trap: American Association of Petroleum Geologists, Tulsa, Applied Source-Rock Geochemistry, p. 93–120.

Rassenfoss, S., 2016, Pores to predictions—nanoscale clues to larger mysteries: Journal of Petroleum Technology, v. 68, no. 12, p. 27–33, Society of Petroleum Engineers, December.

Renner, T.A., 1988, Measurement and correlation of diffusion coefficients for CO_2 and rich-gas applications: SPE Reservoir Engineering, v. 3, p. 517–523.

Roman, F.J.P., and Hejazi, S.H., 2016, Estimation of concentration-dependent diffusion coefficients of gases in heavy oils/bitumen using experimental pressure-decay data: The Canadian Journal of Chemical Engineering, v. 94, p. 2407–2416.

Sanei, H., Wood, J. M., Ardakani, O.H., Clarkson, C.R., and Jianck, C., 2015, Characterization of organic matter fractions in an unconventional tight gas siltstone reservoir: International Journal of Coal Geology, v. 150–151, p. 296–305.

Skinner, J.T., Tovar, F.D., and Schechter, D.S., 2015, Computed tomography for petrophysical characterization of highly heterogeneous reservoir rock: Society of Petroleum Engineers, SPE-177257-MS.

Sorensen, J.A., and Hamling, J.A., 2016, Historical Bakken test data provide critical insights on EOR in tight oil plays: The American Oil & Gas Reporter, v. 59, no. 2, p. 55–61.

Sorensen, J.A., Braunberger, J.R., Liu, G., Smith, S.A., Hawthorne, S.A., Steadman, E.N., and Harju, J.A., 2015, Characterization and evaluation of the Bakken petroleum system for CO_2 enhanced oil recovery: Paper presented at the SPE–AAPG–SEG Unconventional Resources Technology Conference, San Antonio, Texas, USA, 20–22 July 2015, URTeC 2169871.

Sorensen, J.A., Hawthorne, S.A., Smith, S.A., Braunberger, J.R., Liu, G., Klenner, R., Botnen, L.S., Steadman, E.N., Harju, J.A., and Doll, T.E., 2014, CO_2 storage and enhanced Bakken recovery research program: Subtask 1.10 final report for U.S. Department of Energy Cooperative Agreement No. DE-FC26-08NT43291, May, p. 79.

Sorensen, J.A., Kurz, B.A., Smith, S.A., Walls, J., Foster, M., and Aylsworth, B., 2016, The use of advanced analytical techniques to characterize micro- and nanoscale pores and fractures in the Bakken: Paper presented at the SPE-AAPG-SEG Unconventional Resources Technology Conference, San Antonio, Texas, USA, 1–3 August 2016, URTeC 2433692.

Sorensen, J.A., Kurz, B.A., Hawthorne, S.B., Jin, L., Smith, S.A., and Azenkeng, A., 2017, Laboratory characterization and modeling to examine CO_2 storage and enhanced oil recovery in an unconventional tight oil formation: Paper presented at 13th International Conference on Greenhouse Gas Control Technologies, GHGT-13, Lausanne, Switzerland, 14–18 November 2016, published in Energy Procedia, v. 114, p. 5460–5478, Elsevier, July.

Tang, X., Wang, Z., Ripepi, N., Kang, B., and Yue, G., 2015, Adsorption affinity of different types of coal—mean isosteric heat of adsorption: Energy & Fuels, v. 29, p. 3609–15.

Tang, X., Ripepi, N., and Gilliland, E., 2016, Isothermal adsorption kinetics properties of carbon dioxide in crushed coal: Greenhouse Gases: Science and Technology, v. 6, p. 260–74.

Taylor, G.H., Teichmüller, M., Davis, A., Diessel, C.F.K., Littke, R., and Robert, P., 1998, Organic petrology: Berlin and Stuttgart, Gebrüder Borntraeger, p. 704.

Tharanivasan, A.K., Yang, C., and Gu, Y., 2004, Comparison of three different interface mass transfer models used in the experimental measurement of solvent diffusivity in heavy oil: Journal of Petroleum Science and Engineering, v. 44, p. 269–282.

Todd, H.B., and Evans, J.G., 2016, Improved oil recovery IOR pilot projects in the Bakken Formation: Proceedings of the SPE Low Perm Symposium, SPE-180270, Denver, Colorado, May 5–6, 2016.

Tovar, F.D., Eide, O., Graue, A., and Schechter, D.S., 2014, Experimental investigation of enhanced recovery in unconventional liquid reservoirs using CO_2—a look ahead to the future of unconventional EOR: Proceedings of the SPE Unconventional Resources Conference, SPE 169022, The Woodlands, Texas, April 1–3.

Trevisan, O.V., Araujo, S.V., Santos, R.G.D., and Vargas, J.A., 2013, Diffusion coefficient of CO_2 in light oil under reservoir conditions using x-ray computed tomography: Presented at the Offshore Technology Conference, OTC Brasil, OTC-24454-MS, October.

Upreti, S.R., and Mehrotra, A.K., 2000, Experimental measurement of gas diffusivity in bitumen—results for carbon dioxide: Industrial & Engineering Chemistry Research, v. 39, p. 1080–1087.

U.S. Department of Energy National Energy Technology Laboratory, 2008, Carbon sequestration atlas of the United States and Canada (2nd ed.).

U.S. Department of Energy National Energy Technology Laboratory, 2010a, Carbon sequestration atlas of the United States and Canada (3rd ed.).

U.S. Department of Energy National Energy Technology Laboratory, 2010b, Carbon dioxide enhanced oil recovery: untapped domestic energy supply and long term carbon storage solution. Strategic Center for Natural Gas and Oil (SCNGO), National Energy Technology Laboratory, March.

U.S. Department of Energy National Energy Technology Laboratory, 2012, Carbon sequestration atlas of the United States and Canada (4th ed.).

Walls, J., and Armbruster, M., 2012, Shale reservoir evaluation improved by dual energy x-ray CT imaging: Journal of Petroleum Technology, v. 64, no. 11, p. 28–32.

Wang, S., Feng, Q., Javadpour, F., Xia, T., and Li, Z., 2015, Oil adsorption in shale nanopores and its effect on recoverable oil-in-place: International Journal of Coal Geology, v. 147, p. 9–24.

Wang, S., Javadpour, F., and Feng, Q., 2016a, Fast mass transport of oil and supercritical carbon dioxide through organic nanopores in shale: Fuel, v. 181, p. 741–58.

Wang, D., Zhang, J., Butler, R., and Olatunji, K., 2016b, Scaling laboratory-data surfactant-imbibition rates to the field in fractured-shale formations: SPE Reservoir Evaluation & Engineering, v. 19, no. 3.

Wang, D., Seright, R.S., and Zhang, J., 2012, Wettability survey in Bakken shale using surfactant formulation imbibition: Society of Petroleum Engineers Reservoir Evaluation & Engineering, v. 15, no. 6.

Wargo, E.A., Kotaka, T., Tabuchi, Y., and Kumbur, E.C., 2013, Comparison of focused ion beam versus nano-scale x-ray computed tomography for resolving 3-D microstructures of porous fuel cell materials: Journal of Power Sources, v. 241, p. 608–618.

Xiong, Y., Winterfeld, P., Wang, C., Huang, Z., and Wu, Y.S., 2015, Effect of large capillary pressure on fluid flow and transport in stress-sensitive tight oil reservoirs, *in* Proceedings of SPE Annual Technical Conference and Exhibition: Houston, Texas, September 28–30, SPE-175074.

Yin, H., Zhou, J., Jiang, Y., Xian, X., and Liu, Q., 2016, Physical and structural changes in shale associated with supercritical CO_2 exposure: Fuel, v. 184, p. 289–303.